
Doctoral Dissertations

Student Theses and Dissertations

Summer 2020

Advanced control methods on three-phase inverters in distributed energy resources

Sara Yazdani

Follow this and additional works at: https://scholarsmine.mst.edu/doctoral_dissertations



Part of the [Electrical and Computer Engineering Commons](#)

Department: **Electrical and Computer Engineering**

Recommended Citation

Yazdani, Sara, "Advanced control methods on three-phase inverters in distributed energy resources" (2020). *Doctoral Dissertations*. 2925.

https://scholarsmine.mst.edu/doctoral_dissertations/2925

This thesis is brought to you by Scholars' Mine, a service of the Missouri S&T Library and Learning Resources. This work is protected by U. S. Copyright Law. Unauthorized use including reproduction for redistribution requires the permission of the copyright holder. For more information, please contact scholarsmine@mst.edu.

ADVANCED CONTROL METHODS ON THREE-PHASE INVERTERS IN
DISTRIBUTED ENERGY RESOURCES

by

SARA YAZDANI

A DISSERTATION

Presented to the Graduate Faculty of the

MISSOURI UNIVERSITY OF SCIENCE AND TECHNOLOGY

In Partial Fulfillment of the Requirements for the Degree

DOCTOR OF PHILOSOPHY

in

ELECTRICAL ENGINEERING

2020

Approved by

Mehdi Ferdowsi, Advisor

Jagannathan Sarangapani

Jonathan W. Kimball

Pourya Shamsi

Ali Rownaghi

Copyright 2020
SARA YAZDANI
All Rights Reserved

PUBLICATION DISSERTATION OPTION

This dissertation has been prepared using the publication option and is composed of three papers:

Paper I : Pages 7-36, "Internal Model Based Smooth Transition of a Three-Phase Inverter Between Islanded and Grid-Connected Modes." Published in *IEEE Trans. Energy Conversion*, vol. 35, no. 1, pp. 405-415, March 2020.

Paper II : Pages 37-73 "Advanced Current-Limiting and Power-Sharing Control in a PV-Based Grid-Forming Inverter Under Unbalanced Grid Conditions," Published in *IEEE Journal of Emerging and Selected Topics in Power Electronics*, vol. 8, no. 2, pp. 1084-1096, June 2020.

Paper III : Pages 74-111, Internal Model Power Synchronization Control of a PV-Based Voltage Source Converter in Weak-Grid and Islanded Conditions. Submitted to *IEEE Transactions on Sustainable Energy*, under second revision.

ABSTRACT

This research is an endeavor to apply new and well-established control methodologies to improve transient response, stability and reliability of three-phase inverters in grid-connected and isolated mode of operation. In the course of studying the effect of these methodologies, model-based control is introduced and is extensively applied which is relatively a new approach. In addition, the application of this concept has been studied on developing “grid-forming” controls to allow wind and solar inverters to support voltage and frequency levels like traditional generators.

This research encloses the details of three major works of this research and their possible contributions on improving the performance of three-phase inverters in grid-connected and isolated mode of operation. The first one employs the concept of *adaptive control using multiple models* and a hierarchical control approach to smoothly switch between isolated and grid-connected modes of operation. In the second work, the features of the first research work have been applied and more nourished to control a "grid-forming" unit. The interactions of this grid-supporting converter with a "grid-forming" unit is the main subject of discussion in this work. The last work applies the concept of *internal-model control* to introduce a new control methodology in power-synchronization method. This approach has tackled the non-minimum phase issue attributed to power-synchronization methodology and offers a robust solution.

Furthermore, in this research, detailed stability analysis of all the proposed control structures have been presented. Along with all simulation verification, FPGA-Based Hardware-in-the-Loop (HIL) has been utilized to verify the performance of the discrete control structure.

The details of plant modeling, controller design, HIL and experimental results are presented for all of the proposed schemes in each section.

ACKNOWLEDGMENTS

I would like to sincerely thank Dr. Mehdi Ferdowsi, for not saying no to my application and giving me the opportunity to work in a new environment and get to know myself more. I would like to acknowledge his patience with me and the financial and technical support given to me for the research work during the time I spent at Missouri University of Science and Technology. I would like to express my gratitude to Dr. Masoud Davari for his help and critique of my work and for teaching me to not expect great results in a short time. I am so grateful to my committee members, Dr. Jagannathan Sarangapani, Dr. Jonathan W. Kimball, Dr. Pourya Shamsi and Dr. Ali Rownaghi for their valuable support. My special thanks to Dr. Sarangapani for his encouragement to apply control methodologies in different applications, which helped me a lot to choose my future research goals.

My heartfelt gratitude to Reza, whose patience, support and encouragement allowed me to take this journey alone and give my life a better direction. I thank my lovely parents who have always tried to pull my strings to touch the reality of life and run with a more realistic pace. I thank Atousa and Mahyar for their support and criticisms to adjust myself with the rules of life. My last but the most special thanks goes to Vikram, for his unconditional brotherly support without which I would not have been able to go through this journey. I will always be so grateful to his help, our discussions, criticisms, and fights that have hopefully put me on the right path to realize my own *vojoud*.

TABLE OF CONTENTS

	Page
PUBLICATION DISSERTATION OPTION	iii
ABSTRACT	iv
ACKNOWLEDGMENTS	v
LIST OF ILLUSTRATIONS	x
LIST OF TABLES	xiv
 SECTION	
1. INTRODUCTION	1
 PAPER	
I. INTERNAL MODEL BASED SMOOTH TRANSITION OF A THREE-PHASE INVERTER BETWEEN ISLANDED AND GRID-CONNECTED MODES.....	7
ABSTRACT	7
1. INTRODUCTION	8
2. SYSTEM CONFIGURATION AND MODEL DERIVATION.....	11
3. PROPOSED CONTROL ARCHITECTURE	14
3.1. INTERNAL MODEL CONTROL.....	14
3.2. ADAPTATION AND LEARNING BY USING MULTIPLE MODELS	16
3.3. SWING EQUATION BASED POWER SYNCHRONIZATION CONTROL.....	19
4. SMALL SIGNAL STABILITY ANALYSIS	20

5.	HARDWARE CO-SIMULATION AND RESULTS	23
5.1.	SMOOTH TRANSITION BETWEEN GRIDTIED AND ISLANDED MODES	26
5.2.	SMOOTH TRANSITION WITH OPTIMIZED SWITCHING RULE	26
5.3.	EVALUATION THROUGH COMPARISON WITH EXISTING TECHNIQUES	27
5.4.	LOAD SWITCHING AND PARAMETER CHANGES	30
6.	CONCLUSION	32
	REFERENCES	33
II.	ADVANCED CURRENT-LIMITING AND POWER-SHARING CONTROL IN A PV-BASED GRID-FORMING INVERTER UNDER UNBALANCED GRID CONDITIONS	37
	ABSTRACT	37
1.	INTRODUCTION	38
2.	SYSTEM CONFIGURATION	42
3.	CONTROL STRUCTURE.....	46
3.1.	OUTER POWER CONTROL LOOP.....	46
3.2.	INNER VOLTAGE AND CURRENT CONTROL LOOPS.....	51
3.3.	AUGMENTED POWER PROPORTIONAL RESONANT CON- TROL	52
4.	STABILITY ANALYSIS	55
4.1.	GRID-FORMING SMALL-SIGNAL DYNAMIC ANALYSIS	56
4.2.	GRID-FOLLOWING SMALL-SIGNAL DYNAMIC ANALYSIS ...	56
5.	HARDWARE CO-SIMULATION RESULTS AND DISCUSSIONS	57
5.1.	POWER-SHARING CONTROL IN ISLANDED AND GRID- CONNECTED MODES OF OPERATION	60

5.2.	POWER-SHARING CONTROL IN ISLANDED AND UNBALANCED-GRID-CONNECTED MODES OF OPERATION.	61
5.3.	PR CONTROLLER PERFORMANCE EVALUATION IN UNBALANCED-GRID-CONNECTED MODES OF OPERATION.	64
5.4.	POWER-SHARING CONTROL IN ISLANDED AND UNBALANCED-GRID-CONNECTED MODES OF OPERATION AND CHANGE IN IRRADIATION	67
5.5.	COMPARISON WITH A CONVENTIONAL SYNCHRONVERTER EQUIPPED WITH CURRENT-LIMITING LOOP	67
6.	CONCLUSION	68
	REFERENCES	70
III.	INTERNAL MODEL POWER SYNCHRONIZATION CONTROL OF A PV-BASED VOLTAGE SOURCE CONVERTER IN WEAK-GRID AND ISLANDED CONDITIONS	74
	ABSTRACT	74
1.	INTRODUCTION	75
2.	SYSTEM CONFIGURATION	79
2.1.	POWER SYNCHRONIZATION CONTROL STRUCTURE	79
3.	PROPOSED CONTROL ARCHITECTURE	85
3.1.	INTERNAL MODEL CONTROL.....	86
3.1.1.	IMC-IAE.....	90
3.1.2.	IMC-ISE	92
3.1.3.	Low Damping Stable Zero	92
4.	STABILITY ANALYSIS	95
5.	EXPERIMENTAL RESULTS.....	98
5.1.	EXPERIMENTAL EVALUATION OF THE CONTROLLER BY USING A CONVERTER	99
5.2.	HIL TESTING FOR FAULT CASES	101

5.3.	DC-BUS CONTROL AND IMPROVEMENTS IN NON-MINIMUM PHASE BEHAVIOR	104
5.4.	FRT AND CURRENT-LIMITING CAPABILITIES IN WEAK-GRID CONDITIONS	104
5.5.	OPERATION IN ISLANDED MODE	105
6.	CONCLUSIONS	107
	REFERENCES	108
SECTION		
2.	CONCLUSION	112
	REFERENCES	114
	VITA	115

LIST OF ILLUSTRATIONS

Figure	Page
1.1. Typical configuration of a DER based on IEEE 399	2
1.2. Typical configuration of a grid-forming converter in a DER based on IEEE 399.	3
1.3. Typical configuration of a grid-forming and grid-following converter in a DER based on IEEE 399	6
 PAPER I	
1. General overview of the system under study	11
2. Simplified diagram of DER system under study	12
3. General block diagram of a simple closed loop control and IMC structure	14
4. Block diagram of multiple internal model control.....	16
5. Block diagram of multiple internal model control.....	17
6. Frequency response to change of inertia (a) Standalone mode (b) Grid-connected mode	21
7. Frequency response to change of λ (a) Standalone mode (b) Grid-connected mode	22
8. General overview of the system with incorporated delay	23
9. Closed-loop pole placement based on IMC parameter	24
10. Transition from grid-connected Mode to Standalone - Proposed control Method (a) Voltage at PCC and current - One small division for voltage is 26.154 v, One small division for current is 5 A (b) Active and reactive power	24
11. Transition from Standalone Mode to grid-connected - Proposed control Method (a) Voltage at PCC and current - One small division for voltage is 26.154 v, One small division for current is 5 A (b) Active and reactive power	25
12. Transition from grid-connected mode to standalone (a) Switching rule is based on the error (b) Switching rule is based on the square of the error (c) Switching rule is based on optimized switching rule	28

13. Comparison in back and forth transition between grid-connected and standalone modes of operation - (a) Proposed control method (b) Passive islanding detection based on under/over voltage (c) Passive islanding detection based on under/over frequency - One small division for voltage is 53.30 v, One small division for current is 13.33 A.....	29
14. Comparison in back and forth transition between grid-connected and standalone modes of operation - (a) Proposed control method (b) Passive islanding detection based on under/over voltage (c) Passive islanding detection based on under/over frequency - One small division for active power is 1.25 KW and for reactive power is 1.25 KVAR	31
15. Dynamic response of the system (a) when there is a load switching in standalone mode (b) when there is a parameter change in standalone mode	32

PAPER II

1. General overview of the system under study	43
2. Simplified diagram of the system under study	44
3. General overview of the control structure of the system under study	45
4. Active and reactive power control block diagram using power-synchronization method	47
5. Eigenvalue trace of grid-forming PVSG's (a) active power and (b) reactive power	54
6. Eigenvalue trace of grid-following PVSG's (a) active power and (b) reactive power.....	54
7. Closed-loop Bode plot of (a) grid-forming active power and (b) grid-following active power	54
8. The transient from grid-connected to isolated mode of operation (Active Power: 1 kW/div; Reactive Power: 1 kvar/div; Voltage: 34 V/div; Current: 8 A/div; and Frequency 0.15 Hz/div); (a) active and reactive power of grid-forming and grid-following inverters and commanded frequencies (ω_{GF}) and (ω_{GL}) and PCC frequency measured by PLL, (b) PCC voltage and grid-forming currents of phases A and B, and (c) PCC voltage and grid-following currents of phases A and B	58

9. The transient from isolated mode of operation grid-connected (Active Power: 1 kW/div; Reactive Power: 1 kvar/div; Voltage: 34 V/div; Current: 8 A/div; and Frequency 0.15 Hz/div); (a) active and reactive power of grid-forming and grid-following inverters and commanded frequencies (ω_{GF}) and (ω_{GL}) and PCC frequency measured by PLL, (b) PCC voltage and grid-forming currents of phases A and B, and (c) PCC voltage and grid-following currents of phases A and B 59
10. The transient from isolated mode of operation to unbalanced-grid-connected mode (Active Power: 1 kW/div; Reactive Power: 1 kvar/div; Voltage: 34 V/div; Current: 8 A/div; and Frequency 0.15 Hz/div); (a) active and reactive power of grid-forming and grid-following inverters and commanded frequencies (ω_{GF}) and (ω_{GL}) and PCC frequency measured by PLL, (b) PCC voltage and grid-forming currents of phases A and B, and (c) PCC voltage and grid-following currents of phases A and B 62
11. The transient from unbalanced-grid-connected mode to isolated mode of operation (Active Power: 1 kW/div; Reactive Power: 1 kvar/div; Voltage: 34 V/div; Current: 8 A/div; and Frequency 0.15 Hz/div); (a) active and reactive power of grid-forming and grid-following inverters and commanded frequencies (ω_{GF}) and (ω_{GL}) and PCC frequency measured by PLL, (b) PCC voltage and grid-forming currents of phases A and B, (c) PCC voltage at and Grid-following currents of phases A and B 63
12. The transient from balanced grid-connected mode to unbalanced-grid-connection followed by PR control disconnection (a) active and reactive power of grid-forming and grid-following inverters and commanded frequencies (ω_{GF}) and (ω_{GL}) and PCC frequency measured by PLL, (b) PCC voltage and grid-forming currents of phases A and B, and (c) PCC voltage and grid-following currents of phases A and B 65
13. The transient in isolated mode of operation followed by the reduction in irradiation and reconnecting to an unbalanced grid condition (Active Power: 1 kW/div; Reactive Power: 1 kvar/div; Voltage: 34 V/div; Current: 8 A/div; and Frequency 0.15 Hz/div); (a) active and reactive power of grid-forming and grid-following inverters and commanded frequencies (ω_{GF}) and (ω_{GL}) and PCC frequency measured by PLL, (b) PCC voltage and grid-forming currents of phases A and B, and (c) PCC voltage and grid-following currents of phases A and B 66
14. The operation evaluation of a conventional synchronverter (Voltage: 34 V/div; and Current: 8 A/div); (a) PCC voltage and current injected by a PVSG controlled as a synchronverter and (b) PCC voltage and current injected by a converter with a current control loop 69

PAPER III

1.	General overview of the system and the proposed controller	79
2.	One dimensional IMC-active power and reactive power control structures	83
3.	The damping ratio criteria for the numerator in G_P and G_Q	88
4.	(a) Active-power and (b) Reactive-power step-response of the closed-loop system and the control effort— $E_0 = 1.0$ pu, $V_0 = 1.0$ pu, $\omega L = 1.0$ pu, $R = 0.05$ pu, and $\theta_0 = 50^\circ$	91
5.	Stability criteria of the active-power and reactive-power based on $\lambda_{P,Q}$	93
6.	Active and reactive power response to irradiation changes.....	97
7.	The cost function monitoring during persistent fault occurrence	99
8.	Test rig used in the experiments	100
9.	Experimental results associated with the applied active/reactive power changes; the actual active power, its reference, the actual reactive power, and its reference have been shown by traces in blue, cyan, magenta, and lawn green respectively, with 0.5 pu/div (for both active and reactive power, whose “pu” values have been noted at the left-bottom corner of the figures) and 200 ms/div .	101
10.	Operation under three-phase voltage fault (a) active and reactive power response to fault (b) PCC voltage and current response—each small division for active power is 2 kW, for reactive power is 1 kW, for voltage is 21 V, and for current is 5 A	103
11.	Operation under three-phase voltage fault (a) active and reactive power response to fault (b) PCC voltage and current response—each small division for active power is 2 kW, for reactive power is 1 kvar, for voltage is 21 V, and for current is 5 A	106

LIST OF TABLES

	Page
PAPER I	
Table 1. System Parameters	19
PAPER II	
Table 1. System Parameters	53
PAPER III	
Table 1. System Parameters	98
Table 2. Parameters of Figure. 9	102

SECTION

1. INTRODUCTION

The concept of Distributed Energy Resources (DERs) is commonly utilized in modern power system that includes renewable energy resources such as wind generators and solar panels to generate electricity. Distributed Generation is an approach that employs small-scale technologies in modular generators to produce electricity close to the end users of power. The foundation of DERs is based on three different IEEE standards. The first one is IEEE 1547 (version 2018) which is the standard for interconnection and inter-operability of Distributed Energy Resources with associated electric power system interfaces [1]. The technical specifications along with testing environment and equipment in interconnecting and inter-operation between utility electric power systems (EPSs) and DERs are the focus of this standard. Installation of DER on radial primary and secondary distribution systems is the main emphasis of this document, although the advances in control methodologies and power electronic based converter designs results in several revisions of this standard and it is constantly going through several redrafting. As the converters are becoming more versatile the standard constantly adjusts and improves general requirements of power converters. This standard is written considering that the DER is a 60 Hz source. The second standard is IEEE 1559 (2009) [2], which is the standard for inertial systems terminology. The integration of power-electronic based converters to the conventional power-system structure with synchronous machines that are inherently inertial systems can jeopardize the stability of the generating network. The last standard is IEEE 399 (1997) which recommends practice for industrial and commercial power systems analysis (Brown Book) [3]. This standard is a source of information competitive business environment forces plant and building management and the total owning cost of power distribution systems.

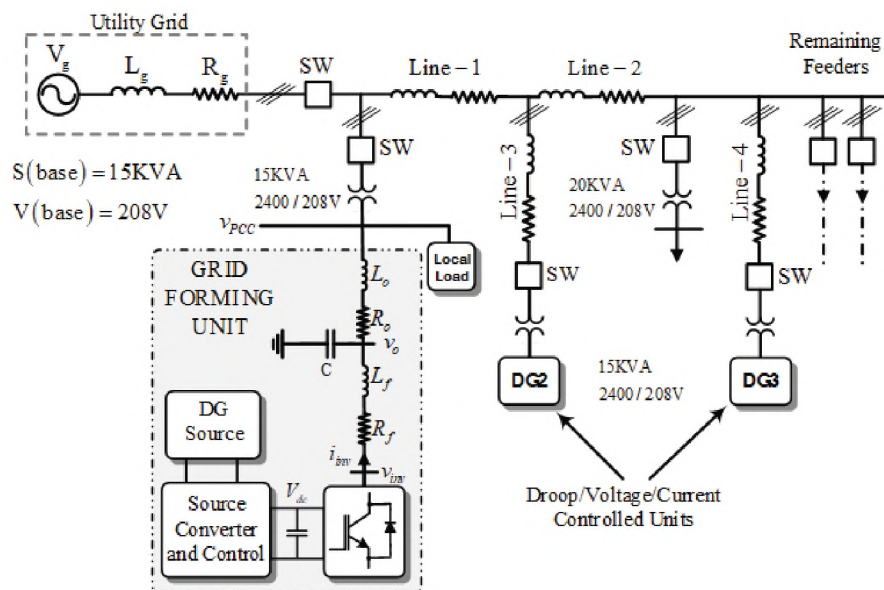


Figure 1.2. Typical configuration of a grid-forming converter in a DER based on IEEE 399

By the introduction of the concept of grid-forming inverters, the rest of the power-electronic based converters are considered as grid-following units. A “grid-following” inverter is a voltage/current-source converter that follows a grid-forming unit in voltage and frequency in PCC. Based on the definitions a following unit should have the following is introduced as (Figure 1.2):

- The grid-following unit is a current source (PQ bus)
- This unit follows the grid forming converter in terms of voltage and frequency stability
- It should be capable of injecting active and reactive power to the load
- In case of PV-Generators it must have fast response to the intermittent irradiation levels (no buffer)

Employing HVDC technology, mainly represented by wind or pv-based converters connected to the bulk-power-system, has found its place in the state-of-the-art of generic dynamic models of Distributed-Energy-Resources (DERs) [4]. The technical advantages

of this system such as reactive-power support to the ac-system and sustainable operation in weak grid condition equipped with synchronization methods as an alternative to PLL make it a suitable candidate to take its own role in common mode of energy transmission. As the power flow of an HVDC link can be independently controlled of the phase angle, it can improve the stability of the network against disturbances due to rapid changes in power.

Different control methodologies, such as power-angle control and vector-current control have already been adopted to realize the potential benefits of a VSC-HVDC [5] and [6]. Power-synchronization is also a similar method that adopts the phase-angle and voltage magnitude to directly control the active and reactive power [7]. In this method, no synchronization unit is required as the power control loop produces the voltage unit vector which generates the PWM switching signals. By incorporating a high-pass filter in the small-signal model of the active power versus load angle and reactive power versus voltage magnitude, the typical problems of the power-angle control such as resonant peak at grid frequency and converter over-current limitations have been rectified to some extent. The crucial purpose of integrating voltage-source converters for HVDC applications is to generate non-oscillatory power in weak grid conditions. However, the typical low-frequency resonance problem still persists [8]. On the other hand, the emerging demands on the operation of the VSCs in isolated mode and as grid-forming inverters to stabilize the voltage and frequency at the point-of-common-coupling (PCC). Therefore, the control of a VSC as virtual synchronous machine has attracted considerable attention. The mathematical implementation of the dynamics of synchronous machines in the control structure of the switching converters have been investigated [9]. In a simpler approach the power-frequency swing equation is solved every control cycle to emulate inertia [10]. However, in weak-grid condition, the proposed control methods might fail to sustain low-frequency resonances or severe voltage faults. In this paper, a new PID (proportional-integral-derivative) control method has been applied. In this method, both swing equation and frequency-droop-based approaches, that resembles the primary frequency control of a synchronous machine are

implemented to tune the PID control gains. Switching power-electronic based converters are mostly controlled through PI control architectures. The derivative term, which is used to add damping to the system is usually avoided. In PWM-based switching converters with large time constant, using the derivative will amplify the large frequency noise. However, power-synchronization based small signal model of the system is severely under-damped and demonstrates non-minimum phase behavior due to the presence of Right-Half-Plane (RHP) zeros. Therefore, to cancel the oscillatory under-damped terms, the derivation can be implemented through adding a high-pass filter [11]. In the present work, the proportional and derivative gains of the PID control have been calculated based on solving the swing and the governor equations of a synchronous machine and the PID controls the plant that has been derived through the power synchronization control law. This control methodology shows significant improvement in the performance of the controller in canceling the voltage imbalances and nonlinear loads on non-oscillatory power generation [12].

In this research, the focus has been on the design of a grid-forming three-phase inverter which functions as a PV-source and is capable of performing in both isolated and grid-connected modes of operation. In the first section, we have discussed the details of designing the control structure for such a converter based on hierarchical control design. The results of this paper have been published in a paper with the title of "*Internal Model Based Smooth Transition of a Three-Phase Inverter Between Islanded and Grid-Connected Modes*". The interaction between a grid-forming and a grid-following unit is described in another paper with the title of "*Advanced Current-Limiting and Power-Sharing Control in a PV-Based Grid-Forming Inverter Under Unbalanced Grid Conditions*". However, the hierarchical control has limitations that requires more observations. The limitations of hierarchical control can be enumerated as follows (Figure 1.3):

- Hierarchical control just focuses on parts of granular level of any system therefore it becomes an immense challenge to ensure whether the system constraints are violated for any system equipped with a high level control structure.

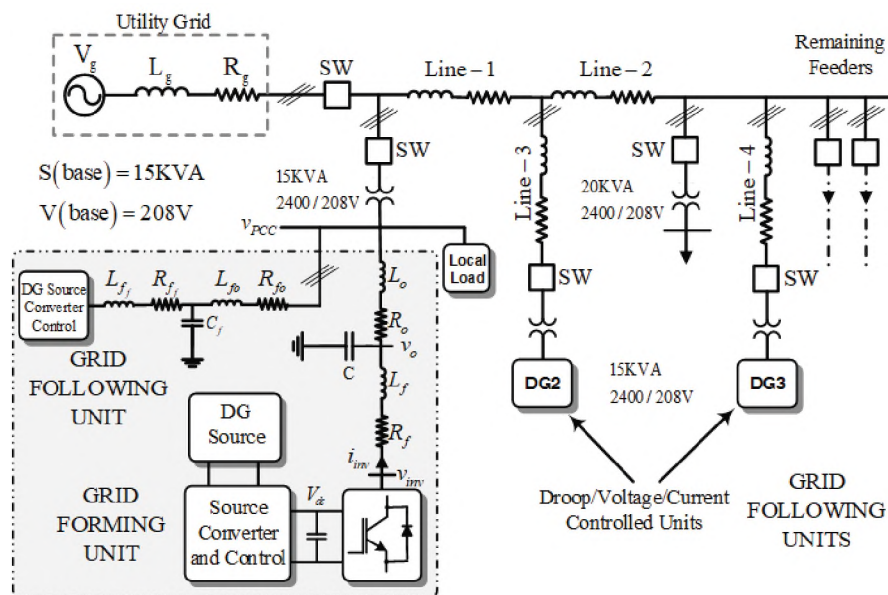


Figure 1.3. Typical configuration of a grid-forming and grid-following converter in a DER based on IEEE 399

- Higher level control always deals with large amount of data as they act as a system level controller. Therefore, it becomes a challenge to store the huge amount of data and process them.
- With such an architecture, the control has to be implemented in either centralized costly platforms or if they are implemented in a low cost decentralized manner time coordination will be an issue. Both of these adds to the complexity of the system.
- Any communication between the devices if has to be carried out would require high cost communication protocols and can always suffer from the limitation of bad data.

In the third paper with the title of "*Internal Model Power Synchronization Control of a PV-Based Voltage Source Converter in Weak-Grid and Islanded Conditions*", the details of a new control methodology based on internal model control has been proposed which will rectify the limitations attributed the the hierarchical power control in three-phase inverters.

PAPER

I. INTERNAL MODEL BASED SMOOTH TRANSITION OF A THREE-PHASE INVERTER BETWEEN ISLANDED AND GRID-CONNECTED MODES

ABSTRACT

Recent technical advances in control, protection and interconnection of distributed power generation units imply that it is practically viable and economically profitable to keep them as backup generators in isolated operating modes. Therefore, along with the development of islanding detection techniques, seamless operation in transition between islanded and grid connected modes is required and more sophisticated control strategies are needed to recognize the existing working condition and adjust the performance to meet the strict standards of grid interconnection. This paper presents a new adaptive control structure, based on internal model control (IMC), which uses multiple models and an inherent islanding detection method through an optimized switching mechanism to tune the operation of a three-phase inverter under transitions between islanded and grid-tied conditions. By applying a power synchronization method, the system emulates the operation of a synchronous machine which is needless to rely on a phase-locked loop to synchronize during the transitions. Hardware co-simulation environment in Simulink/PLECS and Xilinx System Generator have been utilized to evaluate the transient behavior of the controller in discretized domain and verify its robustness during parameter variations and load switching conditions. Various switching rules have been applied and a comparison of their effect in transient response is demonstrated. The results, taken from several case studies, confirm the significant robustness of the proposed control methodology.

1. INTRODUCTION

Distributed energy resources encompass a broad range of sizes and electrical characteristics which varies from serving rural customers to large commercial clients. The present diversity in modern distribution systems contributes to more complexities which makes it impossible to create a general interconnection standard that can address all scenarios. Nevertheless, any devised regulation must regard safety, reliability and economical prerequisites as indispensable. Considering safety concerns as the most important compulsion, IEEE (1547) standard, for interconnection and interoperability of DERs with associated electric power system interfaces [1], prevents unintentional power supply from DER to neighboring customers or to the utility grid when there is an upstream fault in the grid system. Accordingly, as DERs generally utilize inverters to interface the grid, their design should contain necessary protection to counteract unintentional islanding, or, conventional ancillaries must be installed to affect the same protection. Regardless of the availability of the power supply, when there is an outage in the main grid, local generation systems are forced to trip. However, more recent trends provide more flexible approaches to design, operation and integration of future DERs in intentional islanding condition and gives them the capability to disconnect and reconnect to part of the grid while providing power to neighboring customers [2].

Several advanced islanding detection algorithms are available [3,4]. Local islanding detection techniques are basically based on system parameter measurements and mainly include three main categories: passive, active and hybrid methods. On the whole, the ability of DERs to feed the line in a microgrid with intentional islanding capabilities along with the development of islanding detection methods alleviates the anti-islanding requirements, but intensifies the need to develop a control mechanism to detect and offer a seamless operation both in islanded and grid-connected modes without affecting the overall power generating procedure.

Different studies have been performed to address the microgrid transition between standalone and gridtied modes during grid-losses and undesired transients and disturbances [5–9]. Regular DER interactive inverters are dominantly operated by current control mode which switches to voltage control mode by the occurrence of an intentional islanding to feed the emergency loads. However, the transition and delays in islanding detection may result in instabilities in the output voltage of the inverter [10, 11]. Different control methodologies for seamless transition between islanded and gridtied modes of operation have been proposed [12, 13]. A direct control strategy treats the interfaced voltage source converter by a voltage control (VC-VSC) which provides control over frequency and voltage at PCC [14]. Despite being straight forward, this methodology does not comply with the extended operation range of microgrids and the essential hierarchical control structure in modern DER [15]. In a more recent approach, a synchronous power controller (SPC) has been proposed as a suitable alternative which permits PV plants to operate seamlessly in grid connected and islanded modes, with no need of changing the control structure [16]. This method offers a controller with virtual inertia which can elude the anti-islanding algorithm of the connected PV inverters and ensure soft transitions. However, the LCL filter and a trap filter for switching frequency along with the proportional resonant (PR) controller adopted for the current control give rise to a 7th order system and the tuning of parameters becomes cumbersome.

A fixed hierarchical power-voltage-current control structure has been utilized by applying a fixed droop control over the active power and an IMC based voltage control [17]. The proposed controller is robust against random disturbances, but its performance in grid connected mode is dependent on a resonant filter along with the PLL. To generate the reference frequency in standalone mode, the processor internal clock is used. The coupling effect and interactions between PLL and system impedance network is still an issue which can lead to instabilities when multiple inverters are connected and the nonlinear behavior of PLL endangers the effectiveness of the control system in weak grid condition [18, 19].

In the light of the aforementioned information and by considering the fact that the continuous operation of an inverter, either in islanded or grid-connected modes, fits well into the adaptation and learning by using multiple models, which has already been decently addressed in control theory [20, 21], this paper presents an adaptive multiple internal model control to render a seamless operation to microgrids in small distribution systems. Internal model based control (IMC) has already been applied to control three-phase grid connected and standalone converters [22–24]. However, in this paper, a new multiple-internal model control scheme with an adaptive switching and tuning structure has been proposed which is occupied with an optimized switching rule which takes care of smooth transitions during unprecedented delayed islanding detection phenomenon. By involving the concept of power-synchronization [25], a simple swing equation based control methodology has been applied [26] as a fixed control loop which is augmented with an adaptive multi-model switching control. The proposed control structure

- Emulates a virtual synchronous machine which regulates power both in grid-connected and standalone modes.
- Offers a seamless transition with no need of PLL and is robust during transitions.
- Possesses an optimized switching rule and an inherent islanding detection mechanism.
- Is able to perform efficiently in the presence of parameter uncertainties and loading conditions.

These features incorporated with conventional active damping methodology [27] and current limiting capability can significantly improve the robustness and enhance the system stability, by applying a simple linear control design and simpler parameter tuning requirements. Hardware co-simulation experiments endorses the advantages offered by this internal multi-model control.

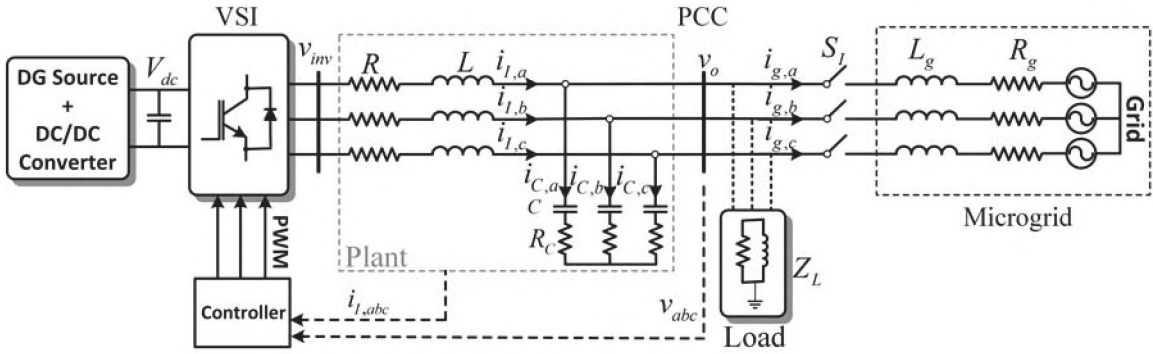


Figure 1. General overview of the system under study

This paper is organized as follows: In section 2, the system configuration is presented. Section 3 will describe the control structure in detail. Small signal stability analysis is explained in Section 4 and Section 5 includes the details about hardware co-simulation method and realtime assessment of the control design through the demonstration of the results. And, in the last section, there will be final discussions and conclusion.

2. SYSTEM CONFIGURATION AND MODEL DERIVATION

The system presented in Figure. 1 is composed of a DER unit and an RL load. This system is required to have a dual-operation under islanded or grid-connected modes when switch S_1 is either open or closed. The system includes a primary energy source and a three-phase VSC interfaced to the PCC by an LC filter and the RL load is connected to the PCC. The main grid is considered as an ideal three-phase voltage source with per phase R_g and L_g components. On the other hand, a quick and safe disconnection from the grid when a disturbance is detected and reconnecting automatically, or with the intervention of an operator, is essential. The main challenge of the this microgrid and the utility is to maintain frequency and voltage at PCC and coordinating the operation of protective relays

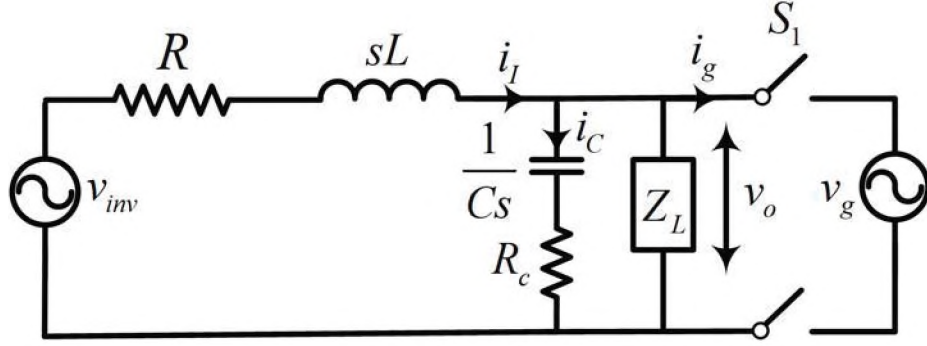


Figure 2. Simplified diagram of DER system under study

and reclosers in compliance with utility standards. The smooth transition and seamless operation of this system requires a robust control infrastructure which is equipped with an accurate islanding detection mechanism.

A simplified diagram of the system is depicted in Figure. 2. The state space representation in both grid-connected and islanded modes is governed by the following equations:

$$v_{inv,abc} = Ri_{I,abc} + L \frac{di_{I,abc}}{dt} + v_{o,abc} \quad (1)$$

$$\dot{i}_{I,abc} = i_{C,abc} + i_{g,abc} = C \frac{dv_{o,abc}}{dt} + i_{g,abc}$$

where, L and C are the filter inductance and capacitance, $v_{inv,abc}$ and $i_{I,abc}$ are vector representation of each phase inverter output voltage and current respectively and $v_{o,abc}$ is the voltage at PCC. To simplify the system representation in gridtie mode, the equations in (1) can be rewritten in stationary reference frame, $\alpha\beta$, by considering the fact that the grid impedance is generally considered to be less than 0.6 per unit of the base impedance. Therefore, without loss of generality, we can consider v_o to be equal to the grid voltage, v_g :

$$v_{inv\alpha} = Ri_{I\alpha} + L \frac{di_{I\alpha}}{dt} + v_{g\alpha} \quad (2)$$

$$v_{inv\beta} = Ri_{I\beta} + L \frac{di_{I\beta}}{dt} + v_{g\beta}$$

and consequently, an ideal model of the system, by considering the nominal values of the filter components in Laplace domain, turns out to be:

$$\tilde{G}_{Pi,\alpha\beta} = \frac{i_{I,\alpha\beta}}{v_{inv,\alpha\beta} - v_{g,\alpha\beta}} = \frac{1}{s\bar{L}_0 + \bar{R}_0} \quad (3)$$

Equation (3) paves the way to apply a model based control (MBC), [28], on the plant in Figure. 1 as long as it is connected to the grid and \tilde{G}_{Pi} is the representation of the model that will be controlled by a current control loop. In standalone mode, v_o will be equal to the voltage across the load and the stationary reference frame representation of the system in islanded mode will be:

$$v_{inv\alpha} = Ri_{I\alpha} + L\frac{di_{I\alpha}}{dt} + v_{C\alpha} \quad (4)$$

$$v_{inv\beta} = Ri_{I\beta} + L\frac{di_{I\beta}}{dt} + v_{C\beta}$$

As in the islanded mode, the challenge is to maintain the voltage across the load, the model of the system based on the voltage across the filter capacitor and inverter output voltage is defined as:

$$\tilde{G}_{Pv} = \frac{v_{C,\alpha\beta}}{v_{inv,\alpha\beta}} = \frac{1}{s^2C_0L_0 + sR_0C_0 + 1} \quad (5)$$

\tilde{G}_{Pv} is the representation of the plant with nominal parameters that is controlled by a voltage control loop. The error generated by the comparison between the output of the plant ($i_{I,abc}$ and $v_{o,abc}$) and the ones generated from each one of the models gives out a signal that can indicate which environment is currently active and switch to the appropriate controller. This is an islanding detection method with nearly no non-detection zone (NDZ) which is innate in IMC based control. The control methodology and the switching rule are thoroughly explained in the next section.

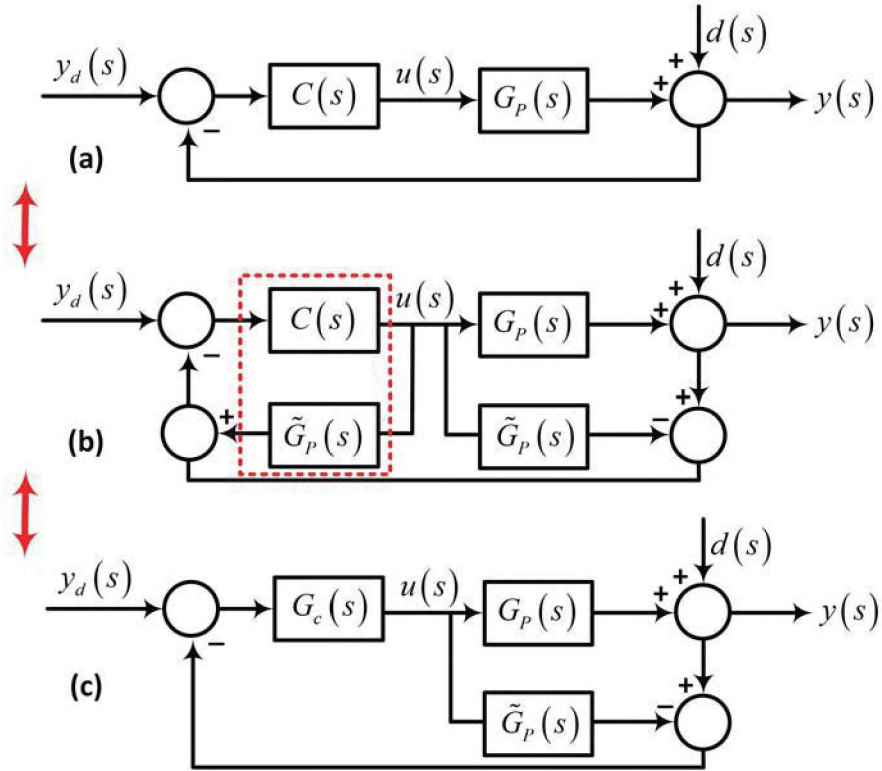


Figure 3. General block diagram of a simple closed loop control and IMC structure

3. PROPOSED CONTROL ARCHITECTURE

3.1. INTERNAL MODEL CONTROL

Classical closed-loop current control is the most common methodology to control converters. This method requires to solve the state space equation of the system which is not accurate for nonlinear and non-minimum phase systems with instabilities. Applying the concept of internal model based control (IMC) which incorporates a reasonably accurate model of the plant by using the nominal values of the system parameters has recently attracted attentions [32–35]. This method works perfectly well when the plant is stable with minimum or non-minimum phases and extra measures can be taken to apply it on unstable plants. As it can be seen in Figure. 3, IMC can simply be transformed into

closed loop by adding and subtracting an accurate model of the plant to the classical closed loop control. Starting from a simple closed loop control, Figure. 3(a), the control law of the system can be written as:

$$y(s) = \underbrace{\frac{C(s) G_P(s)}{1 + C(s) G_P(s)}}_{T(s)} y_d(s) + \underbrace{\frac{1}{1 + C(s) G_P(s)}}_{S(s)} d(s) \quad (6)$$

in which, $T(s)$ is the transfer function of the system and $S(s)$ is the sensitivity. By adding and subtracting the nominal model of the plant, there will be no change on the control structure Figure. 3(b). The IMC structure can be realized after merging the control, $C(s)$, with the model of the system, $\tilde{G}_P(s)$ and the control law is described as:

$$y(s) = \underbrace{\frac{G_c(s) G_P(s)}{1 + G_c(s) (G_P(s) - \tilde{G}_P(s))}}_{T(s)} y_d(s) + \underbrace{\frac{1 - G_c(s) \tilde{G}_P(s)}{1 + G_c(s) (G_P(s) - \tilde{G}_P(s))}}_{S(s)} d(s) \quad (7)$$

If the model exactly matches the plant, $G_P(s) = \tilde{G}_P(s)$, the transfer function and the sensitivity turn out to be:

$$T(s) = G_c(s) G_P(s) \quad (8)$$

$$S(s) = 1 - G_c(s) G_P(s)$$

To have the most accurate control and make the IMC design near optimal and to make y exactly track y_d , the transfer function should be: $T(s) = 1$ and therefore, the controller will be: $G_c(s) = G_P^{-1}(s)$ which can be realized when the plant model is exact, minimum phase and invertible. As the plant models we have (equations: (3) and (5)) are both causal and stable, there is no need to factorize the models and separate the parts which are not

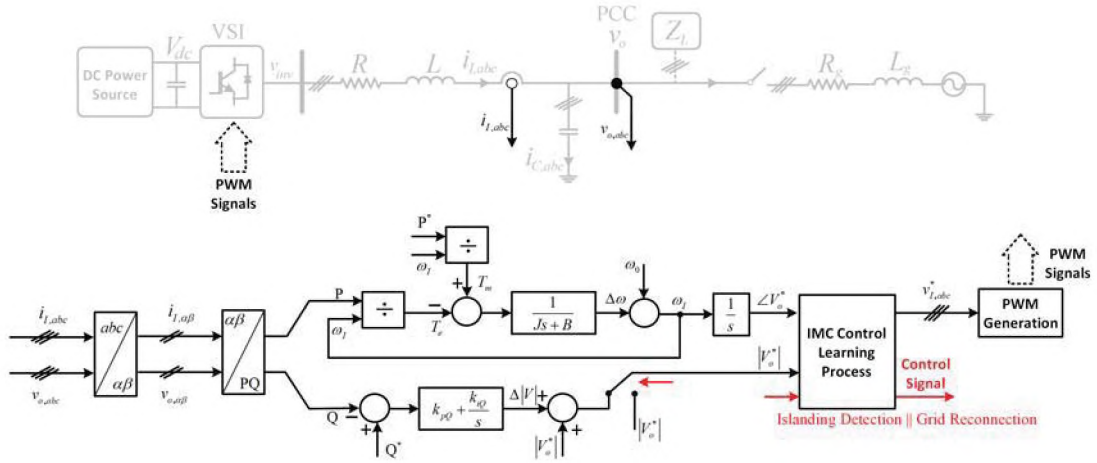


Figure 4. Block diagram of multiple internal model control

invertible and non-minimum phase. However, in order to make the control proper and robust against plant and model mismatches, the controller should be augmented by a low pass filter, $F(s) = 1/(\lambda s + 1)^n$, in which n is chosen in a way to make $G_c(s)$ proper.

The delicacy of designing this controller comes from the fact that tuning parameter, λ_c (filter parameter in G_{ci}) and λ_v (filter parameter in G_{cv}), have inverse relationship with the speed of the closed loop response and favorably, it is not undesirable in this control scheme. As the internal model control structure is primarily cascaded with an inertial power control loop, which is relatively slow, by properly adjusting the λ parameter, the whole control design will demonstrate a suitable stability and robustness. More details about this feature will be explained in coming sections.

3.2. ADAPTATION AND LEARNING BY USING MULTIPLE MODELS

The concept of realizing an intelligent controller through multiple identification models with the capability to recognize the active environment and adjust its controlling operation accordingly has been decently addressed in control theory [20,21]. This structure has proven its credibility and practical operation in several experimental and industrial

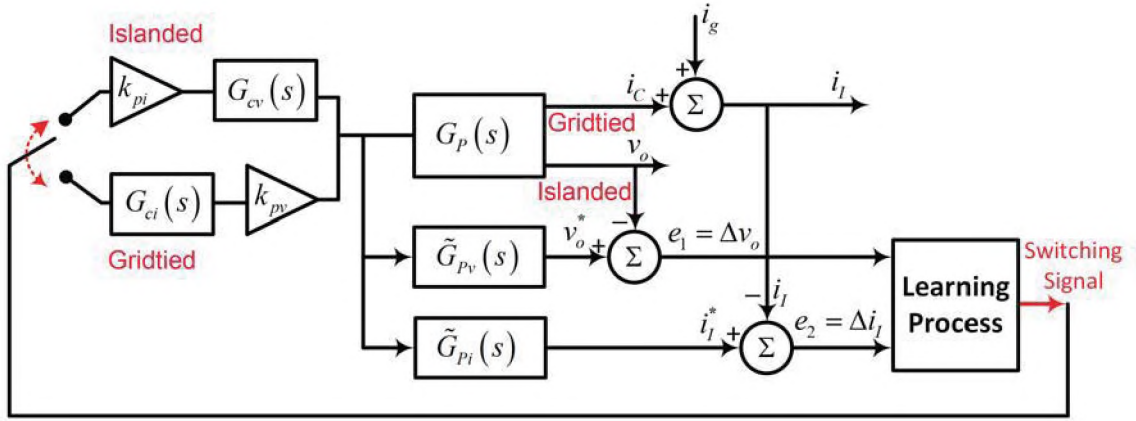


Figure 5. Block diagram of multiple internal model control

applications such as in robotics and aviation [21] and [34]. This methodology can learn about different environments in course of time and act swiftly and accurately. For the current purpose, the switching and tuning should happen during the islanding detection and re-connection to the grid and the mechanism should take care of swift and accurate switching within the learning set and take care of the possible delay in islanding detection.

The structure of the control system applied for this purpose is two different internal models of the system which estimate the standalone and gridtied modes of operation and their corresponding control systems, see Figure. 4. At every instant of time two measures of identification errors are generated, e_1 and e_2 , which are defined as:

$$\begin{cases} e_1 \triangleq v_o^* - v_o = \Delta v_o \\ e_2 \triangleq i_l^* - i_l = \Delta i_l \end{cases} \quad (9)$$

A performance cost, J_{op} , is defined for each of the controllers and to which controller one should switch is determined by the one that minimizes the cost function as follows:

$$J_{op}(t) = \alpha e_j^2(t) + \beta \int_0^t e^{-\xi(t-\tau)} e_j^2(\tau) d\tau \quad (10)$$

$$\alpha \geq 0 \quad \beta, \xi > 0 \quad j = 1, 2$$

The equation has two instantaneous and long-term accuracy measurements, where j is the counting index and α/β are weighing factors. The two internal models of the system are performing in parallel. Considering gridtied as the initial condition, when the islanding occurs, there is a mismatch between the first-order approximated model, (3), and the plant due to the reduction of current at PCC, as the local load is being fed solely by the VSC. The switching must happen as the error between the plant and the first order system starts to rise and the error between the plant and the second order model, (5), starts to diminish as the plant matches with the second-order internal model in islanded mode and it instantaneously minimizes J_{op} .

This way, the detection of the islanded mode is immediate. As in the present application, the delayed islanding detection is not desirable, β is chosen in a way just to rectify the inertial response of the power control loop and the forgetting factor, ξ , determines a memory for the index which is quite useful to keep pace of the switching internal models with the inertial response of the power control loop when the transition happens and act as a low-pass filter to rectify the possible fluctuations due to switchings. As J_{op} is minimized for the error of the second order model, an immediate switching, switches the control to a voltage control which is dominantly used in standalone operation. The voltage control is augmented by a filter, $F(s) = 1/(\lambda_v s + 1)^2$ as the model is second order in standalone mode and a gain, k_{pi} , is also added as an inner current control loop to give current limiting capability to the controller. This ritual can also be applied when the reverse transition occurs to reconnect back to the grid and the filter will be $F(s) = 1/(\lambda_c s + 1)$ as the model is of first order in grid connected mode and a gain, k_{pv} , is used as an outer voltage control loop.

In this application, the choice of IMC rather than a model control is due to the robustness of the IMC when exposed to external disturbances and parameter variations in comparison to more commonly used adaptive model control schemes. Also, the choice of the optimal index switching rule is based on the fact that direct switching based on the

Table 1. System Parameters

Parameter	Value	Parameter	Value	Parameter	Value
R	0.5Ω	<i>J</i>	1Kgm ²	<i>k_{pi}</i>	0.4
L	9.0mH	<i>B</i>	10kgms ⁻²	<i>k_{pV}</i>	100
C	20μF	<i>f</i>	60Hz	<i>ω</i>	377Rad/s
<i>α</i>	2.0	<i>β</i>	10 ⁻²	<i>ξ</i>	1
<i>R_g</i>	1Ω	<i>λ_c</i>	10e ⁻³	<i>R_{Load1}</i>	20Ω
<i>L_g</i>	5mH	<i>λ_v</i>	10e ⁻⁸	<i>R_{Load2}</i>	25Ω
<i>k_{pQ}</i>	5	<i>k_{iQ}</i>	15	<i>L_{Load1,2}</i>	0.5mH

error has very little practical application as it can result in jitters during the switching. The adaptation, in the present application, comes in the identification of the suitable model to appropriately set the controller. The models used in the current application are fixed as the parameter deviations and the disturbances are within a range that can be rectified by the IMC. However, adaptive models can also be applied in more complex applications.

3.3. SWING EQUATION BASED POWER SYNCHRONIZATION CONTROL

The control structure utilized to control power is mostly a simplified version of a synchronverter [26–28], to implement the virtual inertia without using a full detailed model of a synchronous generator. The power-frequency swing equation is solved every control cycle to emulate the inertia which is equivalent to rotor's mechanical inertia in a synchronous generator through the following equations:

$$P^* - P = J\omega_I \left(\frac{d\omega_I}{dt} \right) + B\Delta\omega \quad (11)$$

$$\Delta\omega = \omega_I - \omega_g$$

where, the active power, P , is computed through sensing the inverter output current, $i_{I,abc}$, and the voltage, $v_{o,abc}$, at PCC. J is the emulated inertia and B is the damping factor. The virtual angular frequency, ω_I , is also calculated every control cycle. By minimizing $\Delta\omega$ and considering ω_g as the reference frequency, the frequency at PPC is well-maintained. The underlying equations of this control structure form an enhanced PLL or a sinusoid-locked loop and the synchronization process is innately conserved with the terminal voltage [30].

The basic version of this controller might require a back-up PLL at the start-up to initially synchronize with the grid [31] or during severe ac-system faults. However, for normal operation or during unbalanced grid condition, the synchronization is well-maintained. Similar methodology used in [30] has been applied to derive the transfer function of reactive power versus voltage.

The adopted reactive power control loop, though limited in amount, is required to support the ac system in gridtied mode as its output is added to the voltage reference which alternates in weak ac systems. But, in standalone mode, the voltage magnitude at PCC is adopted as the reference and is directly fed into the voltage control loop in IMC control learning process.

4. SMALL SIGNAL STABILITY ANALYSIS

Small signal dynamic analysis of the proposed control structure has been performed to optimize the parameters and compare them with a conventional cascaded control that does not use the IMC based control. A summary of the parameters used are in Table I. The dynamic response of the proposed controller to the variations of inertia, $0.1 \leq J \leq 100$ (kg/m^2), is depicted in Figure. 6. The frequency response confirms the stability of this system and in comparison to a conventional cascaded architecture, IMC offers a finer stability margin, (phase and gain margins).

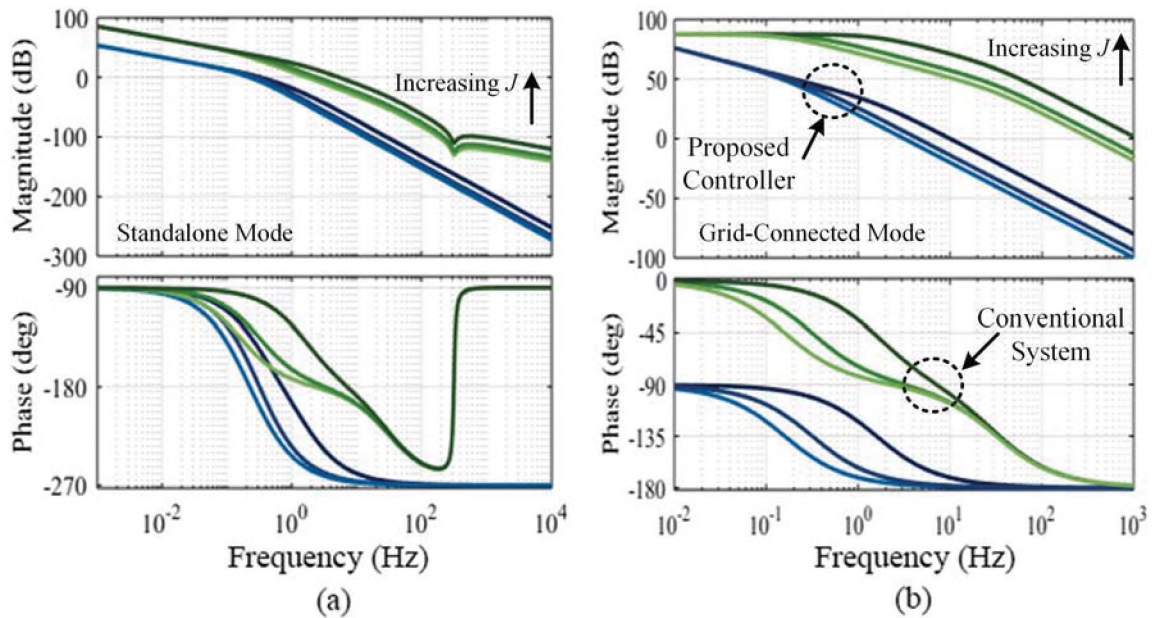


Figure 6. Frequency response to change of inertia (a) Standalone mode (b) Grid-connected mode

Improved bandwidth in both standalone and grid-connected conditions is achieved. Along with it, the variations of λ , ($\lambda_{c,v}$), Figure. 7, illustrate that the choice of λ as IMC filter parameter, should be selected in a way to optimize the performance by keeping the bandwidth of the controller to one-tenth of the switching frequency. This way, gain and phase margins will increase by 8 to 12 degrees on average for both modes of operation. By applying this method, the overall stability margin of the system renders a significant enhanced performance over conventional cascaded control structures.

Another quite important point which should be considered in designing this control architecture is to achieve a balanced speed between the inertial power control loop and the inner IMC loop. Mostly the inertial control structures produce a relative slower response, but the choice of λ , in the IMC controller can rectify this issue by balancing the speed of the cascaded loops of control.

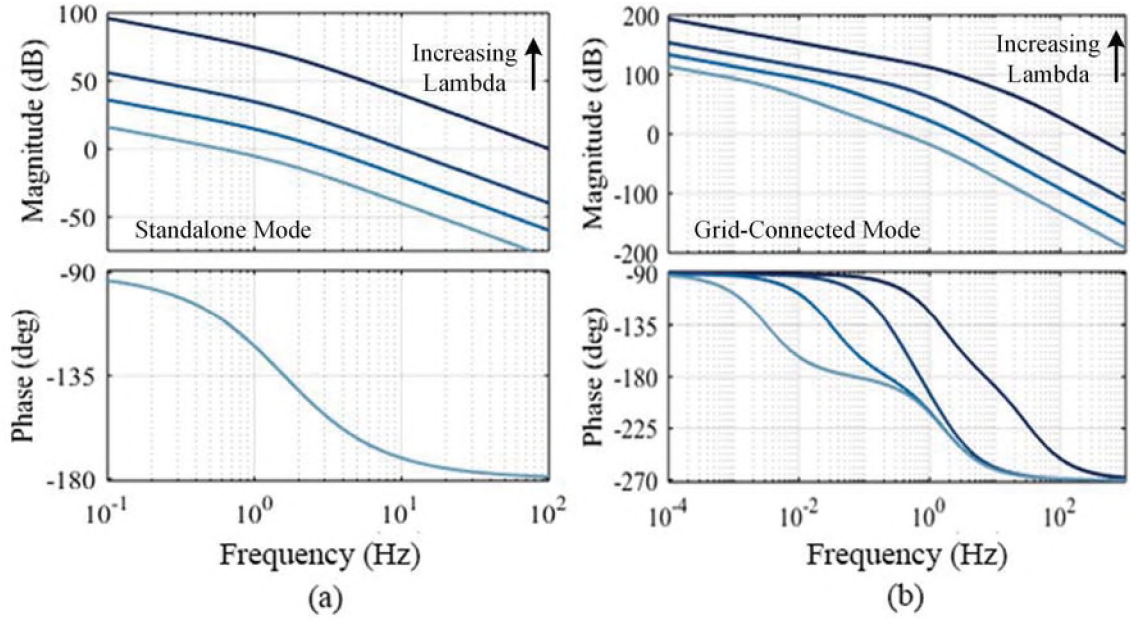


Figure 7. Frequency response to change of λ (a) Standalone mode (b) Grid-connected mode

As mentioned earlier, IMC implementation works best for minimum phase models. However, the implementation in PWM based converters, controller discretization or communication delays in HiL will introduce delays to the system, see Figure. 8. The term $e^{-sT_{samp}}$ will render the system non-casual as the inverse of the model should be incorporated in the controller. Considering this fact, the closed-loop plant models by incorporating the Laplace transform of a time delay of T seconds in one term, $e^{-sT_{samp}}$, for grid-connected and standalone models will be written as:

$$\tilde{G}_{Pv}(s) = \lambda_v s + e^{-sT_{samp}} = 0 \quad (12)$$

$$\tilde{G}_{Pi}(s) = \lambda_c^2 s^2 + 2\lambda_c s + e^{-sT_{samp}} = 0$$

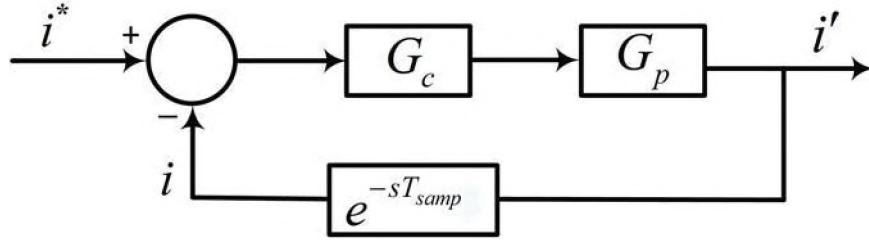


Figure 8. General overview of the system with incorporated delay

Different delay compensation methods have been applied to rectify this problem [37]. Padé approximation of model with time delays is well-known [38]. The exponential transfer function is approximated by a rational transfer function using Padé approximation formulas. In our case, the open-loop transfer functions after using the approximation turns out as:

$$G_{Pv-ol}(s) = \frac{e^{-sT_{samp}}}{\lambda_g s} \approx \frac{1-sT_{samp}}{\lambda_g s} \quad (13)$$

$$G_{Pi-ol}(s) = \frac{e^{-sT_{samp}}}{\lambda_s^2 s^2 + 2\lambda_s s} \approx \frac{1-sT_{samp}}{\lambda_s^2 s^2 + 2\lambda_s s}$$

The numerical solution of the closed-loop transfer functions will result in finding the range of stable poles. For this application, similar method has been applied and the range of λ_c and λ_v applied in both modes of operation have been depicted in Figure. 9.

5. HARDWARE CO-SIMULATION AND RESULTS

Hardware-in-the-loop (HiL) is a testbench environment which is frequently used to emulate different systems to validate the interactive performance of models and physical hardware realistically. This method facilitates emulating large, complex and virtually connected systems. This trend has found its way in several large scale distributed energy systems using distant HiL based simulations to control physical converters [38]. Among all HiL methods, FPGA in the loop technique has become quite popular. Enhanced transient

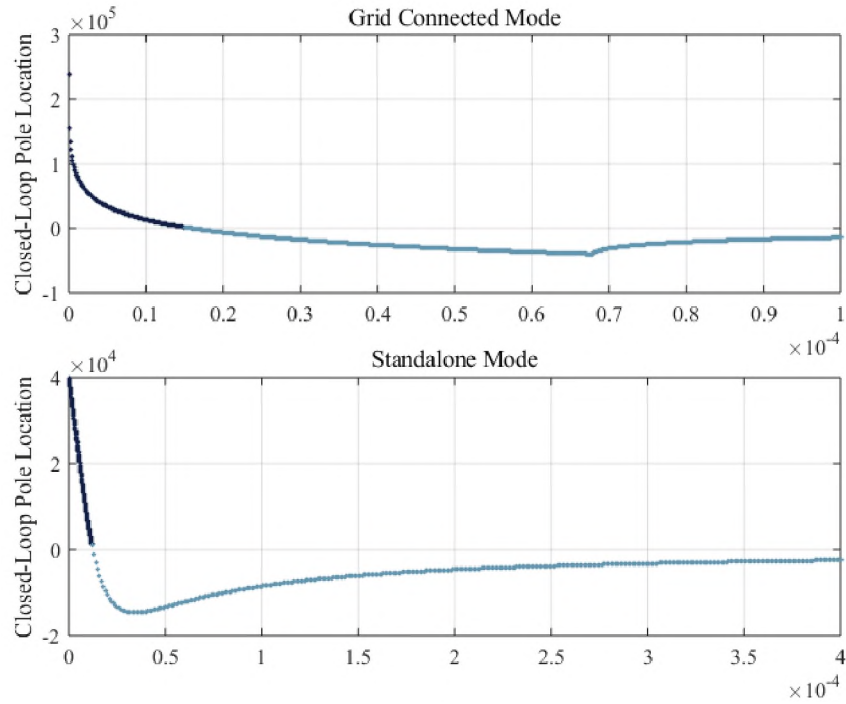


Figure 9. Closed-loop pole placement based on IMC parameter

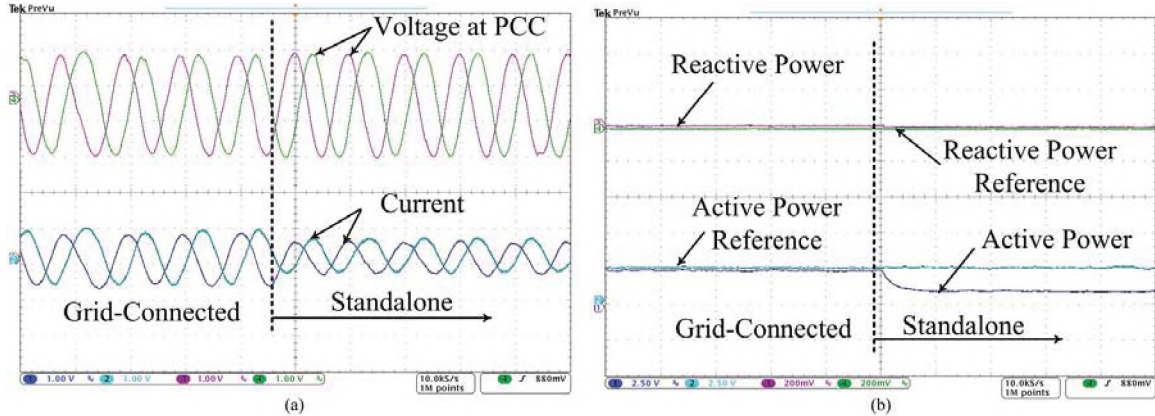


Figure 10. Transition from grid-connected Mode to Standalone - Proposed control Method
 (a) Voltage at PCC and current - One small division for voltage is 26.154 v, One small division for current is 5 A
 (b) Active and reactive power

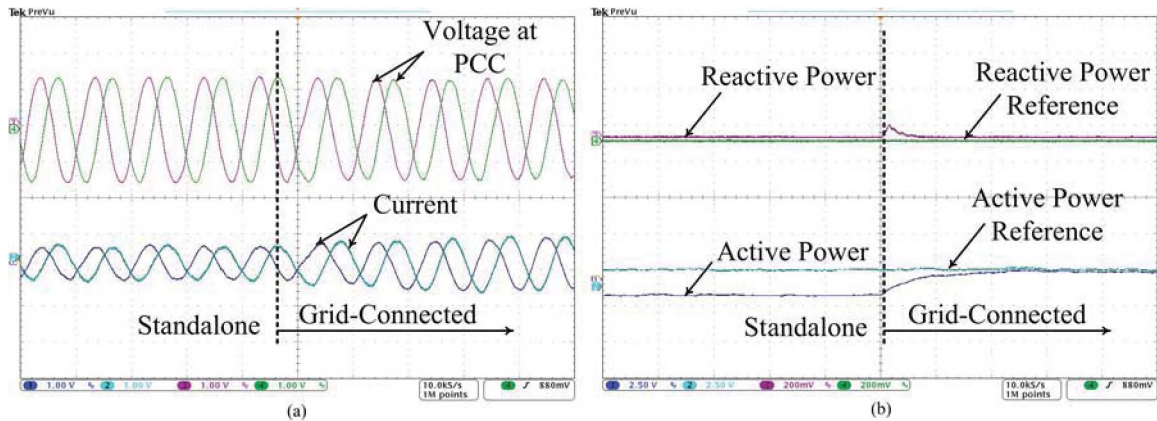


Figure 11. Transition from Standalone Mode to grid-connected - Proposed control Method (a) Voltage at PCC and current - One small division for voltage is 26.154 v, One small division for current is 5 A (b) Active and reactive power

capturing in smaller time steps along with applying hardware pipelining and parallelism reduces the unwanted latencies and delays in the system [39]. In this paper, the schematic block method of Xilinx System Generator in DSP (XSG) with floating number representation and VHDL programming has been applied to implement the control in ZYNQ XC7Z020-CLG484 (Zedboard). The joint test action group, (JTAG) cosimulation interface has been used as it requires minimum resources on FPGA to achieve an optimum hardware consimulation interface. The FPGA clock frequency is chosen to be around 120 MHz at which all modules are found to be compatible with each other. The whole control structure is implemented in System Generator and the switching circuit is realized in PLECS. Logical blocks and VHDL have been used to design the control. Registers have divided the control structure in pipelining stages with minimum latency. The results of the hardware co-simulation are implemented on the board and they have been extracted on the scope by utilizing a DAC module.

5.1. SMOOTH TRANSITION BETWEEN GRIDTIED AND ISLANDED MODES

The first results depicted in Figure. 10 are taken during the transition from grid connected to standalone mode. Phase-a and b of the voltage and current have been extracted during the transition between grid-connected to standalone modes and no discernible fluctuations in the voltage at PCC is observed. In grid-connected mode, reactive power control loop outputs the instantaneous voltage magnitude, when the switching signal occurs, the output of the reactive power loop switches to the fixed reference voltage magnitude and the inner voltage control loop takes care of controlling the voltage at PCC. As the adopted switching ritual observes the changes in the output errors in the corresponding models, the error that minimizes the optimal switching equation, J_{op} , in this case will be $e_1 = \Delta v_o$, so the switching will occur through an optimized scheme which will result in a smooth transition.

Likewise, for the current, the active power loop generates the reference θ which goes through the outer current control loop, k_{pi} . The reverse procedure happens when there is transition from standalone mode to grid-connected and the error that optimizes J_{op} is $e_2 = \Delta i_o$, which directs the control to current control mode, Figure. 11. In addition, Figure. 10(b) and Figure. 11(b), show the control performance of the power control loop. The reactive power command is set to zero and the active power is regulated on the reference value (5kW) in grid-connected mode and it experiences a 2kW of reduction as in standalone mode it just feeds the local load. Similar trend is also observed for power regulation in opposite transition.

5.2. SMOOTH TRANSITION WITH OPTIMIZED SWITCHING RULE

The performance of the applied optimized switching rule is examined by first generating the switching signal through the error between the plant and the model ($J_{op} = e_1$ or $J_{op} = e_2$). Then, the square of the errors with an optimization gain ($J_{op} = \alpha e_1^2$ or

$J_{op} = \alpha e_2^2$) is applied which offers a fast response and instantaneous switching and finally the main switching scheme along with the delay, $J_{op}(t) = \alpha e_j^2(t) + \beta \int_0^t e^{-\lambda(t-\tau)} e_j^2(\tau) d\tau$, is applied to see how the switching scheme affects the performance of the controller during the transitions. In order to see the real effect of switching schemes on the performance, we increased the threshold of the model mismatch with the plant which results in more oscillations around zero error detection and assessed the performance of the switching rule in rectifying the voltage and current fluctuations. The results are summarized in Figure. 12 and the switching happened as there was an islanding event. The transition between grid-connected to standalone mode happens when J_{op} becomes minimum and the error that minimizes it, $e_1 = \Delta v_o$. As it can be seen for the switching adopted as $e_1 = \Delta v_o$, the voltage and current display fluctuations during the transition. It also happens when $e_1 = \Delta v_o^2$, but the optimizing gain rectifies the fluctuations to certain extent. However, incorporating the memory factor, ξ , and the integral in switching scheme has an effect of a low-pass filter that rectifies the unwanted fluctuations and therefore, this switching scheme offers a simultaneous combination of tuning and switching. This feature is more relevant to rectify the delay between the islanding detection and confirmation processes. Applying the optimized cost function reforms the instabilities that occur due to large nondetection zone (NDZ) which is the inherent weakness of passive islanding detection techniques [3].

5.3. EVALUATION THROUGH COMPARISON WITH EXISTING TECHNIQUES

The technique used in the present work lies in the scope of passive islanding detection techniques which basically monitor the system parameters at the point of common coupling. Voltage and frequency variations are the most common parameters that are used to detect the islanding condition. In order to evaluate the performance of the proposed method with other conventional methods, a similar hierarchical control structure is applied by eliminating the internal model control and utilizing an outer power-voltage control loop based on virtual synchronous machine and conventional inner current and voltage control

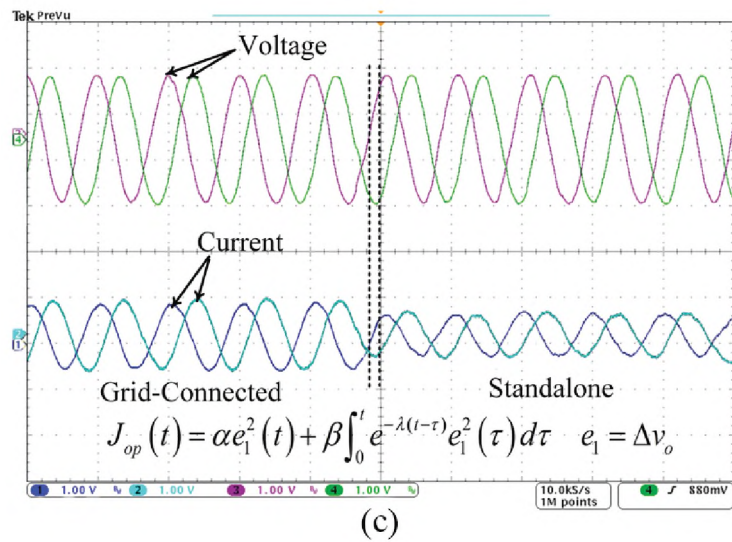
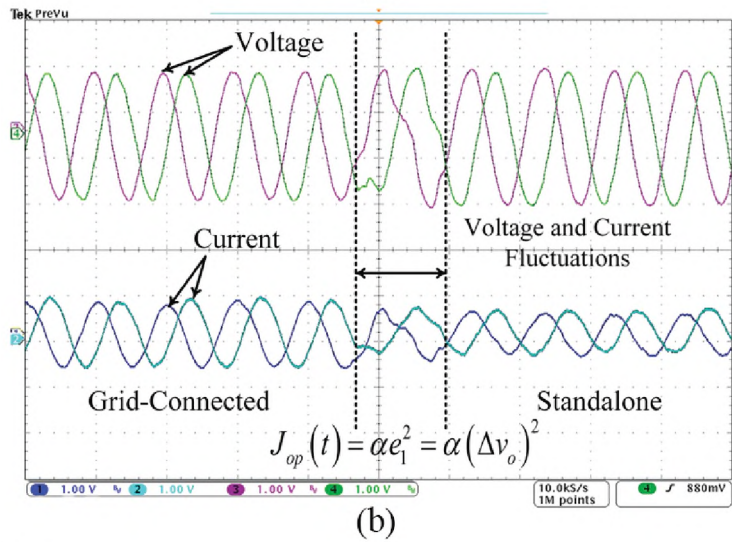
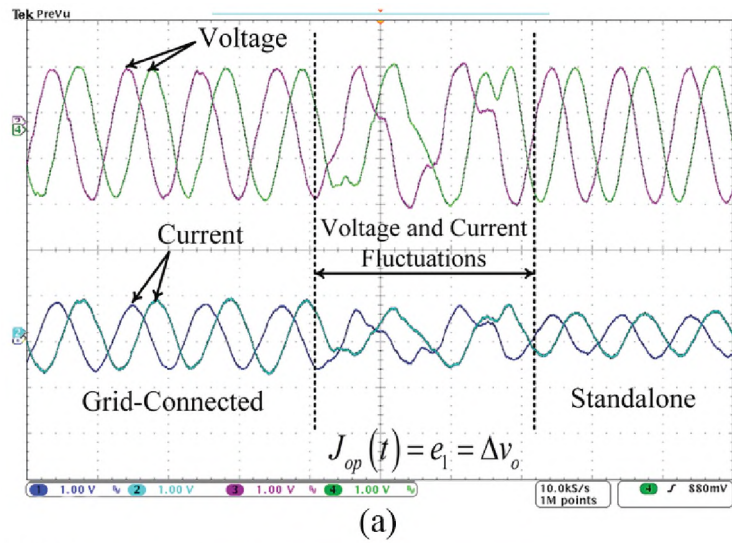


Figure 12. Transition from grid-connected mode to standalone (a) Switching rule is based on the error (b) Switching rule is based on the square of the error (c) Switching rule is based on optimized switching rule

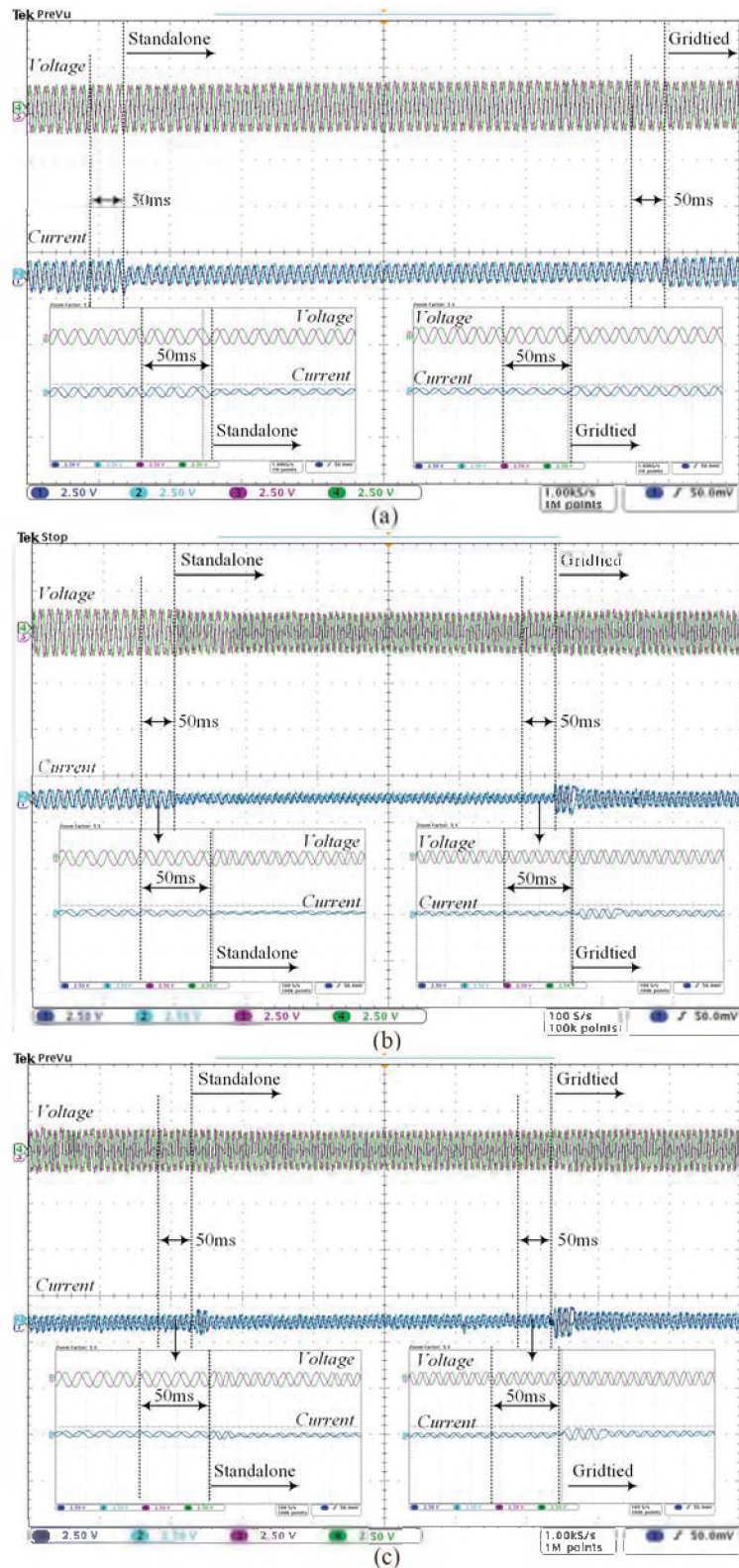


Figure 13. Comparison in back and forth transition between grid-connected and standalone modes of operation - (a) Proposed control method (b) Passive islanding detection based on under/over voltage (c) Passive islanding detection based on under/over frequency - One small division for voltage is 53.30 v, One small division for current is 13.33 A

loops. This control methodology also does not require PLL to detect the phase of the grid voltage. Two conventional passive methodologies, under/over voltage (UVP/OVP) and under/over frequency (UFP/OFP), by observing the frequency deviations through a PLL at PCC, have been separately applied to record the islanding condition. The results of back and forth transition between grid connected and standalone modes of operation due to preplanned islanding and grid-reconnection scenarios by opening and closing the switch S_1 have been depicted in Figures. 13 and Figure. 14.

A rapid PCC voltage/frequency deviation threshold ($\Delta v = 20v$ and $\Delta f = 0.1Hz$) has been applied in $t = 50ms$ to disconnect the grid and similar scenario was applied to connect back. As it can be observed in the results, the voltage and current ride-through capabilities of the proposed control method shows no discernible distortions. Although, for the conventional control structure, the destabilizing effect of the reactive power controller has been limited with a similar technique used in the proposed control structure, distortions can be observed in the voltage and current due to the delay in islanding confirmation ($\cong 20ms$) and phase locking during reconnection to the grid. The power control loop basically takes care of the power flow from the inverter to the grid. However, due to similar reasons, oscillations are also observed in active and reactive power for conventional control loop specially during the transition to reconnect to the grid. The proposed control structure smoothly operates between the two modes of operation and has better ride-through capabilities in comparison to more conventional control structures. The effect of the low-pass filter in the optimized switching rule based on minimizing the cost function results has no NDZ and delay which induces seamless operation during transitions.

5.4. LOAD SWITCHING AND PARAMETER CHANGES

Figure. 15(a) demonstrates a loading transient in standalone mode. As a 1kW load is added, the current increases and the active power injected from the DG unit is adjusted based on the load transition. This phenomenon has no effect on synchronization and

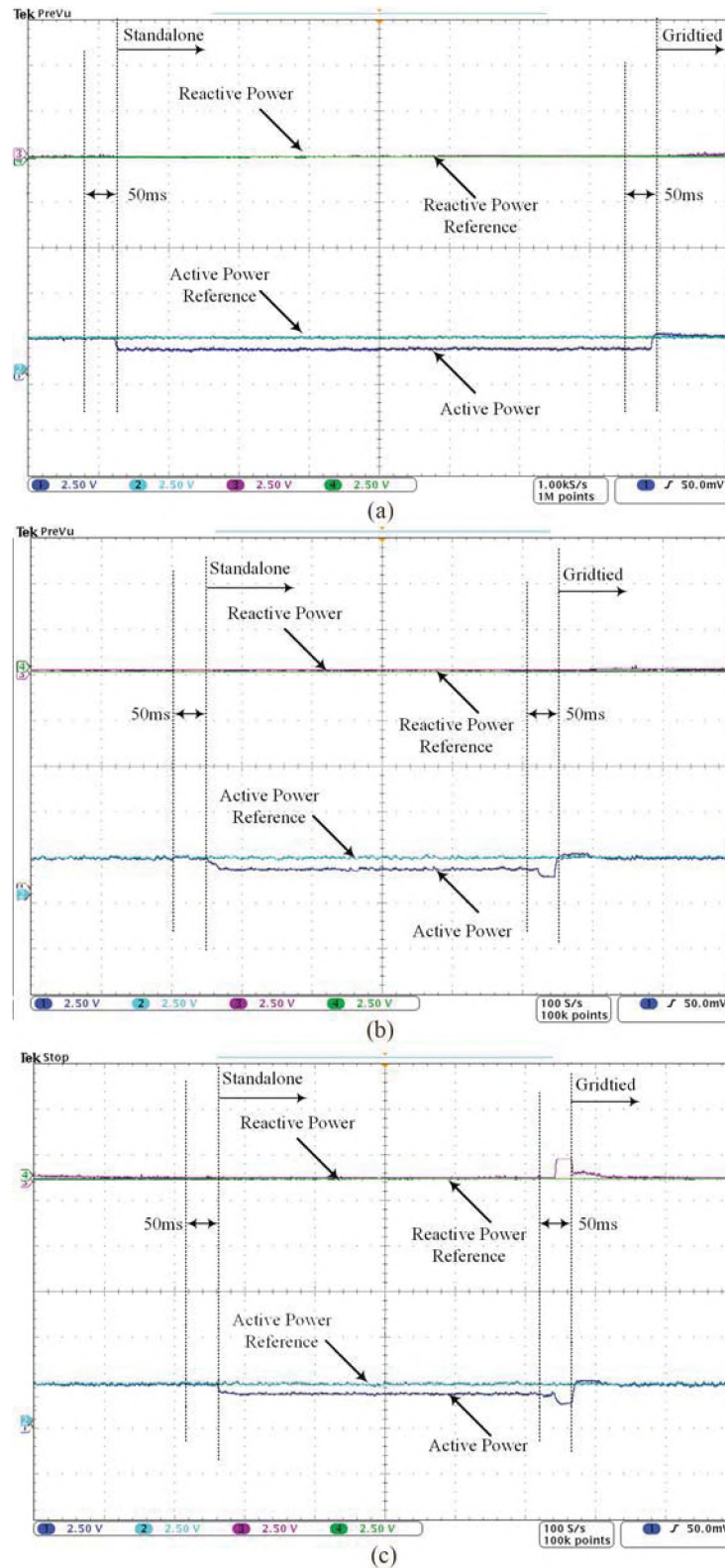


Figure 14. Comparison in back and forth transition - (a) Proposed control method (b) Passive islanding detection based on under/over voltage (c) Passive islanding detection based on under/over frequency - One small division for active power is 1.25 KW and for reactive power is 1.25 KVAR

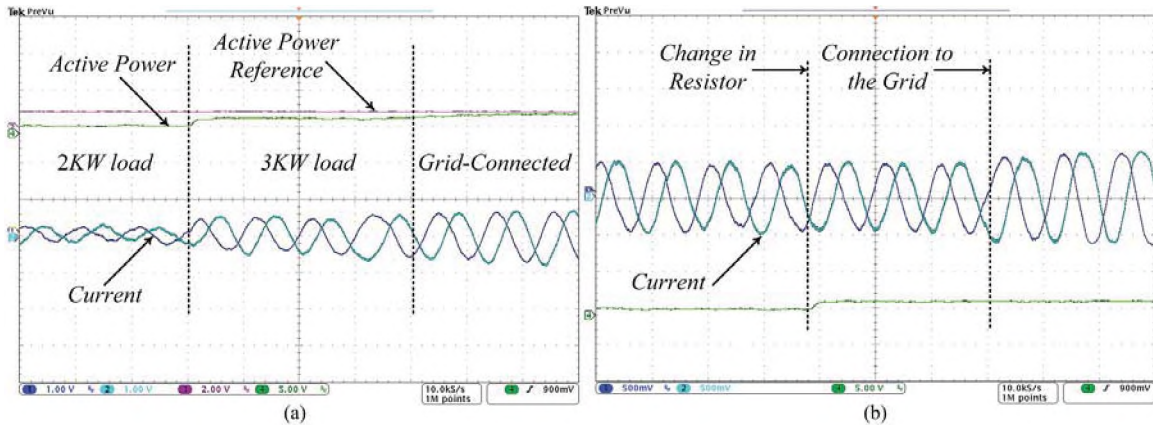


Figure 15. Dynamic response of the system (a) when there is a load switching in standalone mode (b) when there is a parameter change in standalone mode

connection to the grid. The proposed controller acts robustly to reject the sudden loading disturbance yielding no voltage disturbance at PCC while the current and power are adjusted based on the switched load. This event has no effect on the synchronization to the grid. Also, Figure. 15(b) shows the capability of the proposed controller to handle filter parameter changes. In the presence of a step change in a parameter in the standalone mode, there is no discernible change in the current and the voltage at PCC also remains intact. In addition, the changes in the parameter has no effect on re-synchronizing to the grid.

6. CONCLUSION

An adaptive multi internal model based controller for smooth transition between islanded and grid connected modes of operation has been presented in this paper. The proposed control is composed of simple and linear control structures that facilitates flexible operation of a DER. The performance of the proposed controller under load switching conditions and parameter changes proves the robustness of the proposed controller which can robustly deal with the dynamic nature of smart distribution systems.

REFERENCES

- [1] IEEE Standard for Interconnection and Interoperability of Distributed Energy Resources with Associated Electric Power Systems Interfaces," *IEEE Std 1547-2018 (Revision of IEEE Std 1547-2003)* , vol., no., pp.1-138, 6 April 2018.
- [2] T. Basso "IEEE 1547 and 2030 Standards for Distributed Energy Resources Interconnection and Interoperability with the Electricity Grid", *National Renewable Energy Laboratory*, Technical Report, NREL/TP-5D00-63157, December 2014.
- [3] A. Khamisab, H. Shareefa, E. Bizkevelcic and T. Khatiba "A review of islanding detection techniques for renewable distributed generation systems", *Renewable and Sustainable Energy Reviews*, Elsevier, Volume 28, December 2013, Pages 483-493.
- [4] B. Bahrani, H. Karimi, R. Iravani "Nondetection zone assessment of an active islanding detection method and its experimental evaluation", *IEEE Transactions on Power Delivery*, 2011, 26, (2), pp. 517–525.
- [5] S. Lissandron, P. Mattavelli "A controller for the smooth transition from grid-connected to autonomous operation mode", *Energy Conversion Congress and Exposition (ECCE)*, 2014 IEEE, pp. 4298-4305, 2014.
- [6] J. Xiao, P. Wang, and L. Setyawan "Implementation of Multiple-Slack Terminal DC Microgrids for Smooth Transitions Between Grid-Tied and Islanded States", *IEEE Transactions on Smart Grid*, vol. 7, pp. 273-281, 2016.
- [7] G. Liu, T. Caldognetto, P. Mattavelli and P. Magnone, "Power-Based Droop Control in DC Microgrids Enabling Seamless Disconnection From Upstream Grids," *IEEE Transactions on Power Electronics*, vol. 34, no. 3, pp. 2039-2051, March 2019
- [8] Y. Mohamed, H. Zeineldin, M. Salama and R. Seethapathy "Seamless Formation and Robust Control of Distributed Generation Microgrids via Direct Voltage Control and Optimized Dynamic Power Sharing," *IEEE Transactions on Power Electronics*, vol.27, no.3, pp.1283-1294, March 2012.
- [9] I. Serban, C. Marinescu "Control Strategy of Three Phase Battery Energy Storage Systems for Frequency Support in Microgrids and with Uninterrupted Supply of Local Loads," *IEEE Transactions on Power Electronics*, vol.29, no.9, pp. 5010-5020, Sept. 2014.
- [10] J. Stevens, R. Bonn, J. Ginn, S. Gonzalez, and G. Kern, "Development and testing of an approach to anti-islanding in utility-interconnected photovoltaic systems" *Sandia National Laboratories*, Albuquerque, NM, Lab Rep. SAND2000-1939, Aug. 2000.
- [11] H. Kim, T. Yu, S. Choi "Indirect current control algorithm for utility interactive inverters in distributed generation systems", *IEEE Transactions on Power Electronics*, 23, (3), pp. 1342–1347, 2008.

- [12] Sh. Shah, H. Sun, D. Nikovski and J. Zhang "VSC-Based Active Synchronizer for Generators", *IEEE Transactions on Energy Conversion*, vol. 33, no. 1, pp. 116-125, 2018.
- [13] J. M. Guerrero, J. C. Vasquez, J. Matas, L. G. de Vicuña, and M. Castilla, "Hierarchical control of droop-controlled AC and DC microgrids—A general approach toward standardization," *IEEE Transactions on Industrial Electronics*, vol. 58, no. 1, pp. 158–172, Jan. 2011.
- [14] F. Gao and M. R. Iravani, "A Control Strategy for a Distributed Generation Unit in Grid-connected and Autonomous Modes of Operation," *IEEE Transactions on Power Delivery*, vol. 23, pp. 850-859, Apr. 2008.
- [15] Y.R. Mohamed and A.A. Radwan "Hierarchical control system for robust microgrid operation and seamless mode transfer in active distribution systems", *IEEE Transactions on Smart Grid*, 2, (2), pp. 352–362, 2011.
- [16] P. Rodriguez, C. Citro, I. Candela, J. Rocabet, A. Luna, "Flexible grid connection and islanding of SPC-based PV power converters", *Energy Conversion Congress and Exposition (ECCE)*, pp. 450-459, 2015.
- [17] A. Kahrobaeian, Y.A.-R.I. Mohamed "Interactive distributed generation interface for flexible micro-grid operation in smart distribution systems", *IEEE Transactions on Sustainable Energy*, 3, (2), pp. 295–305, 2012.
- [18] S.-K. Chung "A Phase Tracking System for Three Phase Utility Interface Inverters", *IEEE Transactions on Power Electronics*, vol. 15, no. 3, pp. 431-438, May 2000.
- [19] D. Dong, B. Wen, D. Boroyevich, P. Mattavelli and Y. Xue: "Analysis of Phase-Locked Loop Low-Frequency Stability in ThreePhase Grid-Connected Power Converters Considering Impedance Interactions", *IEEE Transactions on Industrial Electronics*, vol. 62, no. 1, pp. 310-321, Jan. 2015.
- [20] K.S. Narendra, J. Balakrishnan and M.K. Ciliz: "Adaptation and learning using multiple models, switching, and tuning", *IEEE Control System Magazine*, June 1995.
- [21] K. S. Narendra and J. Balakrishnan, "Adaptive control using multiple models," in *IEEE Transactions on Automatic Control*, vol. 42, no. 2, pp. 171-187, Feb. 1997.
- [22] M. Yazdani and A. Mehrizi-Sani "Internal model-based current control of the RL filter-based voltage-sourced converter", *IEEE Transactions on Energy Conversion*, vol. 29, no. 4, pp. 873–881, Dec. 2014.
- [23] S. Yazdani and M. Ferdowsi: "Voltage Sensorless Control of a Three-Phase Standalone Inverter Based on Internal Model Control", *IEEE Energy Conversion Congress and Exposition - (ECCE)*, 1478-1482, 2018.

- [24] S. Yazdani and M. Ferdowsi "Co-simulation of Voltage Sensorless Current Control Based on Internal Model Principle", *IEEE Energy Conversion Congress and Exposition (ECCE-2018)*, 1488-1491, 2018.
- [25] L.D. Zhang, L. Harnefors, and H.P. Nee "Power-synchronization control of grid-connected voltage-source converters", *IEEE Transactions on Power Systems*, 25, (2), pp. 809–820, 2010.
- [26] K. Sakimoto, Y. Miura, T. Ise "Stabilization of a power system with a distributed generator by a Virtual Synchronous Generator function", *Proceedings of the 8th International Conference on Power Electronics (ECCE Asia)*, Jeju, Korea, pp. 1498–1505, 30 May– 3 June 2011.
- [27] A. Ghoshal, V. John "Active damping of LCL filter at low switching to resonance frequency ratio", *IET Power Electronics*, 8, (4), pp. 574–582 5, 2015.
- [28] P.S.C. Heuberger, P.M.J. van den Hof, C. Scherer "Model-Based Control: Bridging Rigorous Theory and Advanced Technology", *Springer*, August 5, 2009
- [29] Q.C.Zhong, G. Weiss: "Synchronverters: inverters that mimic synchronous generators", *IEEE Transactions on Industrial Electronics.*, 58, (4), pp. 1259–1267, 2011.
- [30] L.D. Zhang, L. Harnefors and H.P. Nee: "Power-synchronization control of grid-connected voltage-source converters", *IEEE Transactions on Power Systems*, 25, (2), pp. 809–820, 2010.
- [31] Q.-C. Zhong, P.-L. Nguyen, Z. Ma, and W. Sheng, "Self-synchronised synchronverters: Inverters without a dedicated synchronisation unit," *IEEE Transactions on Power Electronics*, vol. 29, no. 2, pp. 617–630, Feb. 2014.
- [32] T. Kobaku, S. C. Patwardhan, and V. Agarwal, "Experimental evaluation of internal model control scheme on a dc-dc boost converter exhibiting nonminimum phase behavior," *IEEE Transactions on Power Electronics*, vol. 32, no. 11, pp. 8880–8891, Nov. 2017.
- [33] S. Saxsena, Y.V. Hote: "Load frequency control in power system via internal model control scheme and model order reduction", *IEEE Transactions on Power Systems*, 28, (3), pp. 2749–2757, 2013.
- [34] S. Leitner, M. Yazdani, S. Ziaei, A. Mehrizi-Sani and A. Muetze, "Internal model based active resonance damping current control of a grid connected voltage sourced converter with an LCL filter," *IEEE Transactions on Power Electronics*, vol. PP, pp. 1-1, 2018.
- [35] J. BoSkoviC and R. Mehra, "Stable Multiple Model Adaptive Flight Control for Accomodation of a Large Class of Control Effector Failures", *Proceedings of the 18th American Control Conference*, pp.1920-1924. 1999.

- [36] G. Lauss, F. Lehfuss, A. Viehweider, and T. Strasser, "Power hardware in the loop simulation with feedback current filtering for electric systems," *Proceedings of 37th Annual Conference IEEE Industrial Electronics Society*, Melbourne, VIC, Australia, pp. 3725–3730, Nov. 2011.
- [37] G. H. Golub, and C. F. Van Loan, *Matrix Computations*, Johns Hopkins University Press, Baltimore, 1989, pp. 557-558
- [38] B. Palmintier, B. Lundstrom, S. Chakraborty, T. Williams, K. Schneider, and D. Chassin, "A power hardware-in-the-loop platform with remote distribution circuit cosimulation", *IEEE Transactions on Industrial Electronics*, vol. 62, no. 4, pp. 2236–2245, Apr. 2015.
- [39] O. Lucia, O. Barragan, L.A. Urriza, I. Burdio, J.M. Navaro "Real-time FPGA-based Hardware-in-the-Loop development testbench for multiple output power converters", *Annual IEEE Applied Power Electronics Conference and Exposition (APEC)*, pp. 309-314, 2010.

II. ADVANCED CURRENT-LIMITING AND POWER-SHARING CONTROL IN A PV-BASED GRID-FORMING INVERTER UNDER UNBALANCED GRID CONDITIONS

ABSTRACT

Grid-forming inverter technology is a novel and evolving concept for systems with high penetration of renewables. The integration of these grid-independent units with the existing conventional generators and gradually replacing them should contribute to stabilizing the power grid. Several control strategies are proposed in order to design grid-forming inverters to emulate the kinetic energy and the self-synchronization features of synchronous machines with robust control on voltage and frequency to deal with the dynamic issues of the grid. In this paper, a PV-based grid-forming inverter with a modified virtual synchronous machine control in parallel with a battery supported inverter with an enhanced droop control has been considered to operate under non-ideal grid voltage conditions and in the isolated mode of operation. The control methodology encloses a photovoltaic synchronous generator along with nonlinear feedback linearization current-limiting control with voltage ride through capabilities that enable the grid-forming PV-inverter and the grid-following battery inverter to seamlessly provide active and reactive power to the load in unbalanced grid conditions. A hardware co-simulation environment in Simulink using the software tool of Piecewise Linear Electrical Circuit Simulation (PLECS) and System Generator from Xilinx has been applied to evaluate the operation of the controller and verify its flexibility and effectiveness in different case studies.

1. INTRODUCTION

The growing tendency toward utilizing a more decentralized electric grid and new types of distributed resources further increases the demand on a variety of technologies and establishing new criteria and requirements for interconnecting DERs to electrical power systems. An increasing number of DER interconnections changes the distribution system interaction with the bulk power system. It also transforms the distribution system into an active source of energy. Consequently, enhanced state-of-the-art capabilities for active power control and reliability services have been reflected in proposed changes in IEEE 1547-2018 Standard for Interconnecting Distributed Resources with Electric Power Systems. In the context of the standard, DER is regarded as a source of electric power that is not directly connected to a bulk power system [1] and more stringent grid support functions such as active voltage regulations, abnormal voltage/frequency ride through, and frequency response capabilities are expected from new generations of energy resources.

Taking the aforesaid into consideration, in recent years, the concept of grid-forming inverter-based resources has proactively attracted the attention of the research community [2–5]. A grid-forming unit can operate independent of grid strength and can autonomously interconnect to a power system. This unit should function as a voltage source and is required to precisely control its output voltage amplitude and frequency to improve the performance of the inverter-based generation. The grid-forming technology can be a viable solution to realize the replacement of the conventional generators with renewable resources [6]. In order to achieve this goal, rigorous operation standards for power system reliability have been devised for inverter-based renewable generation [7]. Basically, the control strategy for electronically coupled DER units is classified into non-interactive and grid-interactive approaches [8]. In the latter, the power control of the grid-following inverter is used in order to control the output power within the microgrid limits.

Grid-forming PV systems are expected to operate as a photovoltaic synchronous generator (PVSG) to inject virtual inertia to the system based on a synchronous generator mechanical properties and as an uninterruptable power supply, PVSG units must have black start capabilities and they should operate in both grid-tied and isolated modes of operation. Different control methodologies have already been proposed to reach these objectives, among which, synchronverters have been highlighted as they successfully propose a control methodology that can emulate a synchronous machine [9]. However, the non-linearities in calculating the active power and the reactive power, and the coupling between the frequency and the field-excitation current loops may result in instabilities in voltage and frequency. By incorporating the nonlinear analysis of the system, the global stability of the system and current limiting capability can be achieved [10, 11].

Furthermore, a performance comparison of grid-following and grid-forming PV sources in providing frequency support in an islanded power system shows that the droop controlled grid-forming inverter has superior frequency control over grid-following inverters with current control [12, 13]. Controlling PV-based VSCs to emulate synchronous generators (which result in PLL elimination due to the existence of damping power providing self-synchronization ability) is also discussed in [14]. In [15], a synchronous machine rotor is emulated by proper dc-link voltage regulation and the dc-link capacitor performs as a virtual rotor. A decentralized control strategy in a grid-forming inverter for overload mitigation, which can autonomously transfer the extra load of the overloaded source to other power suppliers, has been reported in [15]. This control strategy maintains the voltage control of the grid-forming inverter in load transients. However, these control methodologies have not verified the operation of the grid-forming inverter while interacting with other conventional converters as dependent following units.

In a broader view, a generalized eigenvalue perturbation technique for coherency identification has been applied to analyze the performance of large-scale networks of grid-forming droop-controlled inverters in [16]. The multiple-loop voltage regulation incorporat-

ing virtual impedance is able to maintain the plug-and-play capability and innate resiliency of grid-forming droop control. Also, a new decentralized control strategy for multiple three-phase paralleled grid-forming distributed generation units in an islanded microgrid has been proposed by using the filtered tracking error method in [18]. The proposed controller can achieve superior PCC voltage regulation and proportional load power-sharing performance in comparison to droop-based hierarchical control methods. However, this method does not entirely meet the prerequisites of grid-forming inverters as it does not have sufficient provisions for frequency control.

A few reports are available on the operation of grid-forming inverters during unbalanced grid conditions. A dynamic protection integrated model predictive control using a generalized state-space representation of a grid-connected modular multilevel converter is proposed in [18], which enables to reconstruct an ac-grid after a blackout by utilizing a VSC-HVDC system. The method in [18] restores a balanced voltage system under unbalanced grid conditions. However, the operation of this mechanism does not offer a viable solution for grid-following inverters as the cross-coupling of grid-following inverters as dependent units to grid-forming units have not been addressed. Applying conventional current control techniques in grid-following units or treating them as voltage-source converters alters the dynamic model of the network. Consequently, the addition of any dependent constituent varies the prerequisites to maintain the voltage and PCC frequency. More recently, the operation of grid-forming inverters during fault conditions without using PLL has been addressed in the literature. A dynamic virtual damping controller gives the fault ride-through capability to the grid-forming inverter by modifying the outer power reference [19]. In another approach, a PV-based grid-connected converter is controlled through generating an arbitrary phase angle, and a resonant controller gives it a fault ride-through capability [20]. Nevertheless, the interaction of all the proposed methods have been verified in passive grid conditions so far. Besides, the interconnection of grid-following converters—as dependent constituents in active grid environment—has not been addressed. By increasing the en-

trance of DERs into the generation network, the current grid codes are being modified in a way that it will mandate the converter-based generators to have the ability to stay connected and supportive amid transient grid faults and have fault ride-through (FRT) or low-voltage-ride-through (LVRT) capabilities in their control package. Several studies have proposed different control methodologies to enable the voltage-source converters to withstand the grid faults and unbalanced grid conditions. A detailed small-signal modeling analysis, along with a balanced positive/negative sequence control, has been proposed in [21], which mostly just considers the quality of the injected current. Some other studies suggest auxiliary voltage controllers—which can solely be implemented in different control structures to meet the FRT and LVRT requirements [22, 23].

In this paper, a PVSG structure has been proposed as a grid-forming inverter. The voltage-source converter's active power is regulated and stabilized by a loop-shaping approach to the power control loop, which emulates a virtual synchronous machine [24] and provides inertial response to frequency deviations and sets grid voltage and frequency while feeding the load with active and reactive power. The interaction of the grid-forming inverter with a conventional converter is studied by adding a parallel grid-following inverter. In order to investigate the power-sharing capabilities of this system, the grid-following inverter uses a droop control. In this way, a decentralized control mechanism with power-sharing capabilities is achieved in an active grid condition. For fortifying the system to operate during grid voltage unbalanced condition, the outer power control loop is augmented by an auxiliary proportional resonant control tuned to the negative sequence frequency, i.e., double value of the supplied frequency, and the inner current control loop dynamics are eliminated by feedback linearization technique. The proposed PVSG control loop structure

- Emulates a virtual synchronous machine and regulates voltage magnitude and frequency through the grid-forming inverter;
- Possesses power-sharing capabilities by controlling the active and reactive power;

- Operates autonomously in the isolated mode through the grid-forming inverter; and
- Is capable of withstanding grid unbalanced and faulty conditions.

These features are enhanced by the virtual inductance method to ensure the direct controllability of active power and reactive power with the phase angle and the voltage, respectively [25]. Then, they offer the seamless operation of the control scheme in unbalanced grid conditions, in addition to loading and islanding transients.

The remainder of the paper is organized as follows. In section 2., the system configuration is presented. Section 3. describes the control structure in detail. A thorough stability analysis is explained in Section 4. and Section 5., including the information on the hardware co-simulation method and real-time assessments of the control design through demonstrating hardware-in-the-loop (HIL) results. The last section includes the final discussions and concludes this paper's outcomes.

2. SYSTEM CONFIGURATION

The system in Figure. 1 represents a general scheme of the parallel structure of a PV-based grid-forming and a battery-based grid-following inverter as the dc-bus is considered as ideal. This generalized overview of a voltage distribution system can host different types of loads and distributed generators connected to the main feeder. The grid-forming unit can operate in either grid-connected or isolated mode, but the grid-following unit operation is dependent on its connection to the grid-forming inverter as it is not able to work in the isolated mode. Then, the operation of each of the units is studied in different modes of operation. The state-space representation of converters interface dynamics in the natural reference frame is given by the following equations for both grid-forming (GF) and grid-following (GL) inverters.

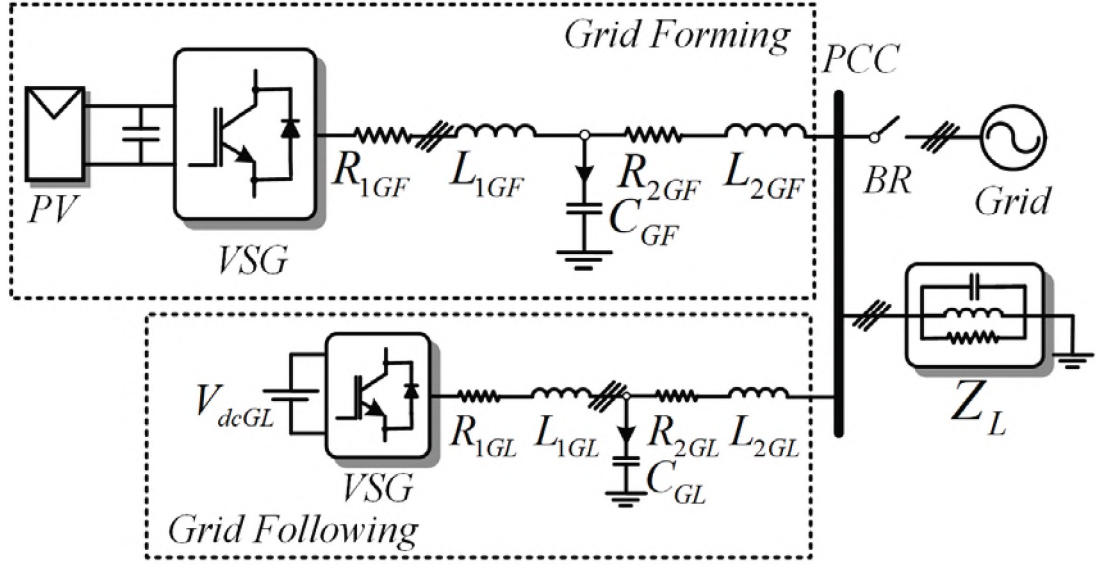


Figure 1. General overview of the system under study

$$v_{GF,abc} = L_{GF} \frac{di_{GF,abc}}{dt} + v_{o,abc},$$

$$v_{GL,abc} = L_{GL} \frac{di_{GL,abc}}{dt} + v_{o,abc}, \quad (1)$$

$$i_{L,abc} = i_{GL} + i_{GF} - i_{C_{eq}}.$$

As the parameters are depicted in Figure. 2, C_{eq} and L_{GF} and L_{GL} are filter capacitance and reactance for both grid-forming and grid-following units and v_{PCC} is the PCC voltage while i_{GF} is the output current of grid-forming and i_{GL} is the output current of grid-following inverter. In order to further simplify the system equations, the dynamic equations are

$$v_{GF,\alpha\beta} = v_{o_{GF,\alpha\beta}} + L_{GF} \frac{di_{GF,\alpha\beta}}{dt} + R_{GF} i_{GF,\alpha\beta},$$

$$v_{GL,\alpha\beta} = v_{o_{GL,\alpha\beta}} + L_{GL} \frac{di_{GL,\alpha\beta}}{dt} + R_{GL} i_{GL,\alpha\beta}, \quad (2)$$

$$i_{L,\alpha\beta} = i_{GL} + i_{GF}.$$

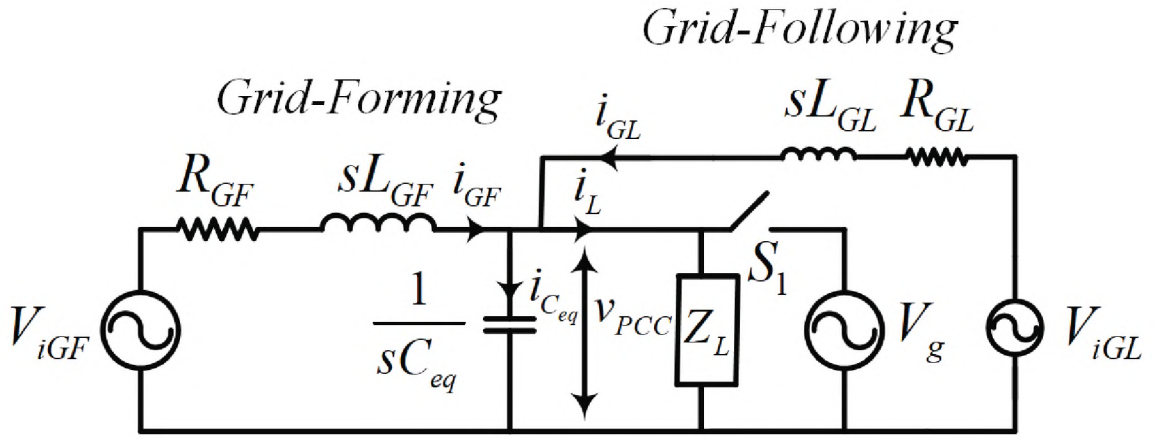


Figure 2. Simplified diagram of the system under study

The third equation is calculated by considering that the capacitance is negligible. To apply the power synchronization control method to both of the inverters, the same procedure in [18] has been applied and the linearized dynamic relation of the active power and the load angle will be

$$\frac{\Delta P_{GF/GL}}{\Delta \theta} = \frac{a_0 s^2 + a_1 s + a_2}{(sL_{GF/GL} + R_{GF/GL})^2 + (\omega L_{GF/GL})^2} \quad (3)$$

where GF and GL stand for Grid-Forming or Grid-Following, respectively, and

$$\begin{aligned} a_0 &= \frac{L_{GF/GL}}{\omega} \left(v_{GL/GF} v_{PCC} \cos \theta_0 - v_{PCC}^2 \right), \\ a_1 &= \frac{R_{GF/GL}}{\omega} \left(v_{GL/GF} v_{PCC} \cos \theta_0 - v_{PCC}^2 \right), \\ a_2 &= v_{GL/GF} v_{PCC} \left(\omega L_{GF/GL} \cos \theta_0 - R_{GF/GL} \sin \theta_0 \right). \end{aligned} \quad (4)$$

Moreover, similar to coupling of the reactive power with the phase angle, the equation will be

$$\frac{\Delta Q_{GF/GL}}{\Delta v_{GF/GL}} = \frac{b_0 s^2 + b_1 s + b_2}{(sL_{GF/GL} + R_{GF/GL})^2 + (\omega L_{GF/GL})^2}, \quad (5)$$

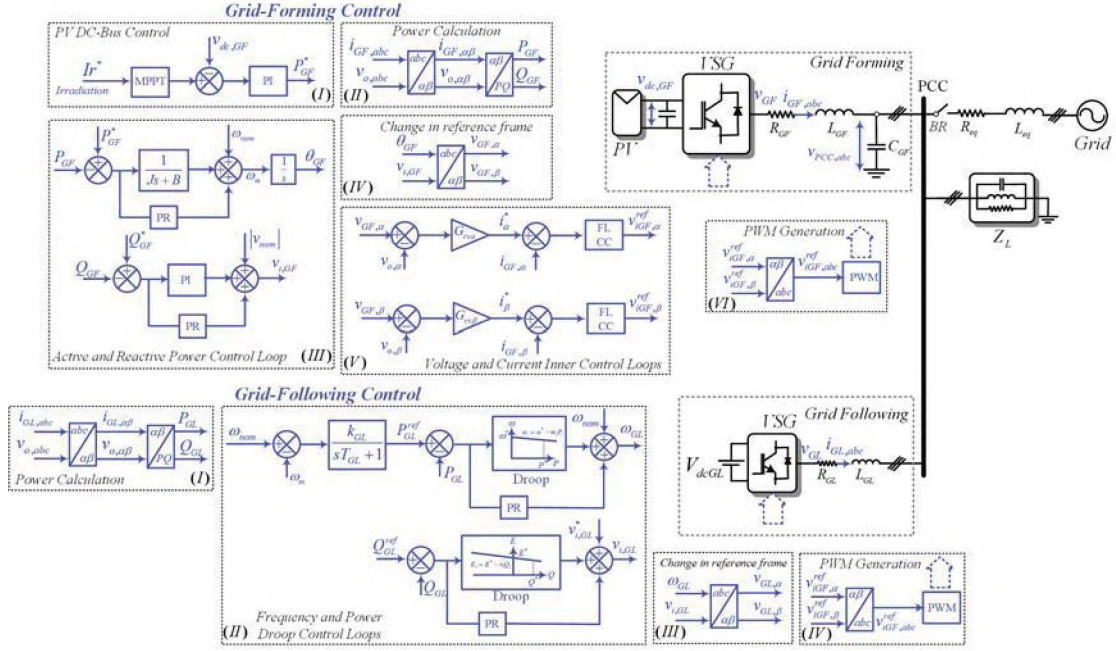


Figure 3. General overview of the control structure of the system under study

where

$$\begin{aligned}
 b_0 &= \frac{L_{GF/GL}}{\omega} (v_{GL/GL} - v_{PCC} \cos \theta_0), \\
 b_1 &= \frac{R_{GF/GL}}{\omega} (v_{GL/GL} - v_{PCC} \cos \theta_0), \\
 b_2 &= \omega L_{GF/GL} (2v_{GL/GL} - v_{PCC} \cos \theta_0) \\
 &\quad - R_{GF/GL} v_{PCC} \sin \theta_0.
 \end{aligned} \tag{6}$$

Consequently, the plant models of each one of the converters are derived, and by utilizing the linearized plant models, the control architecture is designed with a PVSG structure for the grid-forming inverter and a power droop control scheme is being used for the grid-following inverter. The details of the control structure design are described more in detail in the next section.

3. CONTROL STRUCTURE

A fixed hierarchical control structure, including power, voltage, and current control loops in both grid-connected and isolated modes, which are used in the grid-forming converter has been demonstrated in Figure. 3. However, the grid-following inverter operates as it is always connected to the grid since it consistently follows the grid-forming inverter. Today, the distributed renewable energy resources must tackle several challenges as they are becoming more populated in energy generation network [19]. The first challenge that such a system faces is the intermittent nature of PV daily output power. Next is the frequency stability issue that has risen from fluctuations of the net load due to DER variability, decoupling from grid frequency due to PLL dynamics, and lack of rotational inertia. Another issue is to sustain the operation of the grid-forming inverters and its dependent followers in unbalanced grid conditions—which is mainly the subject of the present work. A single grid-forming PV-based unit equipped with a primary grid-following reserve has been proposed. Also, each of the above challenges has been addressed in the control structure, considering the point that the proposed system must seamlessly operate during unbalanced grid conditions. Each control step is described in the following subsections.

3.1. OUTER POWER CONTROL LOOP

A photovoltaic synchronous generator has been designed as the grid-forming inverter. A lookup-table-based MPPT has been utilized, [20], and the irradiation, as a time-varying quantity, is the input to the control system. By utilizing curve fitting methods for the characteristics of the PV curves, the reference dc bus voltage is calculated. Figure. 3 shows the entire process (Grid-Forming Control *I*, *II* and *III*). As reactive power-sharing is

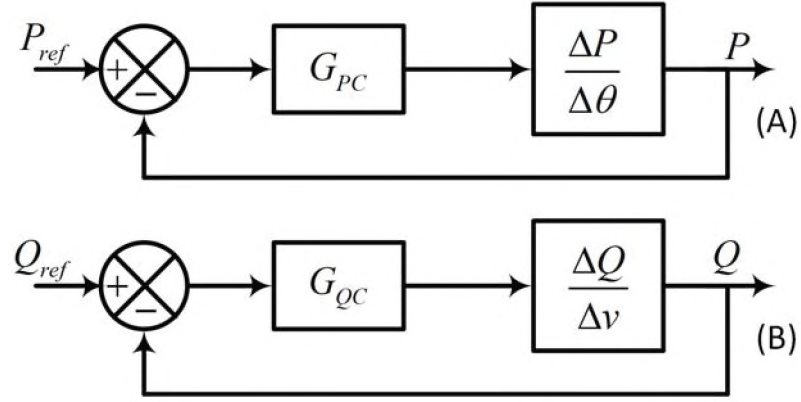


Figure 4. Active and reactive power control block diagram using power-synchronization method

beyond the scope of this paper, the reference reactive power is considered as zero. Actual values of active and reactive power are determined by measuring current and PCC voltage and the reference phase angle of the inverter, ω_m , is regulated as

$$P_{GF}^* - P_{GF} = J\omega_m \left(\frac{d\omega_m}{dt} \right) + D\Delta\omega, \quad (7)$$

$$\Delta\omega = \omega_m - \omega_{nom},$$

where J is the moment of inertia and B is the damping factor. Along with it, the dc-bus in the grid-following inverter is considered as an ideal voltage source and the reference power is obtained through the regulation of the frequency by adopting a simplified governor control model see Figure. 4 (Grid-Following Control *I*, *II* and *III*). Power is controlled through a conventional droop control strategy for inverters with inductive grid impedance which takes the form

$$v_{GL} = v_{GL}^* - n_{FL}\Delta Q_{GL}, \quad \Delta Q_{GL} = Q_{GL}^* - Q_{GL}, \quad (8)$$

$$\omega_m = \omega_{nom} - m_{FL}\Delta P_{GL}, \quad \Delta P_{GL} = P_{GL}^* - P_{GL}.$$

The first equation is the coupling between the reactive power ΔQ_{GL} with the voltage, $v_{GL} - v_{GL}^*$. The second equation is the coupling of the frequency $\omega_m - \omega_{nom}$ and the active power ΔP_{GL} . m_{FL} and n_{FL} are the droop coefficients. As the frequency is being regulated by the swing equation, (7), in the grid-forming inverter, the system does not require PLL to detect the PCC frequency and it is directly fed to the grid-following converter controller loop from the frequency which is set by PVSG. As it is depicted in Figure. 3, by utilizing the transfer functions we obtained in (3) and (5) and using (7) as $G_{PC,GF} = \frac{1}{Js+B}$ as the active power compensator and $G_{QC,GF} = k_{p,GF} + \frac{k_{i,GF}}{s}$, and the reactive power compensator in grid-forming inverter the close-loop transfer functions for the power control loop in the grid-forming inverter turn out to be

$$\frac{P_{GF}}{P_{GF}^*} = \left(\frac{1}{A_0} \right) \frac{a_0 s^2 + a_1 s + a_2}{s^3 + A_1 s^2 + A_2 s + A_3}, \quad (9)$$

where

$$\begin{aligned} A_0 &= JL_{GF}^2, \\ A_1 &= \left(2JR_{GF}L_{GF} + B_{GF}L_{GF}^2 + a_0 \right) / \left(JL_{GF}^2 \right), \\ A_2 &= \left(J \left(R_{GF}^2 + \omega_{GF}^2 L_{GF}^2 \right) + 2R_{GF}L_{GF}B + a_1 \right) / \left(JL_{GF}^2 \right), \\ A_3 &= \left(\left(R_{GF}^2 + \omega_{GF}^2 L_{GF}^2 \right) B + a_2 \right) / \left(JL_{GF}^2 \right). \end{aligned} \quad (10)$$

Similarly, for the reactive power control loop, the close loop transfer function will be

$$\frac{Q_{GF}}{Q_{GF}^*} = \left(\frac{1}{B_0} \right) \frac{b_0' s^3 + b_1' s^2 + b_2' s + b_3'}{s^3 + B_1 s^2 + B_2 s + B_3}, \quad (11)$$

where

$$\begin{aligned} b_0' &= k_{pGF} b_0, \\ b_1' &= k_{pGF} b_1 + k_{iGF} b_0, \\ b_2' &= k_{pGF} b_2 + k_{iGF} b_1, \\ b_3' &= k_{iGF} b_2, \end{aligned} \quad (12)$$

$$\begin{aligned}
B_0 &= L_{GF}^2 + k_{pGF}b_0, \\
B_1 &= (2R_{GF}L_{GF} + k_{pGF}b_1 + k_{iGF}b_0) / (L_{GF}^2 + k_{pGF}b_0), \\
B_2 &= (R_{GF}^2 + \omega_{GF}^2 L_{GF}^2 + k_{pGF}b_2 + k_{iGF}b_1) / (L_{GF}^2 + k_{pGF}b_0), \\
B_3 &= (k_{iGF}b_2) / (L_{GF}^2 + k_{pGF}b_0).
\end{aligned} \tag{13}$$

Likewise, by utilizing the transfer functions in (3) and (5), and by choosing the droop gains as $G_{PC,GL} = m_{GL}$ and $G_{QC,GL} = n_{GL}$, the close-loop transfer functions for the power control loop in the grid-following inverter will be

$$\frac{P_{GL}}{P_{GL}^*} = \left(\frac{m_{GL}}{A_0'} \right) \frac{a_0 s^2 + a_1 s + a_2}{s^2 + A_1' s + A_2'}, \tag{14}$$

where

$$\begin{aligned}
A_0' &= L_{GL}^2 + m_{GL}a_0, \\
A_1' &= (2L_{GL}^2 + m_{GL}a_1) / (L_{GL}^2 + m_{GL}a_0), \\
A_2' &= \omega_m^2 L_{GL}^2 + m_{GL}a_2 / (L_{GL}^2 + m_{GL}a_0).
\end{aligned} \tag{15}$$

Following similar steps, the reactive power loop will look like

$$\frac{Q_{GL}}{Q_{GL}^*} = \left(\frac{n_{GL}}{B_0'} \right) \frac{b_0 s^2 + b_1 s + b_2}{s^2 + B_1' s + B_2'}, \tag{16}$$

where

$$\begin{aligned}
B_0' &= L_{GL}^2 + n_{GL}b_0, \\
B_1' &= (2R_{GL}L_{GL} + n_{GL}b_1) / (L_{GL}^2 + n_{GL}b_0), \\
B_2' &= (\omega_m^2 L_{GL}^2 + R_{GL}^2 + n_{GL}b_2) / (L_{GL}^2 + n_{GL}b_0).
\end{aligned} \tag{17}$$

For further verifying the input/output dynamics of the system and proving the controllability of the system with the proposed controller, the controllable canonical form of the state-space representation has been adopted. The state-space model of each of the systems will have the following forms.

1) *Grid-Forming Inverter's Active Power*: The state-space representation of the grid-forming inverter active power is

$$\begin{aligned} \begin{bmatrix} \dot{x}_{1P_{GF}} \\ \dot{x}_{2P_{GF}} \\ \dot{x}_{3P_{GF}} \end{bmatrix} &= \frac{1}{A_0} \begin{pmatrix} \begin{bmatrix} 0 & 1 & 0 \\ 0 & 0 & 0 \\ -A_3 & -A_2 & -A_1 \end{bmatrix} \begin{bmatrix} x_{1P_{GF}} \\ x_{2P_{GF}} \\ x_{3P_{GF}} \end{bmatrix} + \begin{bmatrix} 0 \\ 0 \\ 1 \end{bmatrix} u \end{pmatrix} \\ y &= \frac{1}{A_0} \begin{bmatrix} a_2 & a_1 & a_0 \end{bmatrix} \begin{bmatrix} x_{1P_{GF}} \\ x_{2P_{GF}} \\ x_{3P_{GF}} \end{bmatrix} \end{aligned} \quad (18)$$

where “ $x_{iP_{GF}}$ ”s ($i = 1, 2, 3$) are states, $y = P_{GF}$ is the actual active power, and $u = P_{GF}^*$ is the active power reference value.

2) *Grid-Forming Inverter's Reactive Power*: The state-space representation of the grid-forming inverter reactive power is

$$\begin{aligned} \begin{bmatrix} \dot{x}_{1Q_{GF}} \\ \dot{x}_{2Q_{GF}} \\ \dot{x}_{3Q_{GF}} \end{bmatrix} &= \frac{1}{B_0} \begin{pmatrix} \begin{bmatrix} 0 & 1 & 0 \\ 0 & 0 & 0 \\ -B_3 & -B_2 & -B_1 \end{bmatrix} \begin{bmatrix} x_{1Q_{GF}} \\ x_{2Q_{GF}} \\ x_{3Q_{GF}} \end{bmatrix} + \begin{bmatrix} 0 \\ 0 \\ 1 \end{bmatrix} u \end{pmatrix}, \\ y &= \frac{1}{B_0} \begin{bmatrix} b_3' - B_3 b_0' & b_2' - B_2 b_0' & b_1' - B_1 b_0' \end{bmatrix} \begin{bmatrix} x_{1Q_{GF}} \\ x_{2Q_{GF}} \\ x_{3Q_{GF}} \end{bmatrix} + b_0' u \end{aligned} \quad (19)$$

where “ $x_{iQ_{GF}}$ ”s ($i = 1, 2, 3$) are states, $y = Q_{GF}$ is the actual reactive power, and $u = Q_{GF}^*$ is the reactive power reference value.

3) *Grid-Following Inverter's Active Power*: The state-space representation of the grid-following inverter active power is

$$\begin{aligned} \begin{bmatrix} \dot{x}_{1P_{GL}} \\ \dot{x}_{2P_{GL}} \end{bmatrix} &= \frac{m_{GL}}{A_0} \left(\begin{bmatrix} 0 & 1 \\ -A_2' & -A_1' \end{bmatrix} \begin{bmatrix} x_{1P_{GL}} \\ x_{2P_{GL}} \end{bmatrix} + \begin{bmatrix} 0 \\ 1 \end{bmatrix} u \right), \\ y &= \frac{m_{GL}}{A_0} \left(\begin{bmatrix} a_2 - A_2'a_0 & a_1 - A_1'a_0 \end{bmatrix} \begin{bmatrix} x_{1P_{GL}} \\ x_{2P_{GL}} \end{bmatrix} + a_0u \right), \end{aligned} \quad (20)$$

where $x_{iP_{GF}}$'s ($i = 1, 2, 3$) are states, $y = P_{GF}$ is the actual active power, and $u = P_{GF}^*$ is the active power reference value.

4) *Grid-Following Inverter's Reactive Power*: The state-space representation of the grid-following inverter reactive power is

$$\begin{aligned} \begin{bmatrix} \dot{x}_{1Q_{GL}} \\ \dot{x}_{2Q_{GL}} \end{bmatrix} &= \frac{n_{GL}}{B_0} \left(\begin{bmatrix} 0 & 1 \\ -B_2' & -B_1' \end{bmatrix} \begin{bmatrix} x_{1Q_{GL}} \\ x_{2Q_{GL}} \end{bmatrix} + \begin{bmatrix} 0 \\ 1 \end{bmatrix} u \right), \\ y &= \frac{n_{GL}}{B_0} \left(\begin{bmatrix} b_2 - B_2'b_0 & b_1 - B_1'b_0 \end{bmatrix} \begin{bmatrix} x_{1Q_{GL}} \\ x_{2Q_{GL}} \end{bmatrix} + b_0u \right), \end{aligned} \quad (21)$$

where " $x_{iQ_{GF}}$ "s ($i = 1, 2, 3$) are states, $y = Q_{GF}$ is the actual reactive power, and $u = Q_{GF}^*$ is the reactive power reference value. The state-space representation of the controller augmented with *PR* control has also been verified, so a thorough pole placement of the stability analysis can be performed as elaborated in Section III.

3.2. INNER VOLTAGE AND CURRENT CONTROL LOOPS

As depicted in Figure. 4 (Grid-Forming Control *IV* and *V*), the power control loops in the grid-forming inverter are followed by a voltage inner control loop, which is implemented in $\alpha\beta$ stationary reference frame. The inner voltage loop, being a proportional controller represented by $G_{cv\alpha/\beta}$, improves the stability and the phase margin of the controller. The voltage control is followed by a nonlinear current control loop which removes the nonlinear dynamics of the current by utilizing the output/input feedback linearization

current control (FL/CC), Figure. 4 (Grid-Forming Control V). This control scheme cancels all nonlinearities of the current control loop and makes an overall linear first-order system—which is much simpler to control. The implementation of the control comes from Kirchhoff's Voltage Law (KVL) equation from the inverter to the grid, i.e.,

$$L_{GF} \frac{di_{GF}}{dt} = R_{GF} i_{GF} + (v_{PCC} - v_g). \quad (22)$$

Here, by choosing the input $u = v_{PCC} - v_g$ and $e = i_{GF} - i_{GF}^*$ (with i_{GF}^* as the reference current), linearizing the dynamics of current is regarded as $\dot{e} = -k_{lin}e$. In order to reach this purpose, the input can be chosen as follows, canceling all the nonlinearities of the current.

$$u = R_{GF} i_{GF} + k_{lin} e, \quad (23)$$

where k_{lin} is a constant. By utilizing this method, the current control loop reduces the system to a linear one through the cancellation of the nonlinearities. As the main control loop is the power control loop, this feedback linearization method performs effectively as a second loop of control and helps stabilize the control structure.

3.3. AUGMENTED POWER PROPORTIONAL RESONANT CONTROL

In an unbalanced grid condition, voltage sag and distortions result in severe oscillations in the generated power of renewable resources. In parallel operation of the converters, the unbalanced grid voltage and rapid power fluctuations jeopardize the power-sharing feature. Several control strategies have been proposed in order to enhance the performance of parallel inverters in unbalanced grid conditions, and modified droop controllers have been designed to improve power-sharing capability in unbalanced grid conditions [30, 31]. A proportional multi-resonant controller is proposed in order to control the output voltage in an unbalanced grid [32], and a similar approach has been employed to augment the power angle synchronization control [33].

Table 1. System Parameters

Parameter	Value	Parameter	Value
R_{GF}	0.1 Ω	J	1 Kgm ²
L_{GF}	5.0 mH	D	10 kgms ⁻²
C_{eq}	20 μ F	m_{GL}	0.4
R_{GL}	0.5 Ω	n_{GL}	1.0
L_{GL}	1.0 mH	K_{PGF}	16
Z_{load}	5 Ω	K_{iGF}	28
R_{eq}	1 m Ω	f	60 Hz
L_{eq}	0.1 mH	T_{GL}	0.25
K_{GL}	2 \times 10 ³	$G_{cv\alpha/\beta}$	0.3

In this paper, the same control methodology has been used in order to augment the virtual synchronous machine control in the grid-forming inverter and the power droop control in the grid-following inverter. This control strategy results in mitigating the power oscillations during unbalanced grid conditions—see Figure. 3 Grid-Forming Control *III*. The primary purpose of this control scheme is to ensure the power-sharing scheme among parallel inverters, and in order to reduce the oscillations in power, distortions in the current are allowed. However, as the proposed power control structure does not have any current-limiting control capability, the inner control loop and the feedback linearization current control keep the current within the limits required. The overall structure utilized for the *PR* control is

$$G_h = \frac{K\omega_{cut}s}{s^2 + 2\omega_{cut}s + (2\omega_0)^2}, \quad (24)$$

where G_h denotes $\Delta\omega$ for active power loop both in PVSG grid-forming and droop control in grid-following inverter and Δv for the reactive power loop. Also, ω_{cut} is chosen in a way to make the controller sufficiently dissipative and attenuate the oscillations in the voltage. The frequency of voltage oscillations in an unbalanced grid condition is double fundamental frequency of the system. Therefore, the resonant frequency has been chosen

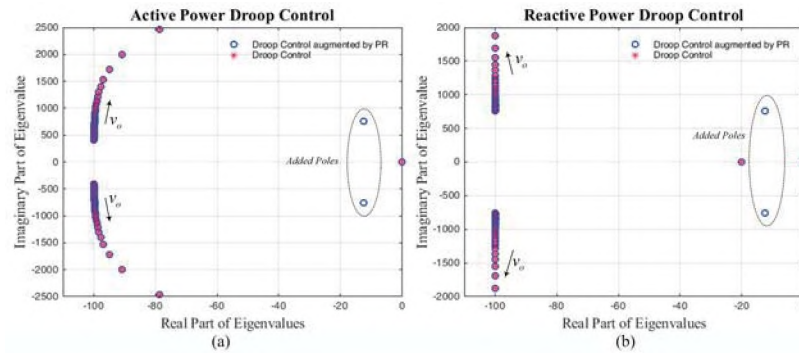


Figure 5. Eigenvalue trace of grid-forming PVSG's (a) active power and (b) reactive power

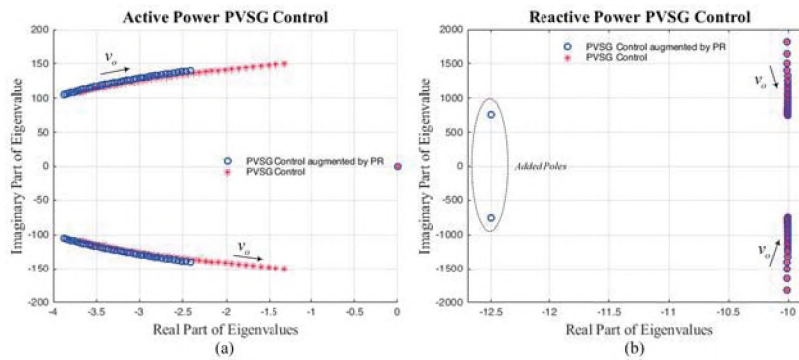


Figure 6. Eigenvalue trace of grid-following PVSG's (a) active power and (b) reactive power

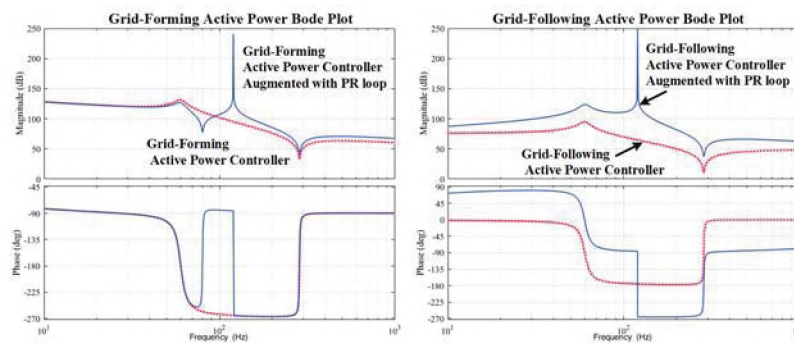


Figure 7. Closed-loop Bode plot of (a) grid-forming active power and (b) grid-following active power

as $2\omega_0$, which is basically the double nominal value of the nominal frequency. The resonant frequency is tuned to the second harmonic, and the rest of the parameters is obtained through the small-signal transfer functions of power obtained in the previous section. In a linear control scheme, the feedforward of a *PR* loop will add a resonating pole at the double fundamental frequency, which is the leading cause of oscillations in power during unbalanced conditions. Figures. 5, 6 and 7 depict the eigenvalues and the Bode plots of the active power for both grid-forming and grid-following inverters. The infinite gains at the double frequency ensure the suppression of any second harmonic oscillations. Also, the added phase at the stated frequency can mitigate any undesired oscillations in power. As the power input to the controller is dc, the elimination of the second harmonic can significantly improve the power-sharing scheme. This strategy is a well-known method applied in linear control scheme, and more details about adjusting the parameters has already been explained in [32–35].

In the overall hierarchical structure of the controller, the outer power loops in both the grid-forming and grid-following inverters have been augmented by the *PR* controller, which enhances the tracking of the dc reference values and improves the bandwidth to achieve the desired transient response. However, the bandwidth of the power control loop is always kept smaller than the inner control loops; hence, the dynamics of the outer loop do not influence the inner loop. As the power control loops are the dominant controllers of both systems, the stability analysis has been performed on the power control loop as explained in the next section.

4. STABILITY ANALYSIS

To further verify the augmented *PR* controller parameters, they are based on the eigenvalues of *A* matrices derived in the previous section. The analysis has been performed

based on the reaction of the stability of the system to gridvoltage sag. The performance of the general control system augmented by PR control is also demonstrated. To this end, the parameters employed in evaluating the stability of the system are summarized in Table 1.

4.1. GRID-FORMING SMALL-SIGNAL DYNAMIC ANALYSIS

5 demonstrates the eigenvalues of grid-forming inverter's close-loop active power dynamics, (17) and (19), along with the eigenvalues of similar matrices when the power control is augmented with a PR controller. 5(a) shows that generally PVSG control system on the grid-forming inverter is stable and the eigenvalues are on the left-half plane. The system response to grid voltage sag shows that the eigenvalues move toward the right-half plane in the active power loop. However, by adding the PR controller, they are shifted more toward the left-half plane with a much slower trend toward instability. On the other hand, in 5(b), the reactive power loop eigenvalues shift toward the right as the grid voltage drops. However, the system is still in a stable region. This observation reveals that the proposed controller for the grid-forming inverter is capable of stabilizing the PCC voltage. Augmenting the reactive power loop with the PR will just add two more poles farther toward the left-half plane, thus pushing the system to more stability in an unbalanced grid condition.

4.2. GRID-FOLLOWING SMALL-SIGNAL DYNAMIC ANALYSIS

6 represents the eigenvalues of grid-following inverter's close-loop active/reactive power dynamics, (20) and (21). The closed-loop dynamics of active power and reactive power are in the stable left-half plane. Besides, the augmentation with PR control adds two more poles in the left-half plane, which renders the system more stable in case of an unbalanced grid condition and the voltage drops.

5. HARDWARE CO-SIMULATION RESULTS AND DISCUSSIONS

As control systems are becoming more intricate and complex, realistic test bench environments are developed in order to test the performance and efficiency of a variety of control methodologies. Recently, hardware-in-the-loop (HIL) implementation has attracted lots of attention. The real-time implementation of the controller can validate the interactive performance of different models and physical hardware. This method facilitates emulating large, complex, and virtually connected systems. This trend has found its way in several large-scale distributed energy systems using distant HIL-based simulations to control physical converters [26].

Among all HIL methods, field-programmable gate array-based (FPGA-based) technique has become quite popular. Enhanced transient capturing in smaller time steps along with applying hardware pipelining and parallel implementation of controller code reduces the unwanted latencies and delays in the system. In this paper, the schematic block method of "System Generator" (from Xilinx) in DSP (XSG) with floating number representation and VHDL programming has been applied to implement the control in ZYNQ XC7Z020-CLG484 (Zedboard). The joint test action group (also known as JTAG) co-simulation interface has been used as it requires minimum resources on FPGA to achieve an optimum hardware consimulation interface. The FPGA clock frequency is chosen to be around 120 MHz at which all modules are found to be compatible with each other. The whole control structure is implemented in Xilinx System Generator, and the switching circuit is realized in the software tool of Piecewise Linear Electrical Circuit Simulation (PLECS). Logical blocks and VHDL have been used to design the control. Registers have divided the control structure into pipelining stages with minimum latency. The results of the hardware co-simulation are implemented on the board, and they have been extracted on the scope by utilizing a DAC module.

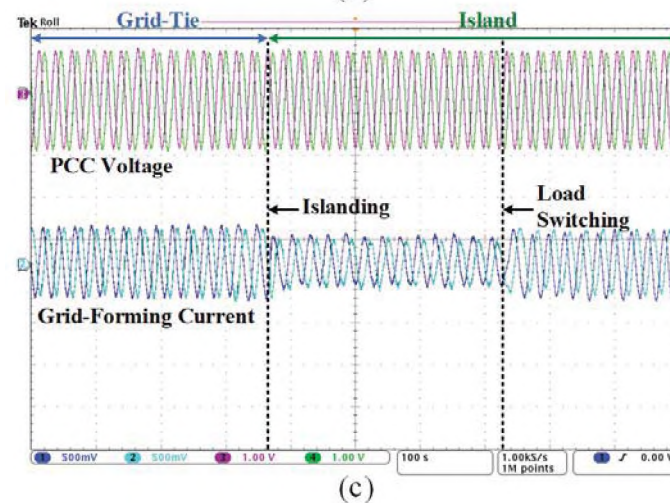
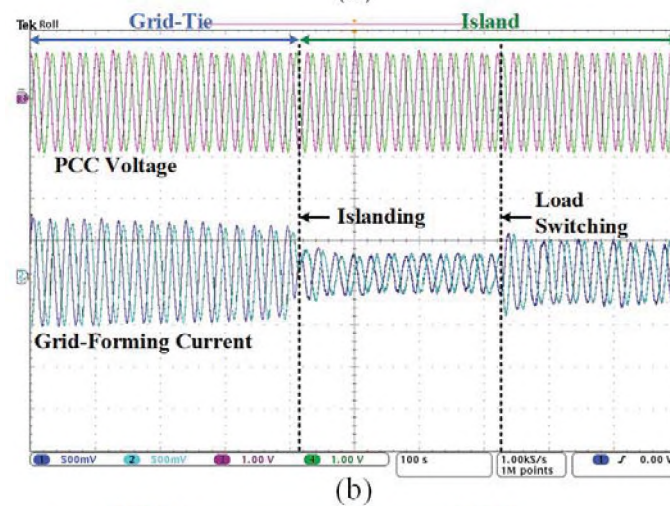
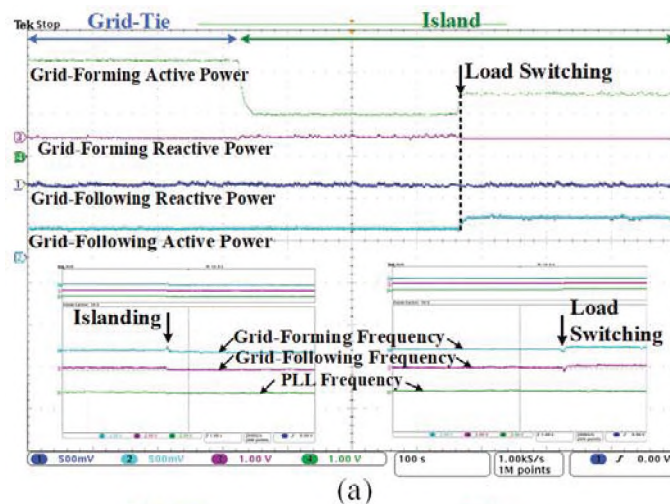


Figure 8. The transient from grid-connected to isolated mode of operation (Active Power: 1 kW/div; Reactive Power: 1 kvar/div; Voltage: 34 V/div; Current: 8 A/div; and Frequency 0.15 Hz/div); (a) active and reactive power of grid-forming and grid-following inverters and commanded frequencies (ω_{GF}) and (ω_{GL}) and PCC frequency measured by PLL, (b) PCC voltage and grid-forming currents of phases A and B, and (c) PCC voltage and grid-following currents of phases A and B

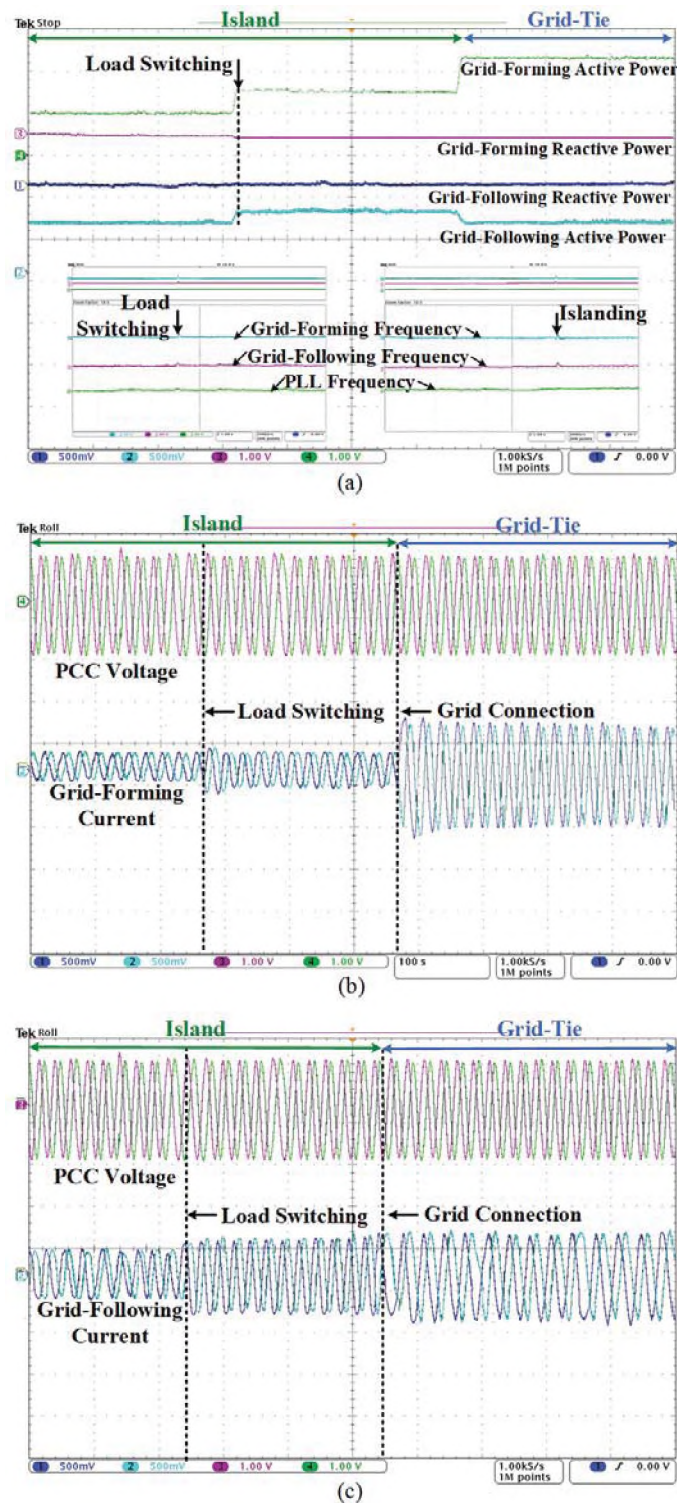


Figure 9. The transient from isolated mode of operation grid-connected (Active Power: 1 kW/div; Reactive Power: 1 kvar/div; Voltage: 34 V/div; Current: 8 A/div; and Frequency 0.15 Hz/div); (a) active and reactive power of grid-forming and grid-following inverters and commanded frequencies (ω_{GF}) and (ω_{GL}) and PCC frequency measured by PLL, (b) PCC voltage and grid-forming currents of phases A and B, and (c) PCC voltage and grid-following currents of phases A and B

5.1. POWER-SHARING CONTROL IN ISLANDED AND GRID-CONNECTED MODES OF OPERATION

HIL results are reported for the proposed system with $10kVA$ power rating for the grid-forming inverter. The grid voltage is maintained at $208V$ (line-to-line rms), and the whole system feeds two local linear loads with the power ratings of $5kW$ and $7.5kW$. The transients in power have been depicted for three modes of operation in Figures. 8 and 9. In Figure. 8, the system is connected to a relatively weak grid with the impedance of $0.1mH$. The reference in the grid-forming active power is calculated through the dc-bus control loop in the isolated mode of operation. Also, the PV-based grid-forming inverter acts as a slack bus in islanded condition. In Figure. 8, the system is first connected to the grid. Afterwards, it disconnects. The transition from grid-connected mode to the isolated operation happens smoothly and as it can be seen in Figure. 8(a), the grid-forming inverter and the grid follower share the power based on the controller parameter gains. As the grid-following unit active power reference generation is sensitive to a change in PCC frequency and it acts as a battery-based converter closer to the load, the active power reference does not change during this transient. However, when there is a switching load transient from $5kW$ to $7.5kW$, the reference generation in the following unit also alters in order to meet the instantaneous load demand. In this way, there is a balance between the active power generated through the grid-forming and the grid-following units—without pushing any of the converters toward their maximum power rating capabilities. An analysis on the frequency commanded by grid-forming and grid-following controllers (see 3, ω_{GF} and ω_{GL}) and the frequency measured at the PCC through a well-tuned PLL shows that the frequency deviations during each transient is within the limits. Moreover, during switching load in the isolated mode of operation, the frequency deviation in both grid-forming and grid-following units does not drift more than $0.5Hz$. Figure. 8(b) and 8(c) show that the PCC voltage has been well stabilized during the transitions, and the voltage phase and

magnitude remain intact. The current injected by the grid former and the grid follower alters according to the power rating of the load in the isolated mode; it is maximum in grid-connected mode as well.

A reverse transition from the isolated mode of operation to grid-connected has been examined in 9. A similar load-switching scheme has been applied in the isolated mode. The inertia of the grid-forming inverter has been chosen in a way that the controller has sufficient bandwidth to control the voltage and frequency at PCC. In such transitions, the grid-forming inverter provides sufficient inertia to keep the frequency oscillations within an acceptable range while the grid follower also takes part in sharing the load during the transition and the outer frequency control loop in the following unit generates sufficient active power.

5.2. POWER-SHARING CONTROL IN ISLANDED AND UNBALANCED-GRID-CONNECTED MODES OF OPERATION

The operation of both grid-forming and grid-following units during an unbalanced grid condition has been examined through synchronizing to an unbalanced grid in which one phase voltage magnitude drops 25% below the nominal value which emulates a faulty condition. 10 depicts the synchronization of both converters to the unbalanced grid from an isolated mode of operation with the proposed control action. The main objective of the controller, which is to provide sufficient power to the load devoid of any oscillations, is met. Along with it, although no frequency measuring units are applied, the frequency commanded through the grid-forming inverter suffices the resynchronization to the grid even in a faulty condition. This condition confirms that the phase angle controlled by the grid-forming inverter, i.e. θ_{GF} , is sufficiently close to that of the grid—which does not affect the performance during resynchronization. Negligible frequency oscillations during the transition from resynchronization to the unbalanced grid condition (lower than 0.7 Hz

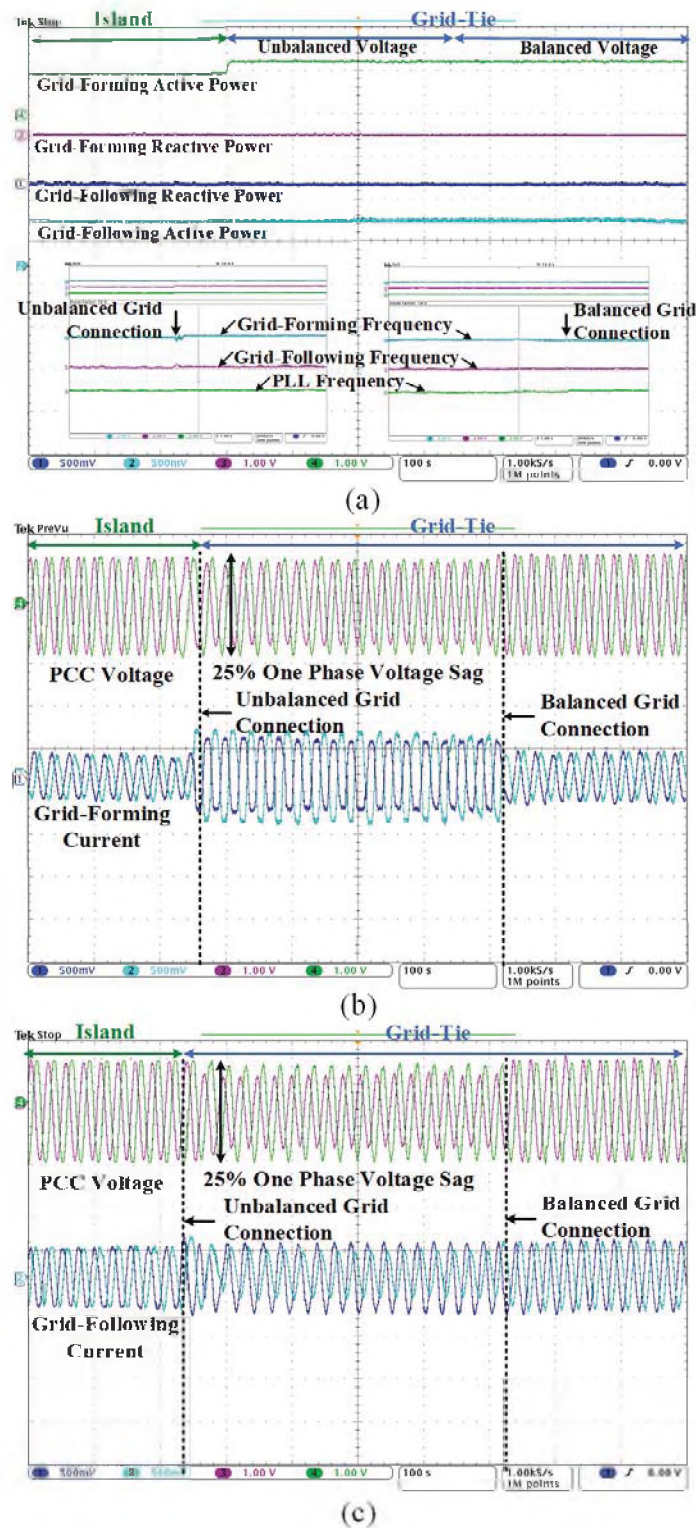


Figure 10. The transient from isolated mode of operation to unbalanced-grid-connected mode (Active Power: 1 kW/div; Reactive Power: 1 kvar/div; Voltage: 34 V/div; Current: 8 A/div; and Frequency 0.15 Hz/div); (a) active and reactive power of grid-forming and grid-following inverters and commanded frequencies (ω_{GF}) and (ω_{GL}) and PCC frequency measured by PLL, (b) PCC voltage and grid-forming currents of phases A and B, and (c) PCC voltage and grid-following currents of phases A and B

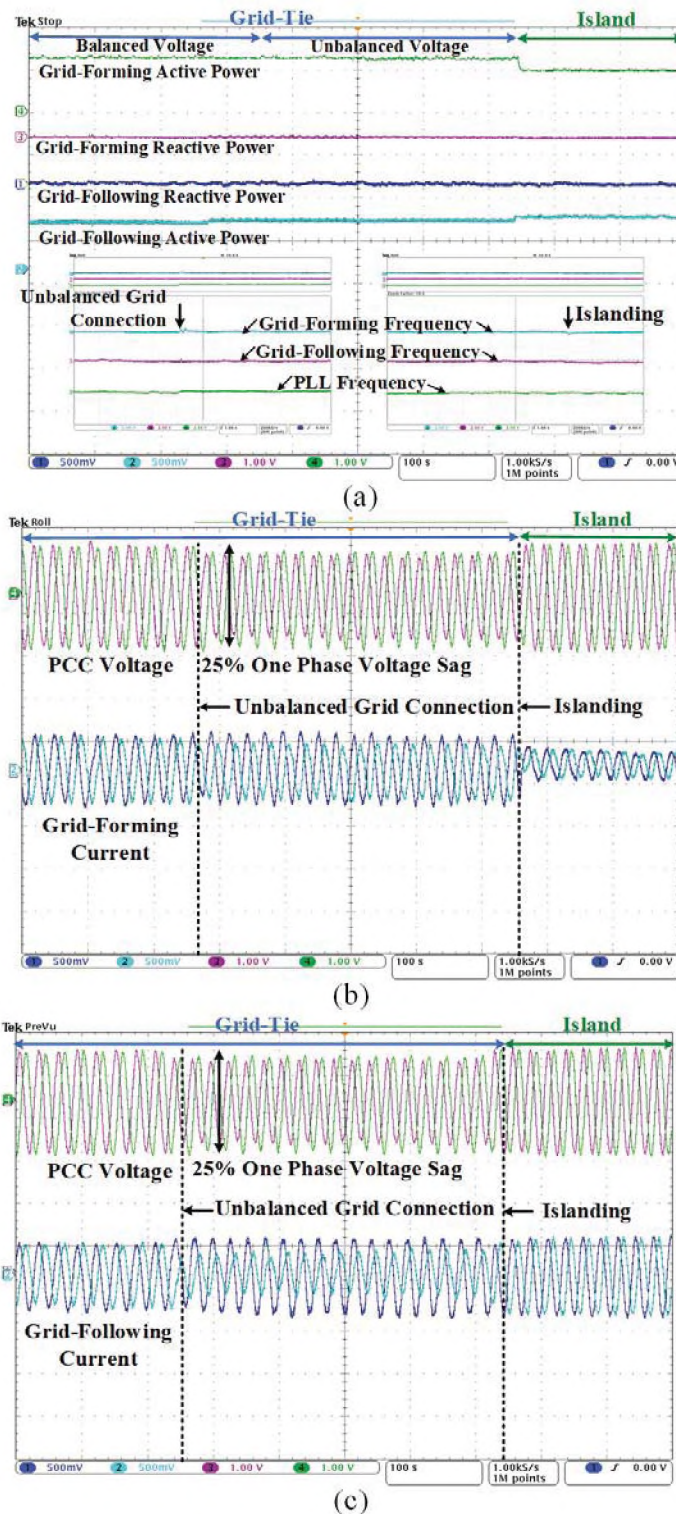


Figure 11. The transient from unbalanced-grid-connected mode to isolated mode of operation (Active Power: 1 kW/div; Reactive Power: 1 kvar/div; Voltage: 34 V/div; Current: 8 A/div; and Frequency 0.15 Hz/div); (a) active and reactive power of grid-forming and grid-following inverters and commanded frequencies (ω_{GF}) and (ω_{GL}) and PCC frequency measured by PLL, (b) PCC voltage and grid-forming currents of phases A and B, (c) PCC voltage at and Grid-following currents of phases A and B

for the grid-forming inverter, i.e., $\Delta\omega_{GF}$), confirm that the controller is robust enough to prevent the inverter to trip when connected to an unbalanced grid condition. Also, in such a severe transition, the current-limiting capability of the controller helps keep the current magnitude within limits as the current magnitude increases when voltage drops in one phase to keep the power tracking the reference value. 10(b) shows the operation of the grid-forming inverter during its resynchronization to an unbalanced grid. The threshold of the feedback linearizing gain used as the current limiting control has been selected to be the highest. This selection examines the current limiting capability of the controller. In the case of the grid-follower, i.e., 10(c), the current shows a usual distortion, and it does not demonstrate any discernible increment in the magnitude because it is, in general, following the grid-forming inverter in terms of sharing power. A reverse transition has been examined from an unbalanced grid-condition to the isolated mode of operation, see 11. This transition confirms that the grid-forming inverter can maintain the voltage magnitude and frequency at the PCC.

5.3. PR CONTROLLER PERFORMANCE EVALUATION IN UNBALANCED-GRID-CONNECTED MODES OF OPERATION

The performance of the PR compensation has been verified during a more severe faulty condition in which there is a 15% voltage magnitude drop in two phases, see 12. The active and reactive power in both grid-forming and grid-following units do not show any discernible oscillations as long as the *PR* compensator is fed forwarded to the power control loop. However, when the *PR* loop is disconnected both active power and reactive power start to oscillate in both units as the current gets distorted when the oscillations are not mitigated by the resonant compensator.

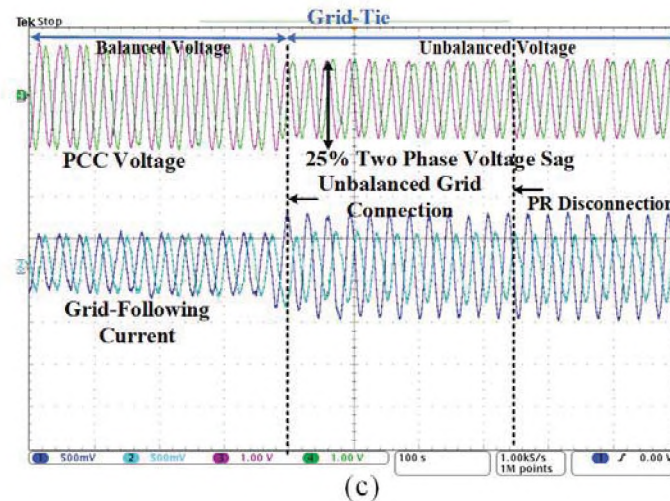
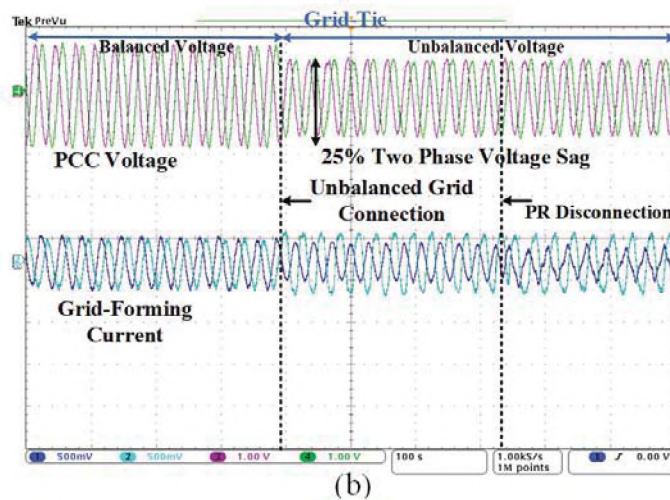
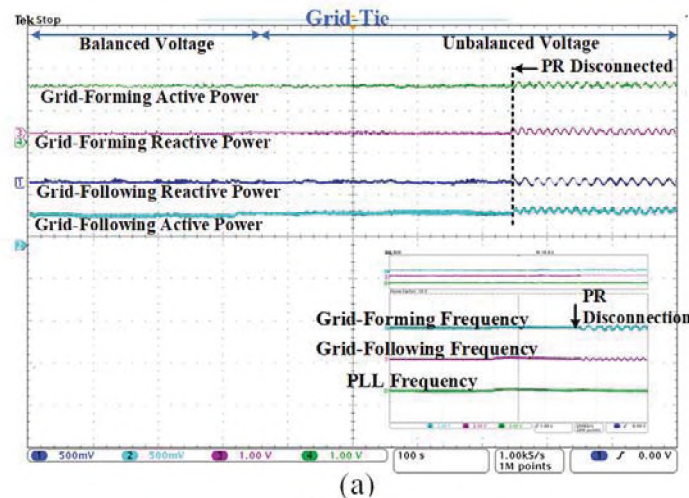


Figure 12. The transient from balanced grid-connected mode to unbalanced-grid-connection followed by PR control disconnection (a) active and reactive power of grid-forming and grid-following inverters and commanded frequencies (ω_{GF}) and (ω_{GL}) and PCC frequency measured by PLL, (b) PCC voltage and grid-forming currents of phases A and B, and (c) PCC voltage and grid-following currents of phases A and B

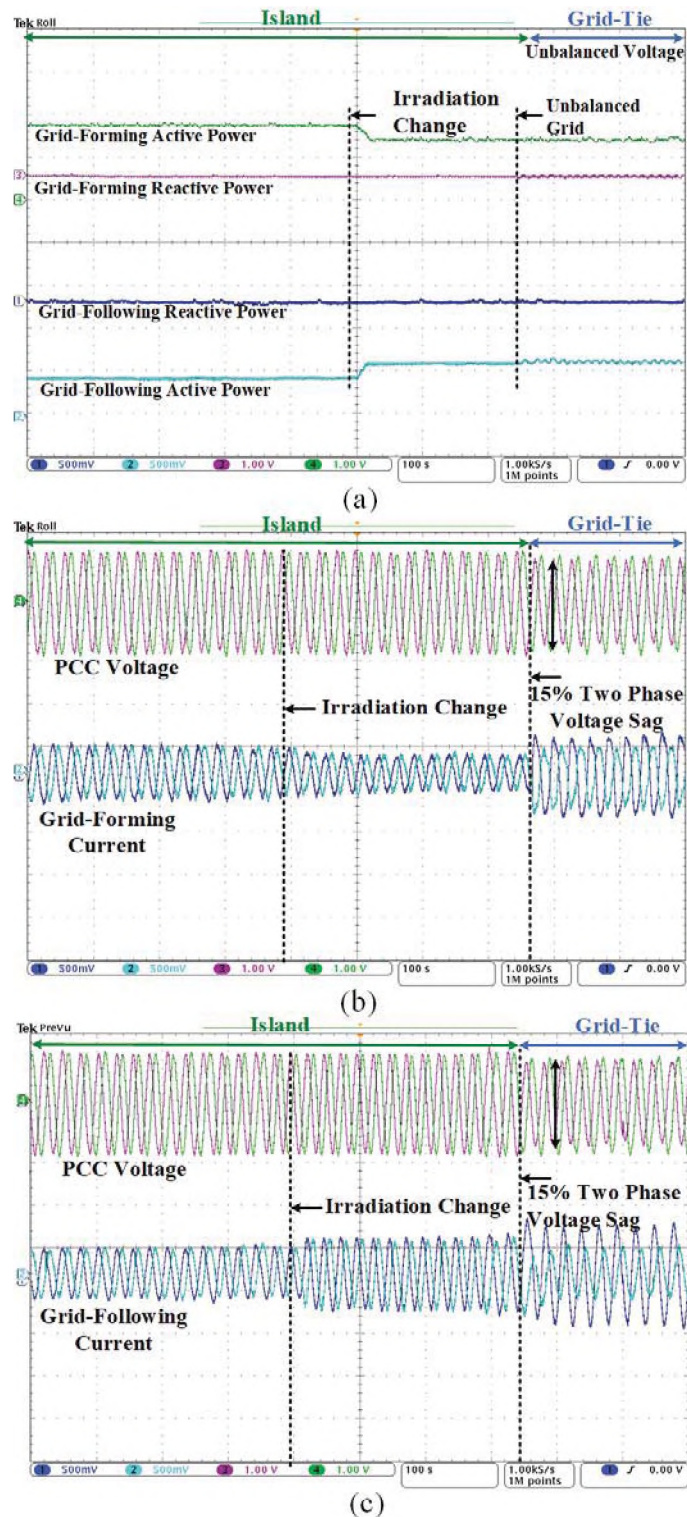


Figure 13. The transient in isolated mode of operation followed by the reduction in irradiation and reconnecting to an unbalanced grid condition (Active Power: 1 kW/div; Reactive Power: 1 kvar/div; Voltage: 34 V/div; Current: 8 A/div; and Frequency 0.15 Hz/div);(a) active and reactive power of grid-forming and grid-following inverters and commanded frequencies (ω_{GF}) and (ω_{GL}) and PCC frequency measured by PLL, (b) PCC voltage and grid-forming currents of phases A and B, and (c) PCC voltage and grid-following currents of phases A and B

5.4. POWER-SHARING CONTROL IN ISLANDED AND UNBALANCED GRID-CONNECTED MODES OF OPERATION AND CHANGE IN IRRADIATION

The performance evaluation of the proposed control architecture during the change in the solar irradiation has also been presented in 13. The active power reference of the grid-forming inverter drops as the irradiation decreases to 50% of its full load value and accordingly the current injected by the grid-forming inverter to the load in the isolated mode reduces—see 13. However, as the grid-following unit is also equipped with a power control loop and acts as a voltage source, it is able to supply the balanced load demand. In this case, the choice of a droop control for the following unit is a proper choice as long as it can switch from a “following” unit to a “forming” one, when the PVSG is vulnerable due to the changes in irradiation. Nevertheless, the frequency commanded by the grid-forming inverter should still take care of the resynchronization to the grid, which means that the phase generated by the grid-forming inverter at the point of common coupling should not be dependent on the irradiation. This phenomenon has been tested in a severe case by reconnecting the system to an unbalanced grid. The performance depicted in 13 reveals that even by the reduction in irradiation, the grid-forming inverter is still able to synchronize to an unbalanced grid and the current in both forming and following units does not show an undesired overshoot.

5.5. COMPARISON WITH A CONVENTIONAL SYNCHRONVERTER EQUIPPED WITH CURRENT-LIMITING LOOP

The operation of PV-based converters as Photovoltaic Synchronous Generators (PVSG) has been recently the subject of discussion as the PV-based converters are capable of emulating a synchronous generator in active and reactive power generation by applying a similar control architecture in [9, 14]. The proposed voltage-source converters can maintain the voltage magnitude and PCC frequency. However, their operation in resynchronizing to an unbalanced grid condition is not yet evaluated. In addition, their interaction as a grid-

forming inverter with grid-following inverters has also not been verified. Grid followers are generally regarded as current-controlled inverters whose operations are dependent on the voltage and the frequency that is stabilized by a grid-forming unit. However, as long as the grid-forming inverters emulate a synchronous machine (with a fixed inertia), in case the chosen moment of inertia slows down the control operation, the settling time of the controller becomes higher by resynchronization to the grid. This process results in oscillations in power and frequency. In such a condition, the current controller which its performance is dependent on the measured PCC frequency will not have a stable operation.

A similar control structure applied in [14] has been utilized to reproduce the transient behavior of a grid-forming inverter during the reconnection to an unbalanced grid condition, see 14. The current shows an overshoot and higher settling time during the resynchronization to the unbalanced grid with 25% voltage sag in one phase. Besides, a current-controlled converter operation in parallel with this converter has been evaluated. As discussed, during the transitions, the current controller shows current overshoots and high settling time performance. Consequently, the choice of the current control architecture for a grid-following unit might not be a feasible solution. The droop control augmented with the governor frequency control loop can be a better candidate to improve the power oscillations and keep the frequency oscillations within the accepted range. By using this approach, there is no adaptive alternating moment of inertia implemented in the linear control structure and in the absence of a stable nonlinear control scheme.

6. CONCLUSION

A hierarchical control methodology based on a virtual synchronous machine for power control has been proposed for a PV-based inverter. This system is capable of having

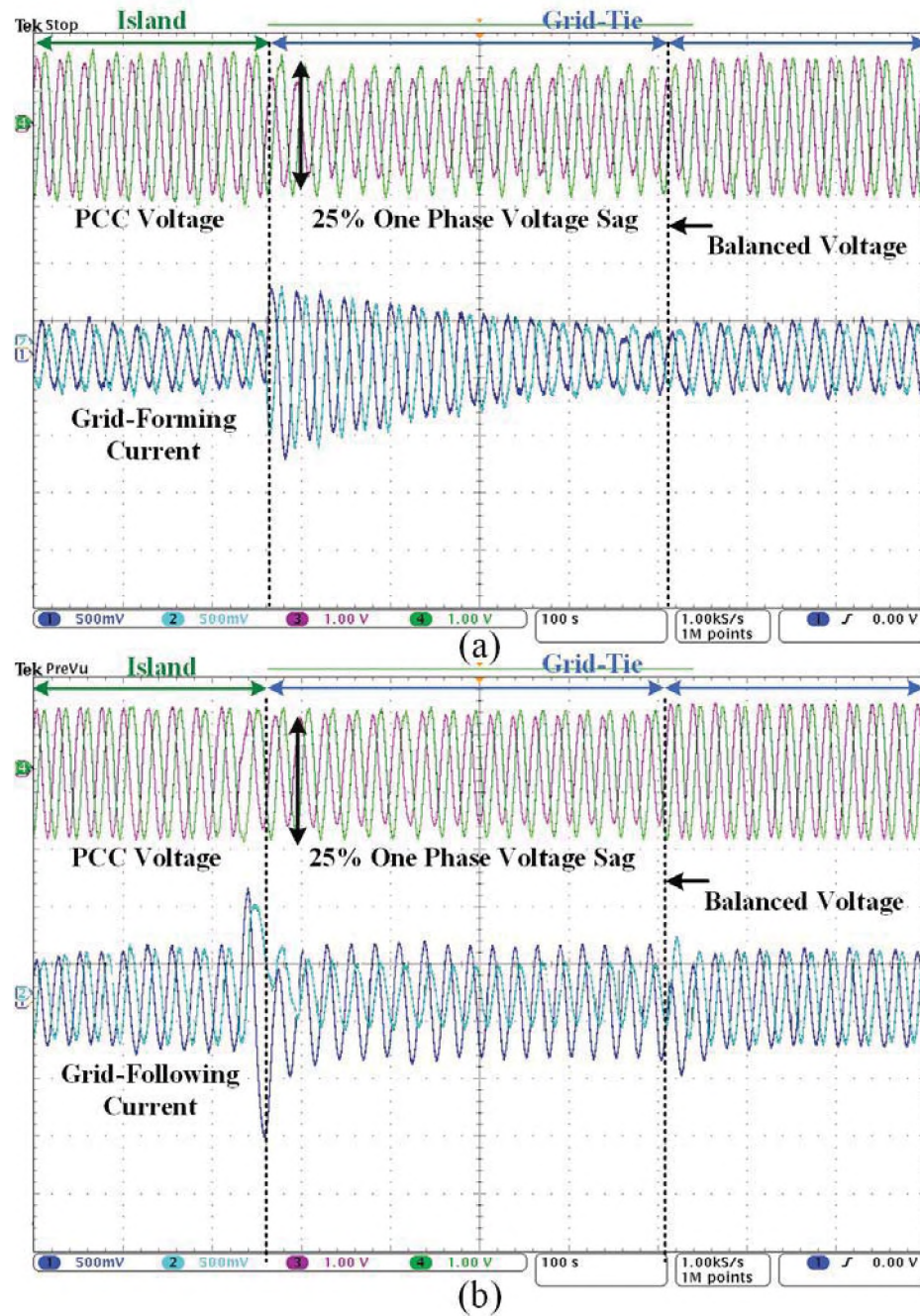


Figure 14. The operation evaluation of a conventional synchronverter (Voltage: 34 V/div; and Current: 8 A/div); (a) PCC voltage and current injected by a PVSG controlled as a synchronverter and (b) PCC voltage and current injected by a converter with a current control loop

an embedded frequency regulator, it can operate autonomously with self-synchronizing capabilities. This system is followed by a more dependent unit called a grid-following inverter. The droop control of this unit helps enhance the power-sharing capabilities of the overall system. In this paper, a PR control is augmented in the power loop controls, thus significantly improving the operation of the converters during unbalanced grid conditions and reducing the oscillations in the power loop. The performance of both systems in three modes of operation reveals the efficiency of the proposed controller. For further evaluations, the operation and the power-sharing feature have been more investigated during different load-switching scenarios. Hardware-in-the-loop co-simulation results have been provided in order to demonstrate the effectiveness of the approaches proposed in this paper.

REFERENCES

- [1] C. Stice and J. C. Boemer, "Bulk system opportunities from new distributed energy resource interconnection and inter-operability standards," *NERC SPIDER WG Meeting*, January 2019.
- [2] A. Paquette, M. Reno, R. Harley, and D. Divan, "Sharing transient loads: Causes of unequal transient load sharing in islanded microgrid operation," *IEEE Industry Applications Magazine*, vol. 20, pp. 23 – 34, December 2013.
- [3] A. D. Paquette and D. M. Divan, "Virtual impedance current limiting for inverters in microgrids with synchronous generators," *IEEE Transactions on Industry Applications*, vol. 51, pp. 1630 – 1638, August 2014.
- [4] D. Zhang and J. Fletcher, "Operation of Autonomous AC Microgrid at Constant Frequency and with Reactive Power Generation from Grid-forming, Grid-supporting and Grid-feeding Generators," *TENCON 2018 - 2018 IEEE Region 10 Conference*, Jeju, Korea (South), pp. 1560-1565, 2018.
- [5] L. K. Gan, J. K. H. Shek and M. A. Mueller, "Modelling and experimentation of grid-forming inverters for standalone hybrid wind-battery systems," *2015 International Conference on Renewable Energy Research and Applications (ICRERA)*, Palermo, pp. 449-454, 2015.
- [6] B. Kroposki, B. Johnson, Y. Zhang, V. Gevorgian, P. Denholm, B. M. Hodge, and B. Hannegan, "Achieving a 100systems with extremely high levels of variable renewable energy," *IEEE Power and Energy Magazine*, vol. 15, pp. 61–73, March 2017.

- [7] "Reliability Guideline BPS-Connected Inverter-Based Resource Performance", *NERC*, September 2018
- [8] F. Katiraei, R. Iravani, N. Hatziargyriou, and A. Dimeas, "Microgrids management," *IEEE Power and Energy Magazine*, vol. 6, p. 54-65, June 2008.
- [9] Q. C. Zhong and G. Weiss, "Synchronverters: Inverters that mimic synchronous generators," *IEEE Transactions on Industrial Electronics*, pp. 1259–1267, 2011.
- [10] Q. C. Zhong, G. C. Konstantopoulos, B. Ren, and M. Krstic, "Improved synchronverters with bounded frequency and voltage for smart grid integration," *IEEE Transactions on Smart Grid*, 2016.
- [11] Q. C. Zhong and G. C. Konstantopoulos, "Current-limiting droop control of grid-connected inverters," *IEEE Transactions on Industrial Electronics*, vol. 64, p. 5963–5973, July 2017.
- [12] M. E. Elkhatab, W. Du and R. H. Lasseter, "Evaluation of Inverter-based Grid Frequency Support using Frequency-Watt and Grid-Forming PV Inverters," *2018 IEEE Power and Energy Society General Meeting (PESGM)*, Portland, OR, 2018, pp. 1-5.
- [13] D. Pattabiraman, R. H. Lasseter. and T. M. Jahns, "Comparison of Grid Following and Grid Forming Control for a High Inverter Penetration Power System," *2018 IEEE Power and Energy Society General Meeting (PESGM)*, Portland, OR, 2018, pp. 1-5
- [14] M. Ashabani and Y. A.-R. I. Mohamed, "Novel comprehensive control framework for incorporating vses to smart power grids using bidirectional synchronous-vsc," *IEEE Transactions on Power System*, vol. 29, pp. 943 – 957, November 2013.
- [15] W. Du and R. H. Lasseter, "Overload mitigation control of droop-controlled grid-forming sources in a microgrid," *2017 IEEE Power and Energy Society General Meeting*, Chicago, IL, 2017, pp. 1-5
- [16] P. J. Hart, R. H. Lasseter, and T. M. Jahns, "Coherency identification and aggregation in grid-forming droop-controlled inverter networks," *IEEE Transactions on Industry Applications*, vol. 55, June 2019.
- [17] X. Huang, K. Wang, L. H. J. Qiu, G. Li, and X. Wang, "Decentralized control of multi-parallel grid-forming dgs in islanded microgrids for enhanced transient performance," *IEEE Access*, vol. 7, pp. 17 958 – 17 968, January 2019.
- [18] F. Mahr and J. Jaeger, "Advanced Grid-Forming Control of HVDC Systems for Reliable Grid Restoration," *2018 IEEE Power and Energy Society General Meeting (PESGM)*, Portland, OR, 2018, pp. 1-5.
- [19] M. G. Taul, P. D. X. Wang, and F. Blaabjerg, "Current limiting control with enhanced dynamics of grid-forming converters during fault conditions," *IEEE Journal of Emerging and Selected Topics in Power Electronics*, July 2019.

- [20] M. Mirhosseini and V. G. A. J. Pou, "Grid-connected photovoltaic power plant without phase angle synchronization able to address fault ride-through capability," *IEEE Journal of Emerging and Selected Topics in Power Electronics*, September 2019.
- [21] S. Mortazavian, M. M. Shabestary, and Y. A.-R. I. Mohamed, "Analysis and dynamic performance improvement of grid-connected voltage source converters under unbalanced network conditions," *IEEE Transactions on Power Electronics*, vol. 32, October 2017.
- [22] P. Piya, M. Ebrahimi, M. Karimi-Ghartemani, and S. A. Khajehoddin, "Fault ride-through capability of voltage-controlled inverters," *IEEE Transactions on Industrial Electronics*, vol. 65, p. 7933–7943, October 2018.
- [23] L. He, Z. Shuai, X. Zhang, X. Liu, Z. Li, and Z. J. Shen, "Transient characteristics of synchronverters subjected to asymmetric faults," *IEEE Transactions on Power Delivery*, vol. 34, June 2019.
- [24] K. Sakimoto, Y. Miura, and T. Ise, "Characteristics of parallel operation of inverter-type distributed generators operated by a virtual synchronous generator," *IEEE Transactions on Power and Energy*, January 2013.
- [25] A. Adib and B. Mirafzal, "Virtual inductance for stable operation of grid-interactive voltage source inverters," *IEEE Transactions on Industrial Electronics*, vol. 66, August 2019.
- [26] K.-K. J. H.-C. Chiang and G.-H. You, "Improved droop control method with precise current sharing and voltage regulation," *IET Power Electronics*, p. 789–800, March 2016.
- [27] K. Wang, X. Huang, B. Fan, Q. Yang, G. Li, and M. L. Crow, "Decentralized power sharing control for parallel-connected inverters in islanded single-phase micro-grids," *IEEE Transactions on Smart Grid*, vol. 9, pp. 6721 – 6730, November 2018.
- [28] D. De and V. Ramanarayanan, "A proportional multiresonant controller for three-phase four-wire high-frequency link inverter," *IEEE Transactions on Power Electronics*, vol. 25, p. 899–906, 2010.
- [29] S. Mukherjee, V. R. Chowdhury, P. Shamsi, and M. Ferdowsi, "Power angle synchronization for grid-connected converter with fault ride-through capability for low voltage grids," *IEEE Transactions on Energy Conversion*, vol. 33, pp. 970 – 979, September 2018.
- [30] M. Davari, W. Gao, and F. Blaabjerg, "A fault-tolerant, passivity based controller enhanced by the equilibrium-to-equilibrium maneuver capability for the DC-voltage power port VSC in multi-infeed ac/dc modernized grids," *IEEE Journal of Emerging and Selected Topics in Power Electronics*, vol. PP, no. 99, pp. 1–24, 2019, Early Access.

- [31] M. Davari and Y. A.-R. I. Mohamed, "Variable-structure-based nonlinear control for the master vsc in dc-energy-pool multiterminal grids," *IEEE Transactions on Power Electronics*, vol. 29, no. 11, pp. 6196–6213, Nov.2014.
- [32] —, "Robust multi-objective control of VSC-based DC-voltage power port in hybrid AC/DC multi-terminal micro-grids," *IEEE Transactions on Smart Grid*, vol. 4, no. 3, pp. 1597–1612, Sep. 2013.
- [33] R. Teodorescu, M. Liserre, P. Rodriguez, and F. Blaabjerg, "Grid converters for photovoltaic and wind power systems- Control of Grid Converters under grid faults". United Kingdom: John Wiley and Sons, 2011.
- [34] L. Zhang, L. Harnefors, and H.-P. Nee, "Power-synchronization control of grid-connected voltage-source converters," *IEEE Transactions on Power Systems*, vol. 25, p. 809–820, May 2010.
- [35] S. H. Mousavi, M. Davari, and H. J. Marquez, "An innovative event based filtering scheme using H1 performance for stochastic LTI systems considering a practical application in smart modernized microgrids," *IEEE Access*, vol. 7, pp. 48 138–48 150, Apr. 2019.

III. INTERNAL MODEL POWER SYNCHRONIZATION CONTROL OF A PV-BASED VOLTAGE SOURCE CONVERTER IN WEAK-GRID AND ISLANDED CONDITIONS

ABSTRACT

The power synchronization control strategy for grid-connected voltage-source converters (VSCs) provides an operation similar to synchronous machines. It is able to avoid the instability caused by a standard phase-locked loop in a weak ac-system connection. However, the non-minimum-phase phenomenon in the developed dynamics places a fundamental limitation on the ac system stability. This paper proposes a one-degree-of-freedom internal-model-based control methodology. It introduces a control approach to incorporate the dynamics of the system nominal model in the control structure. It also rectifies the unwanted effects of the right-half plane zeros. The explicit incorporation of the model enhances the tracking capabilities of the controller in a PV-based VSC. Besides, this article shows that a single-loop of control will suffice to regulate active and reactive power. Experimental results generated by a test rig are provided in order to show the effectiveness of the proposed control in normal operation. Alternatively, for fault cases (which endanger the safety of the personnel and devices), another experimental method based on hardware-in-the-loop (HIL) evaluations is used. To this end, detailed analytical verification of the proposed control structure using HIL evaluations on a PV-Based converter confirm the satisfactory performance of the proposed control architecture.

1. INTRODUCTION

The escalating application of more power electronic converters to interconnect and interoperate with power system utilities with active distribution systems require new power-control schemes. Renewable distributed energy resources (DERs) have provided several benefits such as improved consumer-level resiliency, lower losses, and reduced greenhouse gas emissions [1]. In this regard, the latest updated IEEE 1547—Standard for Interconnection and Interoperability of DERs with Associated Electric Power Systems Interfaces (version 2018) [2]—requires DERs to provide various grid supporting capabilities. Accordingly, all voltage-sourced converters (VSC) shall be capable of actively regulating the point of common coupling (PCC) voltage and ride-through abnormal voltage and frequency oscillations [3]. New power regulatory strategies to transients must be implemented.

Distributed generation based on wind-power and photovoltaics is replacing traditional large-scale generation facilities [4]. The conventional control structures implemented in the power converters mostly rely on the synchronization to a stable grid frequency supported by large rotating inertia. They are not inherently suitable in the paradigm of smart grids [5]. As a result, significant research effort is still devoted towards presenting new control schemes for power electronic converters to address the emerging demands in future smart grids [6]. A feasible approach is the control of power electronic converters to recreate the essential properties of synchronous machines [7]. They are designed to mimic the dynamic response of the synchronous machines and are classified as Virtual Synchronous Machines (VSM) [8]. Various advanced power-angle control techniques have already been proposed to regulate both the phase displacement angle and the voltage amplitude of an inverter [9,10]. Among them, power-angle synchronization control is mainly viewed upon as a combination of power-angle control and vector current control [11–13].

based on the product of current and voltage, several drawbacks are attributed to this control methods [14]. The significant disadvantages are: 1) the limited control bandwidth in the grid frequency synchronization method; and 2) the inability to limit the current flow in both methodologies [15]. In order to overcome the limitations, a hierarchical control structure with primary power control and inner voltage and current control loops is proposed [16]. This method has several features—e.g., such as flexibility and the capability to limit the current. However, incorporating the outer dc-bus controller with this architecture increases the order of the system and tuning the parameters becomes cumbersome which results in slower control response.

Another approach to power-angle control is the power-synchronization control, which is used in the VSC-based high voltage direct current (also known as VSC-base HVDC) system. The proposed control employs the phase angle and voltage magnitude to control active power and reactive power directly [17, 18]. The proposed method introduces a comprehensive small-signal model of the system, and the applied compensator is a conventional PI controller. This approach does not exhibit typical problems related to power-angle control, and this structure has a perfect nominal performance. However, the competing effects of alternating voltages and currents followed by phase angle variations [19] result in RHP zeros. Those RHP zeroes limit the robustness of the control. An analytic gain selection scheme has been utilized to make the design of the power synchronization control more robust. However, this methodology does not tackle the non-minimum phase problem of the transfer functions directly, and the problem may persist [20]. It is noteworthy that dealing with non-minimum dynamics need attention in control designs as they cause both stability and performance issues [21, 33, 34].

A similar power synchronization approach has been adopted in this paper. Because of utilizing that methodology, a robust internal model control has been applied, for eliminating the instabilities attributed to non-minimum phase phenomena. The incorporation of the model of the system in the regulator has long been discussed in control theory [21]. The

synchronization mechanism derived between synchronous machines (SMs) in ac systems leads to obtaining the transfer functions of active power versus load angle and reactive power versus voltage magnitude. The design of a sophisticated regulator is possible as long as these models are available—and control theories have proven that any regulator that is both successful and simple must be isomorphic with the controlled system. It means that deriving the system model is essential to be included in the control design [22].

According to internal model control (IMC) principle, to minimize the output error, while mapping the states of the system to that of the regulator, and obtaining a more straightforward control structure, the regulator must be isomorphic with the system being regulated [23]. The IMC principle has already been applied in several types of research on both single- and three-phase inverters—in both grid-connected and islanded modes of operation [24, 25]. Therefore, the IMC structure has been chosen. It is based on the separation of the “minimum phase” and “non-minimum phase” parts of the plant, which becomes proper by using a low-pass filter. A similar approach has also been utilized in dc-dc boost converters with non-minimum phase behavior in [26]. Small-signal stability analysis of an internal-model-based current and voltage controllers in an islanded inverter-based microgrid system illustrates a distinctive, stable performance compared to conventional PI-based controllers. It is also more robust against parameter uncertainties [27].

In the present work, the linearized dynamic equation between the active power versus the load angle and the linearized dynamic model of the reactive power versus voltage magnitude have been derived and considered. Looking at power synchronization control as a process similar to designing a feed-forward controller, an internal model with a one-degree-of-freedom structure is adopted in order to minimize the model-plant mismatch error. The RHP zeros in the active power versus load angle transfer function and those of the reactive power versus voltage cause the plant to exhibit an inverse step response. This issue adversely magnifies when RHP zeros move toward the origin as the voltage and the phase angle move to their extremes. Such a non-minimum phase phenomenon

will significantly limit the bandwidth of the closed-loop system. Consequently, a thorough investigation on factorizing the non-minimum phase part of the transfer function along with its effect on minimizing the mismatch error between the plant and the model is studied through an internal-model based control scheme. Also, the regulatory and tracking performance of the proposed control structure is examined. This new approach introduces an internal-model-based power synchronization method which:

- Reduces the effects of non-minimum phase phenomena and offers excellent tracking capabilities;
- Is capable of functioning during weak-grid conditions with no dedicated synchronization unit;
- Possesses FRT and current-limiting capabilities; and
- Can switch back and forth between islanded and grid-connected modes.

Moreover, error tuning rules based on the integral of the error squared (ISE) and the integral of the absolute error (IAE) and low-damping characteristics of the transfer function have been examined in order to minimize the mismatch error between the plant and the model of the system. By monitoring the cost function, the method that best applies to the experimental evaluations is the one that provides more reliable step responses and is easier to implement.

This paper is organized as follows. Section II describes the system configuration and investigates the effects of the non-minimum phase on the system stability. Section III introduces the proposed control structure and related plant model identifications. Section IV is about the stability analysis of the proposed method. Section V evaluates the performance of the controller through experimental results, and the last section concludes.

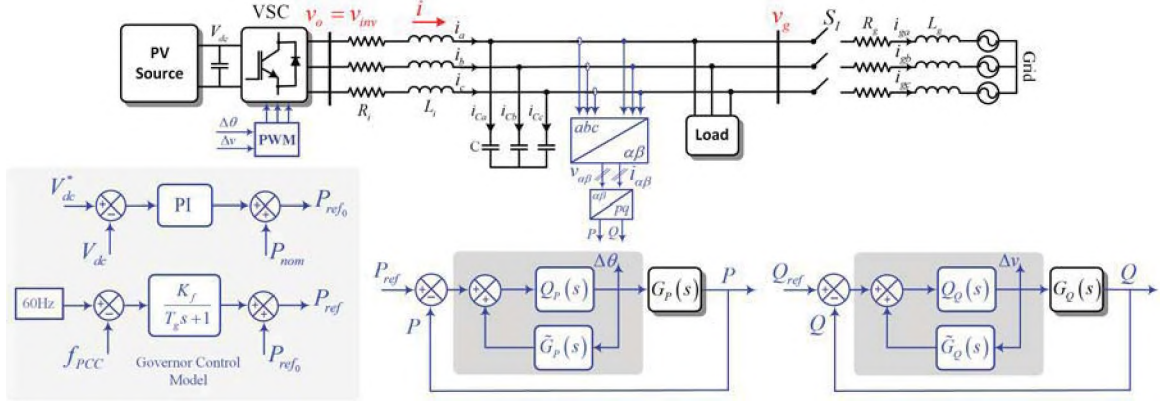


Figure 1. General overview of the system and the proposed controller

2. SYSTEM CONFIGURATION

In this section, the model of the system is derived based on the small-signal analysis of the power synchronization mechanism between synchronous machines. For the VSC system, the power synchronization control structure is designed as an LTI MIMO system so that the feedback of the active and reactive power as the inputs to control will minimize the estimation error.

2.1. POWER SYNCHRONIZATION CONTROL STRUCTURE

1 represents a simple system based on a grid-connected VSC with R_i and L_i as the overall inductance and resistance of the phase reactor and the ac system. The ac capacitor connected to PCC is neglected as it has inappreciable effect on the stability issues as long as the converter is not forced into voltage limitations [10]. v_{inv} is the VSC voltage vector and v_g is the PCC voltage. The power supplied by the VSC is the product of the vector PCC voltage and the vector current, i , of the phase reactor. The transfer functions of the active power based on the load angle and the reactive power based on the VSC voltage magnitude is derived from the KVL equations of the system. It will also include the

electromagnetic transients which is the characteristic of fast power electronic generators. In power synchronization method [18], a VSC is considered as a sinusoidal wave generator with the voltage magnitude of v_{inv} , see 1. The dynamic equations are described as

$$L \frac{d\mathbf{i}^s}{dt} = \mathbf{v}_{inv}^s - \mathbf{v}_g^s - R\mathbf{i}^s. \quad (1)$$

By transforming (1) into the rotating reference frame with the d -axis aligned with \mathbf{v}_g and considering the complex form of the voltage and current as

$$\mathbf{v}_{inv}^s = v_{inv} e^{j\omega t}, \quad \mathbf{i}^s = \mathbf{i} e^{j\omega t}, \quad \mathbf{v}_g^s = v_g e^{j\omega t}. \quad (2)$$

By considering that the dq reference frame of the ac-system leads that of the converter by the load angle θ and voltage magnitude does not exceed the voltage modulus and $\mathbf{v}_{inv} = v_{inv}^{ref} e^{j\theta}$, equation (1) can be divided into following component form

$$\begin{aligned} L \frac{di_d}{dt} &= v_{inv} \cos \theta - v_{gd} - Ri_d + \omega Li_q \\ L \frac{di_q}{dt} &= v_{inv} \sin \theta - Ri_q - \omega Li_d \end{aligned} \quad (3)$$

Now, by considering the inverter voltage magnitude to be constant, $v_{inv} = v_0$, and adding the small-signal deviations to i_d , i_q , and θ around the operating points, one obtains

$$\theta = \theta_0 + \Delta\theta, \quad i_d = I_{d0} + \Delta i_d, \quad i_q = I_{q0} + \Delta i_q. \quad (4)$$

The current is calculated as

$$\mathbf{i}_0 = \frac{\mathbf{v}_0 - \mathbf{v}_{g0}}{R + j\omega L}, \quad (5)$$

which has d - and q -components as

$$\begin{aligned} I_{d0} &= \frac{v_0 \sin \theta_0}{\omega L}, \\ I_{q0} &= \frac{v_{g0} - v_0 \cos \theta_0}{\omega L}. \end{aligned} \quad (6)$$

By neglecting the parasitic resistance R , as it has low effect on the current magnitude, the dq components of complex converter voltage at operating point, and its small-signal derivatives are calculated as

$$\mathbf{v}_0 = v_{d0} + \mathbf{j}v_{q0} = v_0 \cos \theta_0 + \mathbf{j}v_0 \sin \theta_0. \quad (7)$$

The linearized voltage deviation parts, Δv_d and Δv_q , along with linearized sine and cosine functions are also derived in Laplace form as

$$\begin{aligned} \Delta v_d &= sL\Delta i_d - \omega L\Delta i_q, \\ \Delta v_q &= sL\Delta i_q + \omega L\Delta i_d, \\ \sin(\theta_0 + \Delta\theta) &\approx \sin \theta_0 + \cos \theta_0 \Delta\theta, \\ \cos(\theta_0 + \Delta\theta) &\approx \cos \theta_0 - \sin \theta_0 \Delta\theta. \end{aligned} \quad (8)$$

The linearized form of (3) around the operating point of θ_0 by keeping the voltage magnitude, v_0 , constant yields the following equations.

$$\begin{aligned} L \frac{d\Delta i_d}{dt} &= -v_0 \sin \theta_0 \Delta\theta - R\Delta i_d + \omega L\Delta i_q, \\ L \frac{d\Delta i_q}{dt} &= v_0 \cos \theta_0 \Delta\theta - R\Delta i_q - \omega L\Delta i_d \end{aligned} \quad (9)$$

The instantaneous active power value from a VSC is given by $P = \text{Re}\{v\mathbf{i}^*\}$ with per unitized quantities. The linearized form of active power deviation is $\Delta P = \text{Re}\{\mathbf{i}_0^* \Delta \mathbf{v} + v_0 \Delta \mathbf{i}^*\}$ and the component form is:

$$\Delta P = \begin{bmatrix} I_{d0} \\ I_{q0} \end{bmatrix}^T \begin{bmatrix} \Delta v_d \\ \Delta v_q \end{bmatrix} + \begin{bmatrix} v_{d0} \\ v_{q0} \end{bmatrix}^T \begin{bmatrix} \Delta i_d \\ \Delta i_q \end{bmatrix}, \quad (10)$$

By taking the Laplace transformation of (9) and substituting in (10), the linearized dynamic relation between the active power and load angle is derived as

$$G_P(s) = \frac{\Delta P}{\Delta\theta} = \frac{b_{P0}s^2 + b_{P1}s + b_{P2}}{s^2 + a_1s + a_2}. \quad (11)$$

where the numerator coefficients are

$$\begin{aligned} b_{P0} &= \frac{1}{\omega L} \left(v_{g0} v_0 \cos \theta_0 - v_0^2 \right), \\ b_{P1} &= \frac{R}{\omega L^2} \left(v_{g0} v_0 \cos \theta_0 - v_0^2 \right), \\ b_{P2} &= \left(\omega L v_{g0} v_0 \cos \theta_0 - R v_{g0} v_0 \sin \theta_0 \right) / L^2 \end{aligned} \quad (12)$$

and the denominator coefficients are

$$\begin{aligned} a_1 &= 2R/L, \\ a_2 &= \left(R^2 + (\omega L)^2 \right) / L^2 \end{aligned} \quad (13)$$

Similarly for the reactive power, the linearized form of (3) around the operating point of v_0 by keeping the load angle magnitude, θ_0 , constant yields the following equations.

$$\begin{aligned} L \frac{d\Delta i_d}{dt} &= \Delta v \cos \theta_0 - R\Delta i_d + \omega L\Delta i_q, \\ L \frac{d\Delta i_q}{dt} &= \Delta v \sin \theta_0 - R\Delta i_q - \omega L\Delta i_d \end{aligned} \quad (14)$$

The instantaneous reactive power value from a VSC is given by $Q = \text{Im}\{vi^*\}$ with per unitized quantities. The linearized form of reactive power deviation is $\Delta Q = \text{Im}\{\mathbf{i}_0^* \Delta \mathbf{v} + v_0 \Delta \mathbf{i}^*\}$ and the component form is

$$\Delta Q = \begin{bmatrix} I_{d0} \\ -I_{q0} \end{bmatrix}^T \begin{bmatrix} \Delta v_q \\ \Delta v_d \end{bmatrix} + \begin{bmatrix} v_{d0} \\ v_{q0} \end{bmatrix}^T \begin{bmatrix} -\Delta i_q \\ \Delta i_d \end{bmatrix}. \quad (15)$$

By taking the Laplace transformation of (14) and substituting it in (15), the linearized dynamic relation between the reactive power and voltage magnitude is derived as

$$G_Q = \frac{\Delta Q}{\Delta v} = \frac{b_{Q0}s^2 + b_{Q1}s + b_{Q2}}{s^2 + a_1s + a_2}, \quad (16)$$

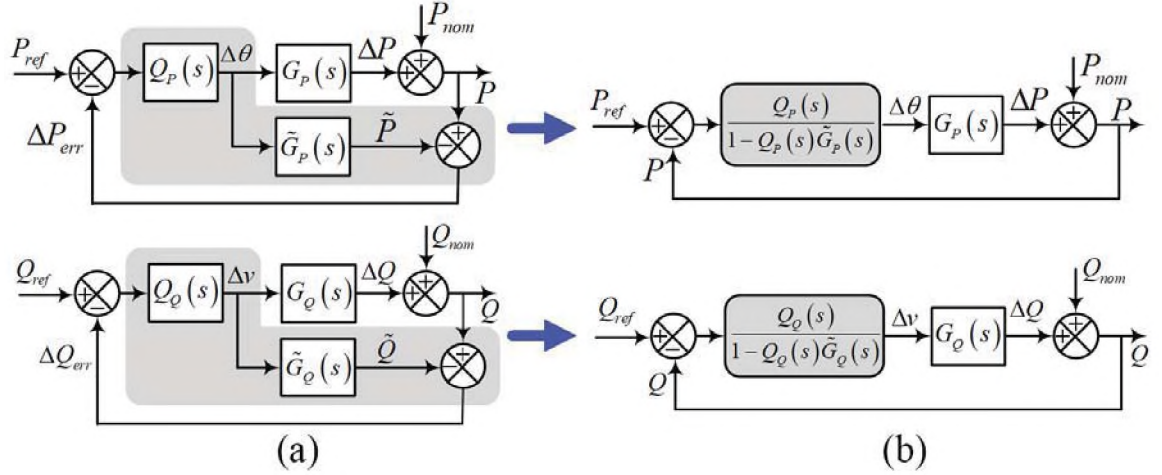


Figure 2. One dimensional IMC-active power and reactive power control structures

where

$$\begin{aligned}
 b_{Q0} &= \frac{1}{\omega L} (v_0 - v_{g0} \cos \theta_0), \\
 b_{Q1} &= \frac{R}{\omega L^2} (v_0 - v_{g0} \cos \theta_0), \\
 b_{Q2} &= (\omega L (2v_0 - v_{g0} \cos \theta_0) + Rv_{g0} \sin \theta_0) / L^2
 \end{aligned} \tag{17}$$

The denominator coefficients are the same as those of active power versus phase angle.

$$\begin{aligned}
 a_1 &= 2R/L, \\
 a_2 &= (R^2 + (\omega L)^2) / L^2
 \end{aligned} \tag{18}$$

The two transfer functions derived are the diagonal derivatives of the load flow Jacobian matrix—considering an inductive grid impedance. In such a configuration, the state variables are not explicitly available, and the problem in defining the state variables is the derivative terms of forcing function. The state variables can be selected to eliminate the derivative terms of the inputs [16]. In order to do so, the MIMO system with two inputs and two outputs is considered as follows.

$$\begin{cases} u_1 = \Delta \theta, \\ u_2 = \Delta v. \end{cases} \quad \begin{cases} y_1 = \Delta P, \\ y_2 = \Delta Q. \end{cases} \tag{19}$$

The four states of the system can be defined as

$$\begin{aligned}
 x_1 &= y_1 - \beta_0 u_1, \\
 x_2 &= \dot{y}_1 - \beta_0 \dot{u}_1 - \beta_1 u_1 = \dot{x}_1 - \beta_1 u_1, \\
 x_3 &= y_2 - \gamma_0 u_2, \\
 x_4 &= \dot{y}_2 - \gamma_0 \dot{u}_2 - \gamma_1 \dot{u}_2 = \dot{x}_3 - \gamma_1 u_2.
 \end{aligned} \tag{20}$$

By this choice of variables, dynamics of state variables are

$$\begin{aligned}
 \dot{x}_1 &= x_2 + \beta_1 u_1, \\
 \dot{x}_2 &= -a_2 x_1 - a_1 x_2 + \beta_2 u_1, \\
 \dot{x}_3 &= x_4 + \gamma_1 u_2, \\
 \dot{x}_4 &= -a_2 x_3 - a_1 x_4 + \gamma_2 u_2.
 \end{aligned} \tag{21}$$

Also, the coefficients are calculated as

$$\begin{cases}
 \beta_0 = b_{p0} \\
 \beta_1 = b_{p1} - a_1 \beta_0 \\
 \beta_2 = b_{p2} - a_1 \beta_1 - a_2 \beta_0
 \end{cases} , \tag{22}$$

$$\begin{cases}
 \gamma_0 = b_{q0} \\
 \gamma_1 = b_{q1} - a_1 \gamma_0 \\
 \gamma_2 = b_{q2} - a_1 \gamma_1 - a_2 \gamma_0
 \end{cases} .$$

This way, the state-space representation of the system is

$$\begin{aligned} \begin{bmatrix} \dot{x}_1 \\ \dot{x}_2 \\ \dot{x}_3 \\ \dot{x}_4 \end{bmatrix} &= \underbrace{\begin{bmatrix} 0 & 1 & 0 & 0 \\ -a_2 & -a_1 & 0 & 0 \\ 0 & 0 & & 1 \\ 0 & 0 & -a_2 & -a_1 \end{bmatrix}}_{\mathbf{A}_{PQ}} \begin{bmatrix} x_1 \\ x_2 \\ x_3 \\ x_4 \end{bmatrix} + \underbrace{\begin{bmatrix} \beta_1 & 0 \\ \beta_2 & 0 \\ 0 & \gamma_1 \\ 0 & \gamma_2 \end{bmatrix}}_{\mathbf{B}_{PQ}} \begin{bmatrix} u_1 \\ u_2 \end{bmatrix}, \\ \begin{bmatrix} y_1 \\ y_2 \end{bmatrix} &= \underbrace{\begin{bmatrix} 1 & 0 & 0 & 0 \\ 0 & 0 & 1 & 0 \end{bmatrix}}_{\mathbf{C}_{PQ}} \begin{bmatrix} x_1 \\ x_2 \\ x_3 \\ x_4 \end{bmatrix} + \underbrace{\begin{bmatrix} \beta_0 & 0 \\ 0 & \gamma_0 \end{bmatrix}}_{\mathbf{D}_{PQ}} \begin{bmatrix} u_1 \\ u_2 \end{bmatrix}. \end{aligned} \quad (23)$$

In this problem, as the state variables are not available for feedback and only the output is measurable, see 2, an observer-based controller, can estimate the state variables that are not directly accessible from the plant. For designing an observer-based controller, the conditions of controllability and observability should be verified. The rank of the controllability matrix, as well as that of the observability matrix, comes as 4. As both matrices are full-rank, it guarantees that the system is fully controllable and observable. As a consequence, designing an observer-based-controller is possible.

3. PROPOSED CONTROL ARCHITECTURE

The conventional power synchronization control (PSC) structure of a VSC is mainly composed of an integrator that converts the power error into a frequency deviation. Additionally, to provide the best voltage support for the system, the reactive power control loop is also required [9]. However, this control architecture cannot compensate for the non-minimum phase phenomenon due to the presence of RHP zeros (in both G_P and G_Q), which results in a limited bandwidth. In order to overcome this issue, a one-degree-of-freedom IMC provides a fractional order controller for an NMP system. It does so by incorporating the minimum phase part of the system model in the control loop. The internal model

principle is inherently an observer-based controller as it monitors the output error of the system. The gain in the IMC filter can also be regarded as the observer gain; it fastens the dynamics of the overall control structure.

3.1. INTERNAL MODEL CONTROL

Internal model control (IMC) originates from the classical control theory that in an open-loop control process, the precise tracking of the desired value, y_d , is only achieved when the controller embeds the inverse of the plant. This way, the transfer function of a typical system will be

$$T(s) = \frac{y(s)}{y_d(s)} = C(s) G(s) \xrightarrow{T(s)=1} C(s) = G^{-1}(s) \quad (24)$$

However, this control structure is not suitable for NMP systems as the inverse of a system with RHP zeros will end up in having RHP poles, and the controller will become unstable. Along with it, this system is not able to sustain noises and input/output disturbances to the system. In classical control theories, this problem is solved through feedback to the system. The control structure is used in order to minimize the tracking error of the system. Still, this closed-loop structure requires a complicated control structure typically to deal with NMP systems.

In this paper, both of the transfer functions of G_P and G_Q exhibit the NMP behavior—as they both have RHP zeros and the undesirable phenomenon becomes more pronounced when the RHP zeros are closer to the origin. If resistance R is neglected in (11) and (16), G_P and G_Q both will have a pair of resonant poles (i.e., $s = -\frac{R}{L} \pm j\omega$ located in the LHP)—and

they both will have two symmetrical zeros as

$$\begin{aligned} G_P(s) = 0 &\Rightarrow s = \pm\omega\sqrt{\frac{v_{0g} \cos \theta_0}{v_0 - v_{0g} \cos \theta_0}}, \\ G_Q(s) = 0 &\Rightarrow s = \pm\omega\sqrt{\frac{2v_0 - v_{0g} \cos \theta_0}{v_{0g} \cos \theta_0 - v_0}}. \end{aligned} \quad (25)$$

Critical RHP zeros in G_P happens when $v_{0g} \cos \theta_0 = 0$ and that is when $\theta_0 = \pm\pi/2$. However, in G_Q , RHP zeros close to the origin happen when $2v_0 - v_{0g} \cos \theta_0 = 0$ which lies in the reverse relation of Δv and ΔQ . By crossing the origin, the increase in voltage magnitude results in reactive power reduction. Therefore, the existence of RHP zeros are more critical in the reactive power loop. In 2(a), $\tilde{G}_P(s)$ and $\tilde{G}_Q(s)$ are considered as an exact estimation of the plants and the closed-loop transfer function for the active power and reactive power loops turns out to be

$$\begin{aligned} P(s) &= \frac{G_P(s) Q_P(s)}{1 + Q_P(s) (G_P(s) - \tilde{G}_P(s))} P_{ref}(s) \\ &+ \frac{1 - G_P(s) Q_P(s)}{1 + Q_P(s) (G_P(s) - \tilde{G}_P(s))} P_{nom}(s), \end{aligned} \quad (26)$$

and

$$\begin{aligned} Q(s) &= \frac{G_Q(s) Q_Q(s)}{1 + Q_Q(s) (G_Q(s) - \tilde{G}_Q(s))} Q_{ref}(s) \\ &+ \frac{1 - G_Q(s) Q_Q(s)}{1 + Q_Q(s) (G_Q(s) - \tilde{G}_Q(s))} Q_{nom}(s). \end{aligned} \quad (27)$$

The exact control is achievable when $G_P(s) = \tilde{G}_P(s)$ and $G_Q(s) = \tilde{G}_Q(s)$, that is when the model exactly matches with the plant and the above equations will simplify to

$$\begin{aligned} P(s) &= \underbrace{G_P(s) Q_P(s)}_{T_P(s)} P_{ref}(s) \\ &+ \underbrace{(1 - G_P(s) Q_P(s))}_{S_s(s)} P_{nom}(s), \end{aligned} \quad (28)$$

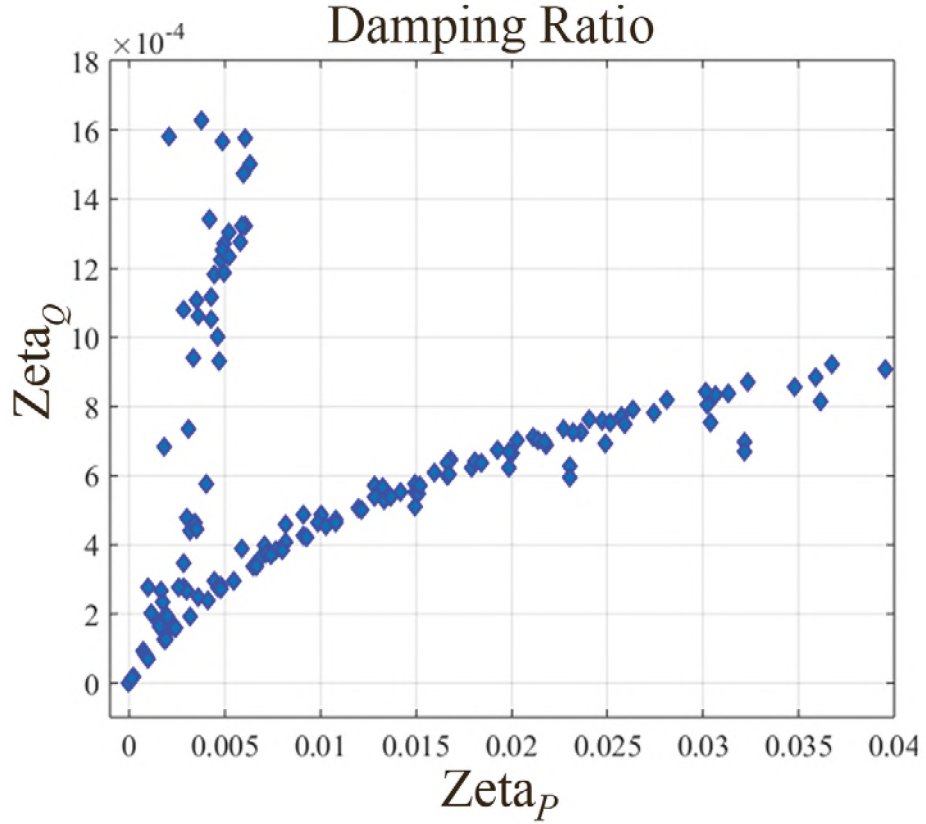


Figure 3. The damping ratio criteria for the numerator in G_P and G_Q

and

$$Q(s) = \underbrace{G_Q(s) Q_Q(s)}_{T_Q(s)} Q_{ref}(s) + \underbrace{(1 - G_Q(s) Q_Q(s))}_{S_Q(s)} Q_{nom}(s). \quad (29)$$

This way, the controller architecture is an open-loop structure that can quickly transform into a classical closed-loop structure—as shown in Figure 2(b). By constructing the model by the nominal values of the plant and writing the closed-loop form of the shaded area in Figure 2(a), the internal-model control structure will be

$$\begin{aligned} C_P(s) &= \frac{Q_P(s)}{1 - Q_P(s) \tilde{G}_P(s)}, \\ C_Q(s) &= \frac{Q_Q(s)}{1 - Q_Q(s) \tilde{G}_Q(s)}. \end{aligned} \quad (30)$$

By considering (28) and (29) and matching the model with the plant as $G_P(s) = \tilde{G}_P(s)$ and $G_Q(s) = \tilde{G}_Q(s)$, the exact control is only achievable when $Q_P(s) = G_P^{-1}(s)$ and $Q_Q(s) = G_Q^{-1}(s)$. However, as G_P and G_Q are NMP, the transfer function can be divided into invertible and non-invertible components as follows.

$$\begin{aligned} G_P(s) &= G_{P+}(s) G_{P-}(s), \\ G_Q(s) &= G_{Q+}(s) G_{Q-}(s), \end{aligned} \quad (31)$$

in which G_{P+} and G_{Q+} are the non-minimum-phase components, and G_{P-} and G_{Q-} are the minimum phase ones. In order to remove the NMP effect from the controller, the non-minimum-phase parts of the transfer function (i.e., $G_{P+(s)}$ and $G_{Q+(s)}$) are removed. Also, in order to make it proper, a filter is added to the minimum-phase part of the transfer functions, so ultimately, the control will look like

$$\begin{aligned} Q_P(s) &= f_P(s) G_{P-}^{-1}(s), \\ Q_Q(s) &= f_Q(s) G_{Q-}^{-1}(s). \end{aligned} \quad (32)$$

By substituting Q_P and Q_Q in (28) and (29), in order to achieve the perfect tracking, the following relations are held.

$$\begin{aligned} T_P(s) &= G_{P-}^{-1}(s) f_P(s) G_{P-}(s) G_{P+}(s) \\ &= f_P(s) G_{P+}(s), \\ T_Q(s) &= G_{Q-}^{-1}(s) f_Q(s) G_{Q-}(s) G_{Q+}(s) \\ &= f_Q(s) G_{Q+}(s), \end{aligned} \quad (33)$$

Furthermore, perfect tracking is achieved when

$$\begin{aligned} T_P(0) = 1 &\Rightarrow f_P(0) = G_{P+}^{-1}(0), \\ T_Q(0) = 1 &\Rightarrow f_Q(0) = G_{Q+}^{-1}(0), \end{aligned} \quad (34)$$

Therefore, the right choice for the filter can be as

$$f_P(s) = \frac{G_{P+}^{-1}(0)}{(1 + \lambda_P s)^n}, \quad f_Q(s) = \frac{G_{Q+}^{-1}(0)}{(1 + \lambda_Q s)^n}. \quad (35)$$

In the present work, three methods of factorization based on integral absolute error (IAE), integral square error (ISE) [17], and low damping (LD) stable zero analysis have applied to deal with the NMP behavior of the system.

3.1.1. IMC-IAE. This method selects the NMP components to minimize the integral of the absolute value of the mismatch error between the plant and the model. Equation (36) reveals this information.

$$\begin{aligned} J_{IAE_P} &= \int_0^{T_s} |P(t) - \bar{P}(t)| dt, \\ J_{IAE_Q} &= \int_0^{T_s} |Q(t) - \bar{Q}(t)| dt. \end{aligned} \quad (36)$$

As the system under discussion is of order two, it has only one RHP zero. Therefore, in order to minimize the cost function of J_{IAE} , the slowest zero of the system (i.e., $\frac{1}{\beta_P}$ and $\frac{1}{\beta_Q}$) is selected as the NMP component. Equation (37) is detailed as below

$$\begin{aligned} G_{P+}(s) &= \beta_P s + 1 \quad \text{Re}(\beta_P) > 0, \\ G_{P-}(s) &= \frac{\beta'_P s + 1}{s^2 + a_1 s + a_2}, \\ G_{Q+}(s) &= \beta_Q s + 1 \quad \text{Re}(\beta_Q) > 0, \\ G_{Q-}(s) &= \frac{\beta'_Q s + 1}{s^2 + a_1 s + a_2}, \end{aligned} \quad (37)$$

in which $\frac{1}{\beta'_P}$ and $\frac{1}{\beta'_Q}$ are the corresponding LHP zeros. In this scheme, the filter that is chosen comes as

$$f_P(s) = \frac{1}{1 + \lambda_P s}, \quad f_Q(s) = \frac{1}{1 + \lambda_Q s}. \quad (38)$$

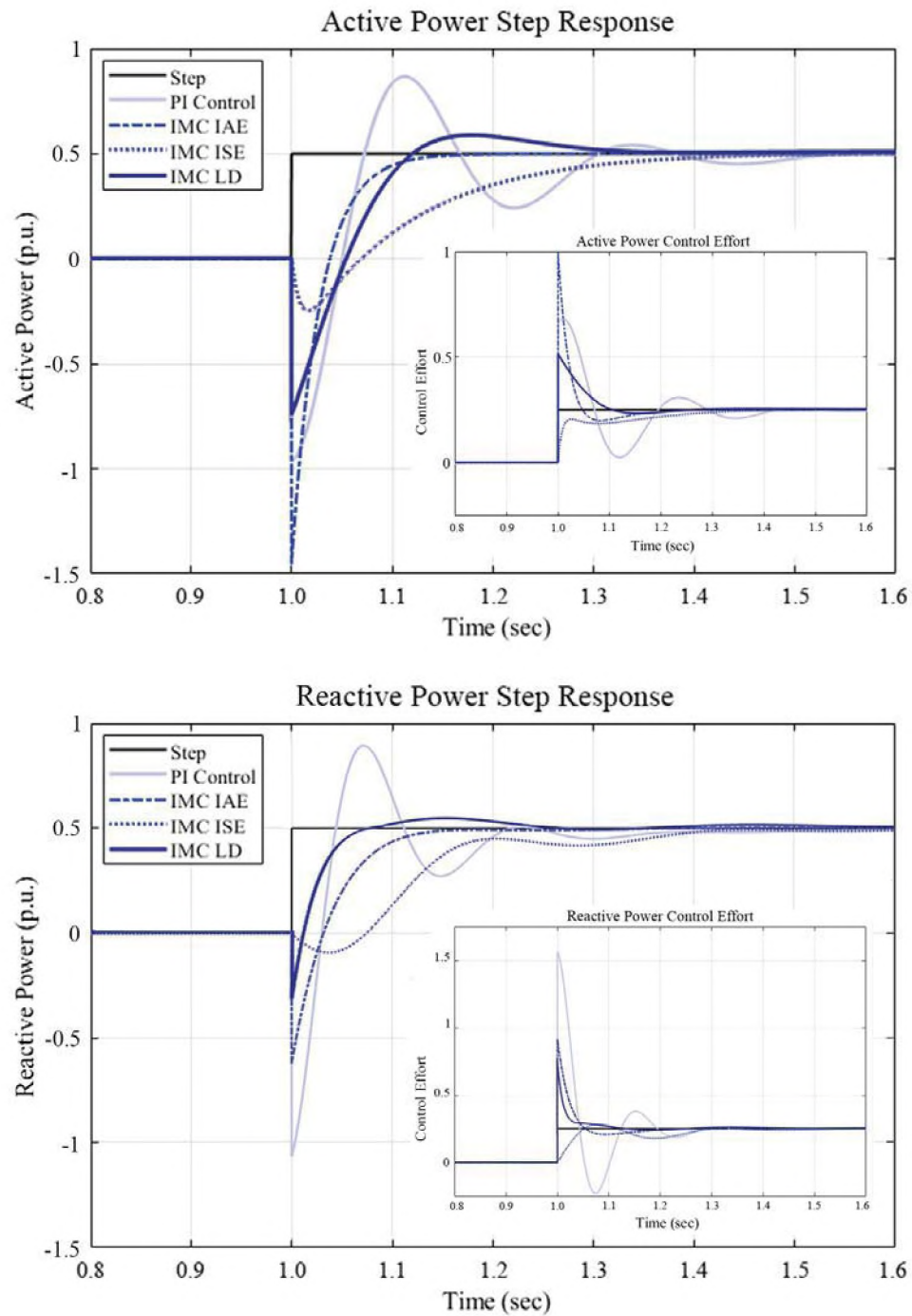


Figure 4. (a) Active-power and (b) Reactive-power step-response of the closed-loop system and the control effort— $E_0 = 1.0$ pu, $V_0 = 1.0$ pu, $\omega L = 1.0$ pu, $R = 0.05$ pu, and $\theta_0 = 50^\circ$

3.1.2. IMC-ISE. This method chooses the NMP components in order to minimize the integral of the square value of the mismatch error between the plant and the model as follows

$$\begin{aligned} J_{ISE_P} &= \int_0^{T_s} (P(t) - \tilde{P}(t))^2 dt \\ J_{ISE_Q} &= \int_0^{T_s} (Q(t) - \tilde{Q}(t))^2 dt \end{aligned} \quad (39)$$

Similarly, in order to minimize the cost function, J_{ISE} , the slowest zero of the system (i.e., $\frac{1}{\beta_P}$ and $\frac{1}{\beta_Q}$) is chosen as the NMP component. Equation (40) is detailed as below

$$\begin{aligned} G_{P+}(s) &= \frac{\beta_P s + 1}{-\beta_P s + 1} \quad \text{Re}(\beta_P) > 0, \\ G_{P-}(s) &= \frac{(\beta'_P s + 1)(-\beta_P s + 1)}{s^2 + a_1 s + a_2}, \\ G_{Q+}(s) &= \frac{\beta_Q s + 1}{-\beta_Q s + 1} \quad \text{Re}(\beta_Q) > 0, \\ G_{Q-}(s) &= \frac{(\beta'_Q s + 1)(-\beta_Q s + 1)}{s^2 + a_1 s + a_2}. \end{aligned} \quad (40)$$

In this scheme, the slowest zeros are compensated by a division by their corresponding LHP poles (i.e., $\frac{1}{-\beta_P}$ and $\frac{1}{-\beta_Q}$) to remove the effect of unstable zeros and it is also multiplied by the minimum phase component. Also, the following low-pass filters are selected to increase the phase margin.

$$f_P(s) = \frac{1}{1 + \lambda_P s}, \quad f_Q(s) = \frac{1}{1 + \lambda_Q s}. \quad (41)$$

3.1.3. Low Damping Stable Zero. Without disregarding $R, 3$, depicts the damping ratio of the numerators of $G_P(s)$ and $G_Q(s)$ for the range of $-\frac{\pi}{2} \leq \theta_0 \leq \frac{\pi}{2}$ and $0 \leq v_0 \leq 2v_{g0}$. This analysis shows that the numerators of $G_P(s)$ and $G_Q(s)$ are under-damped for the range of stable zeros, and apart from the NMP behavior, it exhibits oscillatory response which is undesirable when stable power production is a mandate. In order to minimize the effect of low-damping components of the system model, the whole numerator is regarded as

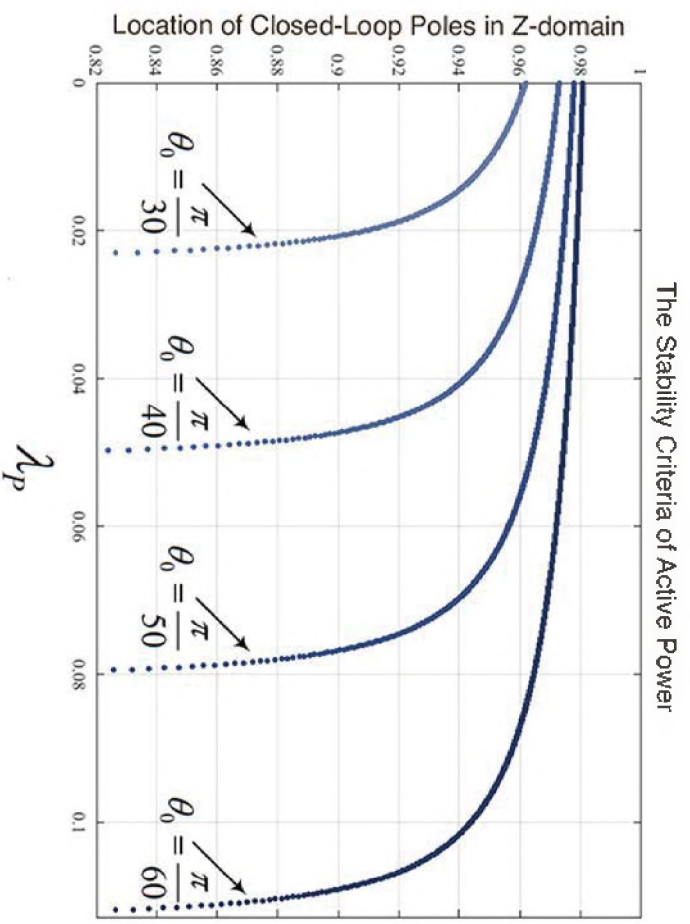
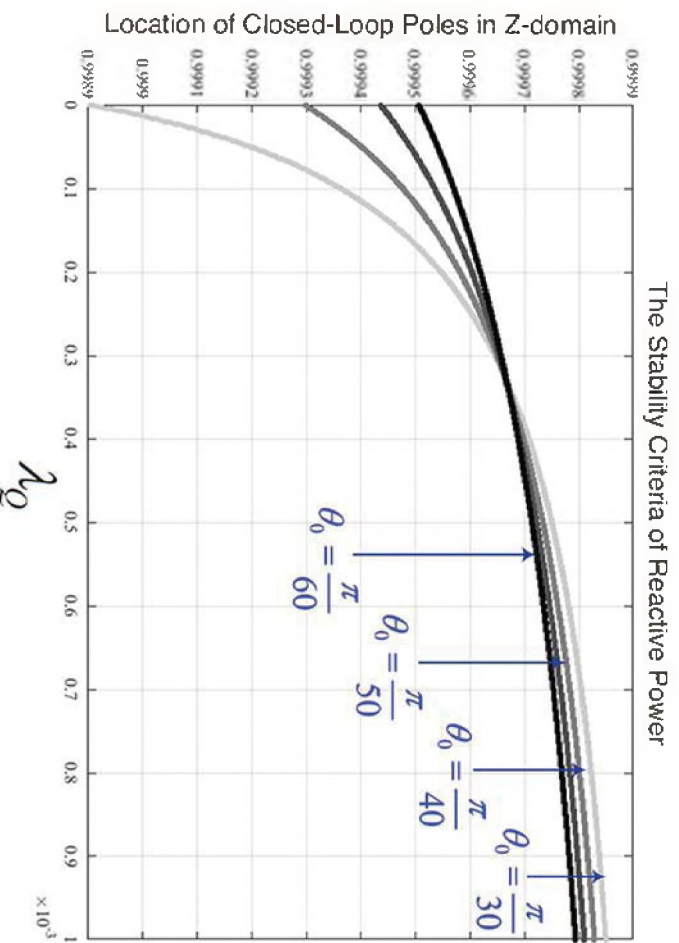


Figure 5. Stability criteria of the active-power and reactive-power based on λ_p, Q



non-minimum phase terms. Additionally, the system model is divided into

$$\begin{aligned}
 G_{P+}(s) &= b_{P0}s^2 + b_{P1}s + b_{P2}, \\
 G_{P-}(s) &= \frac{1}{s^2 + a_1s + a_2}, \\
 G_{Q+}(s) &= b_{Q0}s^2 + b_{Q1}s + b_{Q2}, \\
 G_{Q-}(s) &= \frac{1}{s^2 + a_1s + a_2},
 \end{aligned} \tag{42}$$

In which, G_{P+} and G_{Q+} are the NMP parts and the denominators are the minimum-phase parts. Since the order of the NMP component of the system has increased, the IAE optimization rule is adopted to minimize the error detailed in (43).

$$\begin{aligned}
 J_{IAEP} &= \int_0^{T_s} |P(t) - \tilde{P}(t)| dt, \\
 J_{IAEQ} &= \int_0^{T_s} |Q(t) - \tilde{Q}(t)| dt.
 \end{aligned} \tag{43}$$

Besides, in order to make the control transfer function proper, a higher-order filter is applied as follows

$$f_P(s) = \frac{1}{(\lambda_P s + 1)^2}, \quad f_Q(s) = \frac{1}{(\lambda_Q s + 1)^2}. \tag{44}$$

For the final choice of the control structure, the low damping stable zero method (IMC-LD) has primarily been chosen because of the following three reasons.

- This method does not require to precisely find the RHP zeros of the transfer function as it considers the whole numerator to be NMP.
- It eliminates the power system variables of v_0 , v_g , and θ_0 —whose alterations play a vital role in producing the RHP zeros.
- By proper choice of the filter, it shows a better tracking capability compared to the two other IMC methods (depicted in 4).

4. STABILITY ANALYSIS

The stability of the power synchronization method is dependent on the locations of poles and zeros of the small-signal transfer functions. As mentioned before, the low damping ratio in the numerators in G_P and G_Q is not dependent on the parameters of the system, while it is directly related to the parameters of the power system like v_0 , v_{g0} , and θ_0 . A suitable control structure can compensate the system's RHP zeros. In order to dampen the grid-frequency resonant poles, a high-pass filter has been adopted in [18]; it is able to act as an "active resistor" and to improve the stability margin of the system.

The system's RHP zeros' effect has not been mitigated in the closed-loop transfer function. An analytic gain selection method has been applied to give sufficiently large stability margins to the system in [1] to make power synchronization robust. The selection of the gains mainly depends on the active power complex-transfer-function between $\Delta\theta$ and Δi . However, the minimum gain, which is recommended and proposed in the method, depends upon the variations of the system parameters, i.e., R and L and those of power system, i.e., i , ω , v_0 , and v_g . Neglecting the fact that the active power and reactive power are coupled in nature might limit the robust performance of the proposed controller in large-signal oscillations.

As depicted in 3, the locations of oscillatory RHP zeros are mostly dependent on the phase angle θ_0 in moderate voltage ranges. The NMP systems are generally difficult to control as the RHP zeros introduce internal instabilities to the system. In the IMC approach, the filter design incorporates more tunable variables in the case of NMP systems as compared to minimum-phase systems. Furthermore, the delay created in the response of the NMP system is rectified. Figures. 4 shows the step response of IMC based control structures in comparison to conventional PI controller when θ_0 is relatively large (50°). The results show that the IMC scheme shows at least 30% improvement in settling time.

By factorizing the low-damping numerator as the non-minimum phase part of the transfer function, the rise-time and the peak are reduced compared to other control methodologies. Also, as factorizing the whole numerator is independent of finding the zeros of the system, this control methodology has been adopted in order to examine the control performance experimentally. One more important effect of the IMC control by factorizing the low-damping numerator is to produce a non-oscillatory control effort—which shapes the modulating voltage vector. This feature is significantly essential when the converter performs as a virtual synchronous machine, and the VSC frequency oscillations with regards to changes in active power set-point should be curbed. As the system model is embedded in the control structure, the range of applicable λ cannot be independent of the system's parameters. By applying Routh's stability criterion, λ_P and λ_Q limits will be achieved based on the system parameters, which are

$$\begin{aligned}\lambda_P &> \frac{R}{2\omega} \left(v_{g0}v_0 \cos \theta_0 - v_0^2 \right), \\ \lambda_Q &> \frac{R}{2\omega} \left(v_0 - v_{g0} \cos \theta_0 \right).\end{aligned}\tag{45}$$

By considering R to be negligible, the above conditions shrink to $\lambda_P > 0$ and $\lambda_Q > 0$. However, $\lambda_{P,Q}$ should be curtailed based on the stability criterion of discretized systems. In order to quantify the limits of $\lambda_{P,Q}$, the delay term caused by the PWM switchings and sensors have been generally considered in one term in the feedback. Padé approximation of the models has been employed to write the open-loop transfer functions [30]. The exponential transfer function is approximated by a rational transfer function, considering that the system model is exactly equal to the plant. Then, the final plant transfer function turns out to be

$$\begin{aligned}G_{P-ol} &= \frac{(b_{P0}s^2 + b_{P1}s + b_{P2}) \left(e^{-sT_{P_{samp}}} \right)}{(\lambda_P^2 - b_{P0})s^2 + (2\lambda_P - b_{P1})s + (1 - b_{P2})} \\ &\approx \frac{(b_{P0}s^2 + b_{P1}s + b_{P2}) \left(1 - sT_{P_{samp}} \right)}{(\lambda_P^2 - b_{P0})s^2 + (2\lambda_P - b_{P1})s + (1 - b_{P2})}\end{aligned}\tag{46}$$

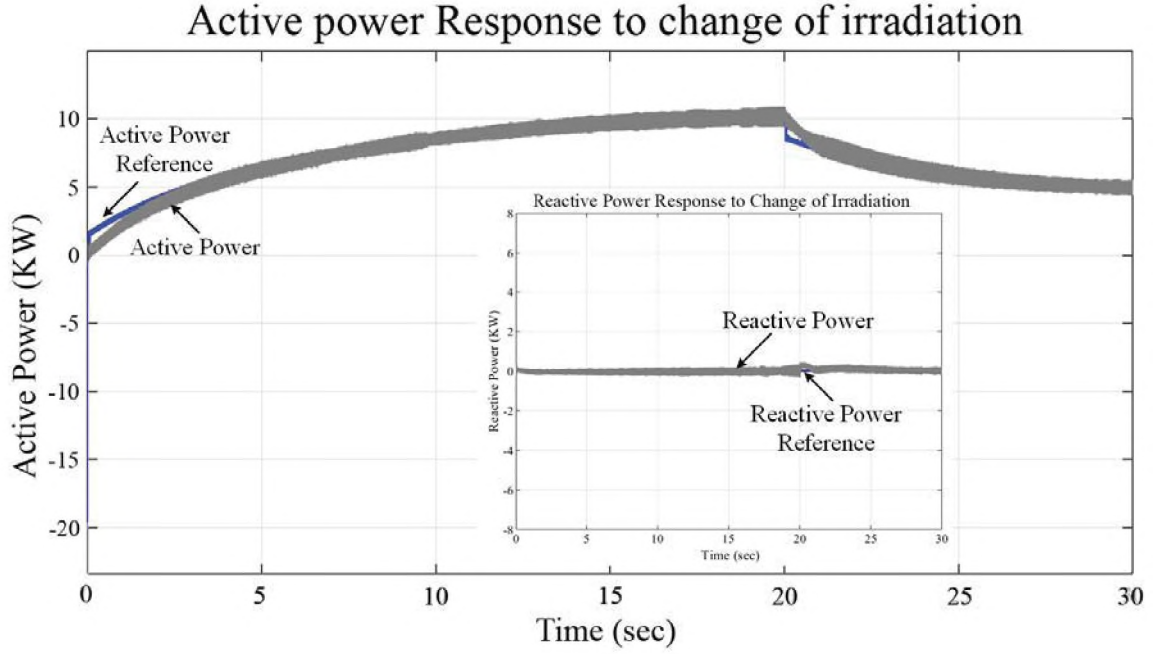


Figure 6. Active and reactive power response to irradiation changes

$$\begin{aligned}
 G_{Q-ol} &= \frac{(b_{Q0}s^2 + b_{Q1}s + b_{Q2}) \left(e^{-sT_{Q_{samp}}} \right)}{\left(\lambda_Q^2 - b_{Q0} \right) s^2 + (2\lambda_Q - b_{Q1}) s + (1 - b_{Q2})} \\
 &\approx \frac{(b_{Q0}s^2 + b_{Q1}s + b_{Q2}) \left(1 - sT_{Q_{samp}} \right)}{\left(\lambda_Q^2 - b_{Q0} \right) s^2 + (2\lambda_Q - b_{Q1}) s + (1 - b_{Q2})}
 \end{aligned} \tag{47}$$

The numerical solution of the closed-loop transfer functions will result in finding a range of the stable poles of the system within the unit circle. Finding the stable poles will furnish a range of $\lambda_{P,Q}$ in the IMC, which will stabilize the system. The stability criteria of the active power and reactive power are represented in Figure. 5. As the poles of both systems are within the unit circle, $\lambda_{P,Q}$ is selected to replace the poles closer to the origin, and this way, the system remains stable. However, the range of available λ_Q is more limited than that of λ_P , which is again related to the inverse relation between the reactive power and the voltage. Finding suitable criteria for $\lambda_{P,Q}$ is essential to adjust the speed of the controller, which is directly related to the inertial reaction of the controller to disturbances.

Table 1. System Parameters

Parameter	Value	Parameter	Value
V_{dc}^*	400 V	V_g	170 V
S_{Rating}	15 kVA	R_i	0.1 Ω
f	60 Hz	L_i	5e ⁻³ H
K_{pPI}	40	R_g	0.1 Ω
K_{iPI}	600	L_g	5e ⁻⁴ H
K_f	2000	T_g	0.003
λ_p	1e ⁻⁶	λ_q	1e ⁻⁴

5. EXPERIMENTAL RESULTS

This section shows the effectiveness of the proposed control. In this regard, in order to reveal the practicality of the introduced controller, first, it has been tested on a single converter prototype. Second, experimental examinations should have a compatible setup as VCSs need to feed faulty networks since the internal-model-based control is required to be robust to withstand grids with faults. Therefore, conducting such tests is almost impossible in our currently available laboratory facilities due to the considerations related to the safety of devices and personnel. Alternatively, the controller performance and response during faults (in the weak-grid conditions) have to be assessed by hardware-in-the-loop (HIL) to show the validity of the proposed control in this research, as detailed in [33]. HIL-based evaluations make various, complex testing scenarios and incorporation of several disturbances/faults in the system possible (for creating real-world dangerous test cases).

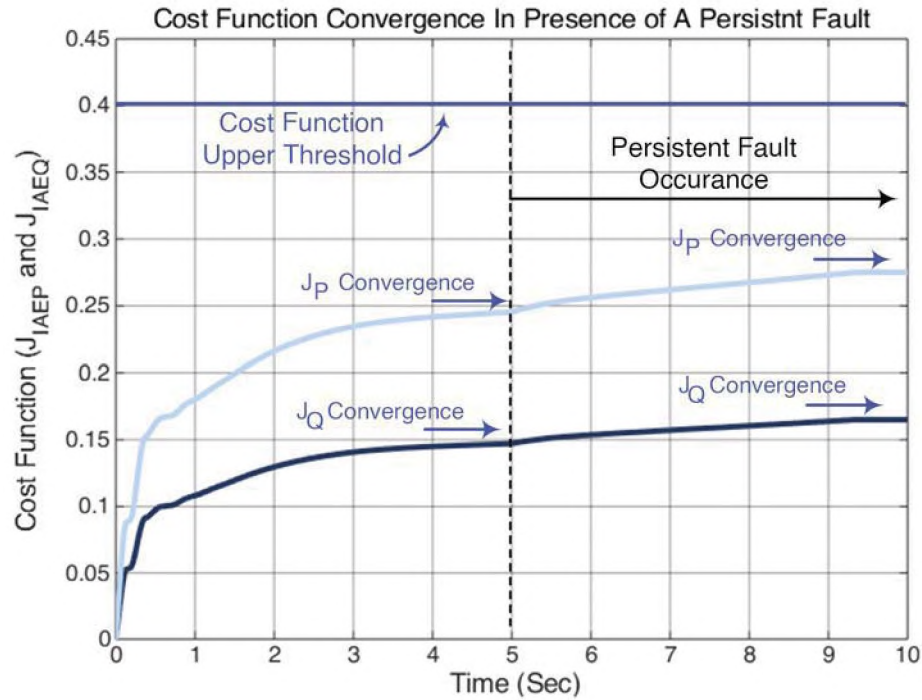


Figure 7. The cost function monitoring during persistent fault occurrence

5.1. EXPERIMENTAL EVALUATION OF THE CONTROLLER BY USING A CONVERTER

Here, the viability of implementing the proposed control is tested during normal operation. To this end, a test rig, which is based at Georgia Southern University, has been used in order to conduct experimental evaluations of the closed-loop system. Figure. 8 shows the setup, which has the same parameters stated in Table 2. It has been utilized to test the converter's performance when the VSC is normally being operated for active/reactive power changes. The VSC is based on intelligent power modules from SEMIKRON, including insulated gate bipolar transistors (IGBTs) built by "SKM 50 GB 123 D" modules, "SKHI 21A (R)" gate drives, and protection circuitry. The switching frequency has been set to 8.1 kHz . The ac-side filter inductance and resistance are 5.0 mH and 0.1Ω , respectively, with an SCR around 3.

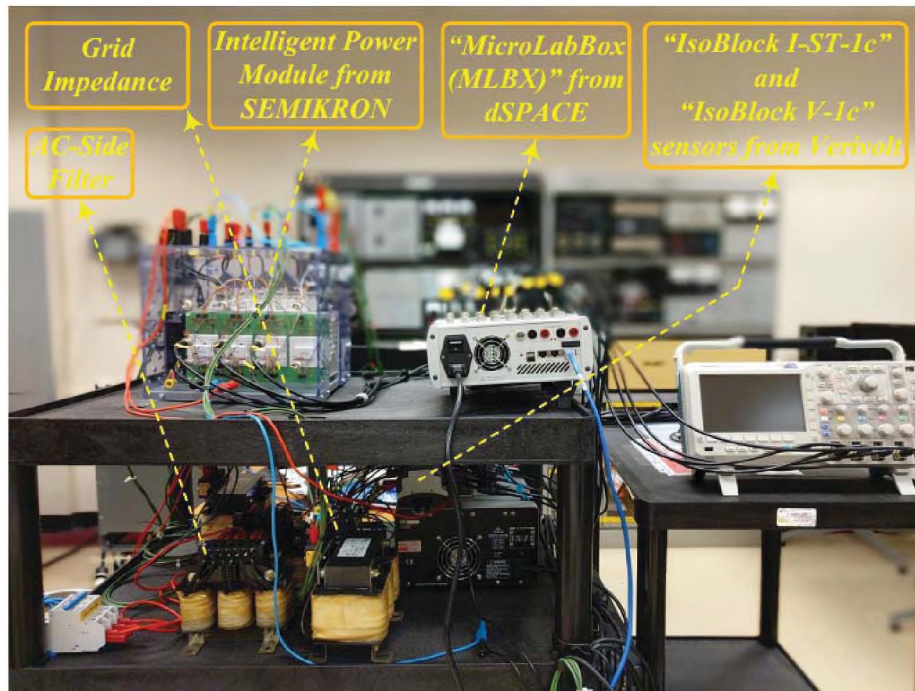


Figure 8. Test rig used in the experiments

The dc-link capacitance and inductance are 2.04 mF and 1.50 mH, respectively. The three-phase converter is operated at 30 A and 208 V (line-to-line rms) and 400 V (dc).

“IsoBlock I-ST-1c” current sensors and IsoBlock V-1c” voltage sensors from Verivolt Company measure the currents and the voltages, respectively. “MicroLabBox (MLBX)” from dSPACE connect the VSC under test to the measurement and drive printed circuit boards. A dual-core, 2 GHz “NXP (Freescale) QorIQ P5020” real-time processor has executed and run the proposed control algorithm. “Xilinx Kintex-7 XC7K325T” field-programmable gate arrays (also known as FPGAs) have generated the pulse width modulation (PWM) signals connected to digital inputs/outputs (I/Os). The MLBX interface board consists of eight 14-bit, 10 megasamples per second (Mps), differential analog-to-

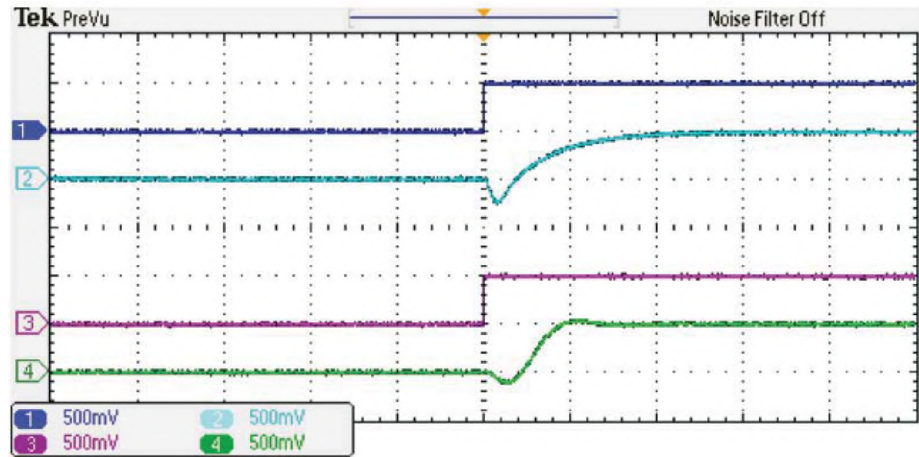


Figure 9. Experimental results associated with the applied active/reactive power changes; the actual active power, its reference, the actual reactive power, and its reference have been shown by traces in blue, cyan, magenta, and lawn green respectively, with 0.5 pu/div (for both active and reactive power, whose “pu” values have been noted at the left-bottom corner of the figures) and 200 ms/div

digital channels to interface the measured signals to the controller (with the functionality of free-running mode). The Real-Time-WorkShop in the MATLAB Simulink environment has generated the software code.

Figure. 9 shows the experimental result of the closed-loop system and demonstrates the effectiveness of the proposed controller quite well. The experiments reveal a good agreement with simulations as well.

5.2. HIL TESTING FOR FAULT CASES

In order to examine the closed-loop system under fault cases, which raise concerns about the safety of devices and personnel, HIL testing has been used alternatively here. Due to the value that it offers in research, education, and manufacturing—as an experimental method and testing procedure—FPGA-based HIL systems have found a wide range of applications in smart grids, power systems, power electronic systems, aircraft and mis-ile industries, automotive industry, motion control, mechatronics, and robotics.

Because of providing ultra-high-fidelity simulations. It is regarded as an alternative testing approach. FPGA-based HIL examination is currently revolutionizing test engineering in many disciplines, including, but not limited to, vehicle and communication systems, smart grids, robotics, aerospace, process control, and naval warships—and even structures in the civil engineering sometimes (see [21, 33, 34] and references therein).

In this subsection, Xilinx System Generator for DSP has been applied to test and implement the discretized control structure on a development board for the Xilinx Zynq-7000 SoC (Zedboard). This design tool provides a realistic environment to verify the interactive performance of control algorithms implemented in the hardware with the rich simulation and verification environment offered by PLECS and Simulink. The optimized control structure is realized through a schematic block method with floating number representation and VHDL programming. The HIL is realized through the joint test action group (JTAG) co-simulation interface, which requires minimum resources on FPGA fabric. The FPGA clock frequency is selected to be around 120 MHz—at which all modules are found to be compatible with each other. Optimized pipelining stages are realized by dividing registers with minimum latencies. The results of the hardware co-simulation (which has been implemented on the board) have been extracted on the scope by utilizing a DAC module.

Table 2. Parameters of Figure. 9

Parameter	Value	Parameter	Value
S_n^1	10.81 kVA	SCC ³	32.42 kVA
L_1/R_1	5 mH/0.1 Ω	f_s^4	8.1 kHz
V_{DC}^2	400 V	$V_{PCC_{Line-to-Line\ rms}}^2$	208 V

¹ Nominal VA ³ PCC Short Circuit Capacity for Calculating SCR

² Nominal Value ⁴ Switching Frequency

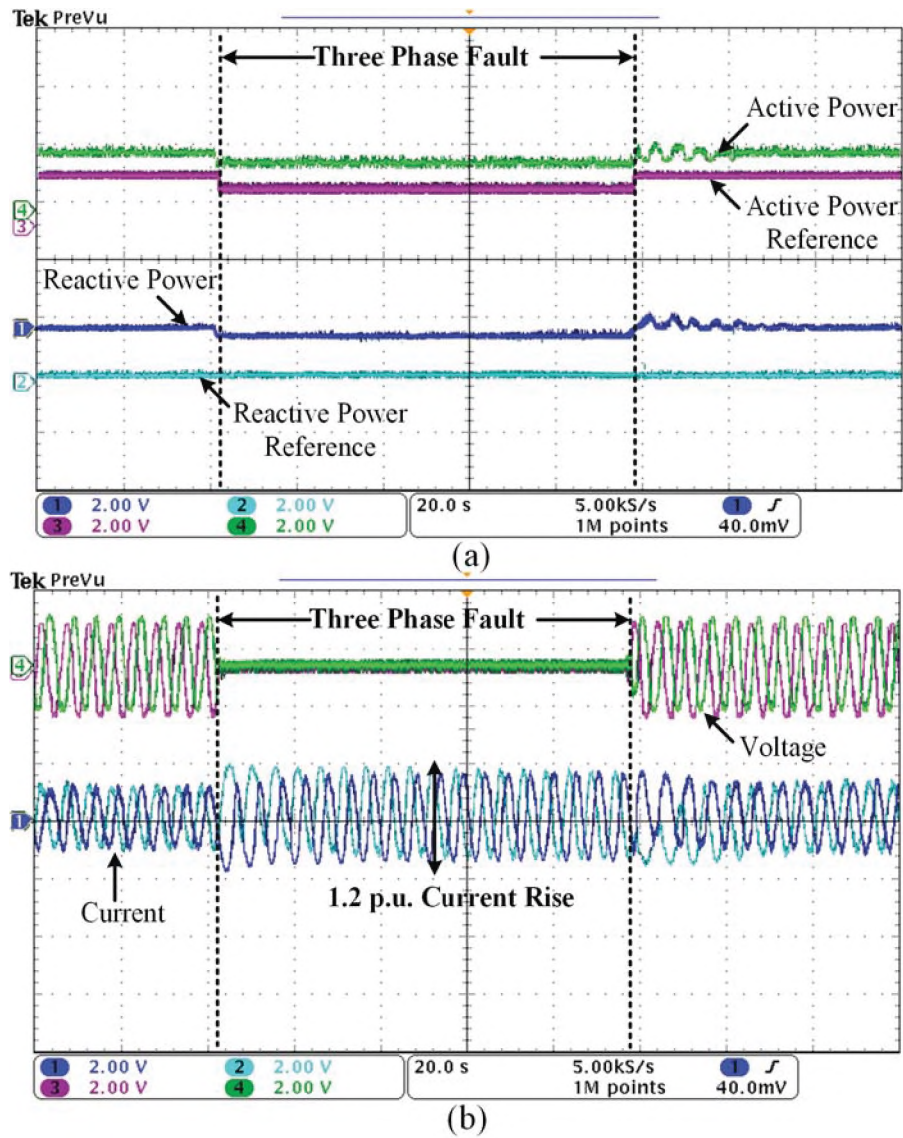


Figure 10. Operation under three-phase voltage fault (a) active and reactive power response to fault (b) PCC voltage and current response—each small division for active power is 2 kW, for reactive power is 1 kW, for voltage is 21 V, and for current is 5 A

5.3. DC-BUS CONTROL AND IMPROVEMENTS IN NON-MINIMUM PHASE BEHAVIOR

In this paper, a PV-based VSC has been studied. In order to emulate a virtual synchronous generator, a dual control loop is applied to the dc-bus. The primary control loop is based on the Power Point Tracking (PPT) of a PV-based dc-bus to extract the maximum available active power for optimal usage of a PV-bus. In the secondary control loop, a linear governor model has been adopted to emulate a virtual synchronous machine and use the frequency information at PCC to control the power supplied by the generator during loading conditions. The frequency measurement at PCC is not used in resynchronization. The intermittent and slow nature of PV-based dc-bus calls for a control structure with fine tracking capabilities. The tracking capability of the controller has been demonstrated in 4. The HIL simulation results show as the irradiation changes to half; the active power reference also changes, and the IMC control loop also tracks the reference power with no steady-state error. Likewise, in the reactive power loop, the actual value tracks the reference and keeps the reactive power zero. This Scenario is examined in a weak grid with $SCR = 2$.

5.4. FRT AND CURRENT-LIMITING CAPABILITIES IN WEAK-GRID BEHAVIOR

In order to further verify the FRT capabilities of the proposed control structure, the operation has been examined in grid-connected mode of operation under a three-phase fault condition. A 10kW resistive load has been activated, the upper limit of the active power set-point is also selected to be 10 kW, and the reactive power set-point is zero. Accurate power tracking for both active and reactive power is achieved while the coupling of active and reactive power dynamics is minimum. The voltage does not show any significant fluctuations as the magnitude of the voltage is fed forward to the reactive power control loop. In order to monitor the controller performance during a persistent fault, the IAE cost function is observed. As shown in Figure. 7, the cost functions of J_P and J_Q do not surpass the upper threshold even though the voltage magnitude has dropped to 0.1 pu. The limited cost function helps curb the current during the fault condition.

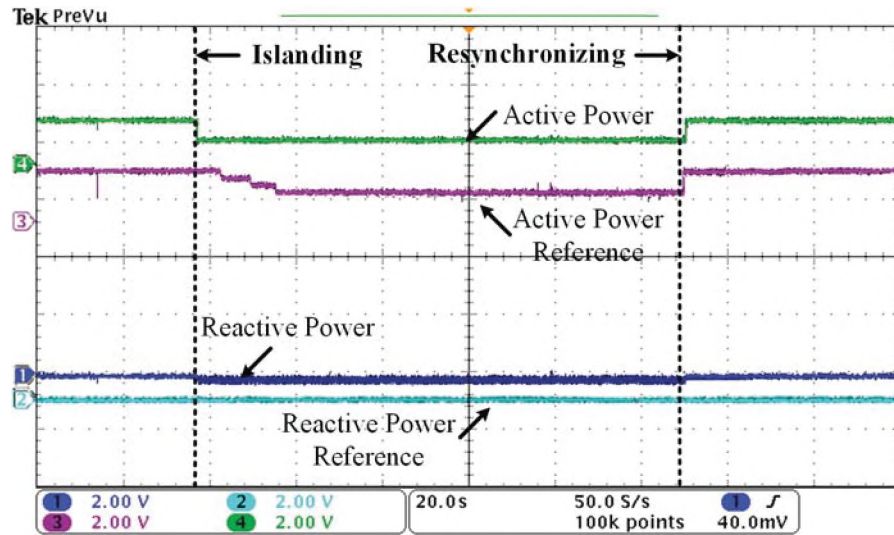
Figure. 10 shows the measured results of active and reactive power along with the VSC current and PCC voltage, when three-phase voltage drops to 0.1 pu for 0.5 s in the weak-grid condition where $SCR = 1$. The results show that the active power reference and the actual active power both drop during the fault.

Nonetheless, the converter continues to inject current to the grid. During voltage re-recovery, the small swing can be observed when the system is re-synchronized to the network. Additionally, the current rise is maintained within 1.2 pu due to the error minimization process in the control structure—which keeps the system's parameters bounded.

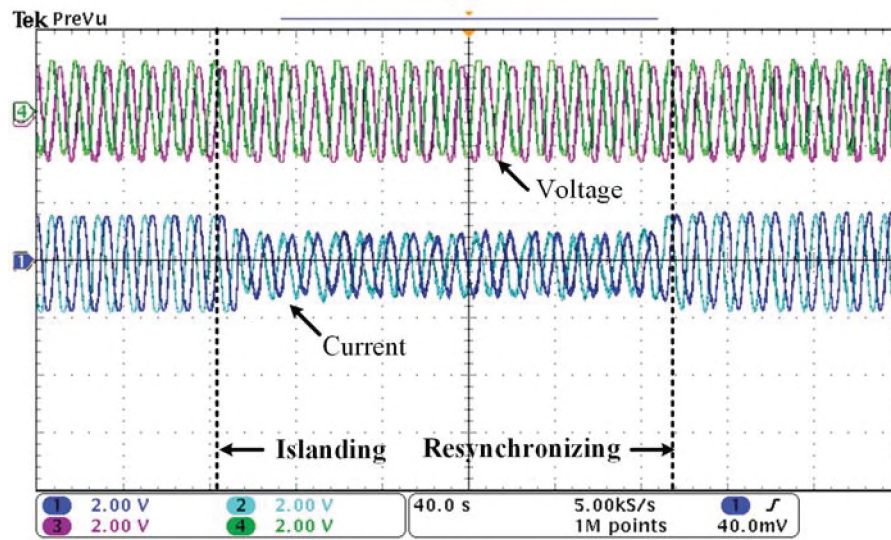
5.5. OPERATION IN ISLANDED MODE

The performance of the proposed control structure is also examined during the islanded mode of operation, and it has been shown in Figure. 11. A conventional under/over voltage (UVP/OVP) technique has been adopted as an islanding detection method—which is a popular method for all grid-connected PV inverters.

The detection of various types of abnormal conditions is monitored through sensing the grid voltage of v_g . In case the voltage starts to exit the limits imposed by the relevant standards [1], an islanding signal turns switch “ S_I ” off and disconnects the converter from the grid to start operating in islanded mode. The isolation is detected immediately, and the none-detection-zone (NDZ) has not been considered. Unlike conventional power control methods, the reactive power loop operates as the converter is disconnected from the grid. The reactive power loop well maintains the voltage magnitude and keeps the voltage magnitude bounded while minimizing the error in the control structure.



(a)



(b)

Figure 11. Operation under three-phase voltage fault (a) active and reactive power response to fault (b) PCC voltage and current response—each small division for active power is 2 kW , for reactive power is 1 $kvar$, for voltage is 21 V, and for current is 5 A

The detection of various types of abnormal conditions is monitored through sensing the grid voltage of v_g . In case the voltage starts to exit the limits imposed by the relevant standards [1], an islanding signal turns switch “ S_I ” off and disconnects the converter from the grid to start operating in islanded mode. The isolation is detected immediately, and the none-detection-zone (NDZ) has not been considered.

Unlike conventional power control methods, the reactive power loop operates as the converter is disconnected from the grid. The reactive power loop well maintains the voltage magnitude and keeps the voltage magnitude bounded while minimizing the error in the control structure.

6. CONCLUSIONS

In this paper, the internal model principle has been applied to the small-signal model representation of the power synchronization method. Therefore, because of the existing non-minimum phase dynamics, its impediments of the corresponding active and reactive power transfer functions have been rectified by considering the LD stable zeros as the non-minimum phase and eliminating their effect by applying the IAE method and cost minimization. A thorough stability analysis, the verifications of the proposed controller operation—during faulty and weak-grid conditions—and its performance in switching grid-connected modes of operation endorse the adequate functionality of the proposed controller. The internal model principle applied in this paper is simple to design and requires only one parameter to be tuned. The outer dc-bus controller, which is composed of an MPP loop and a governor droop emulator, forces the system to perform closer to a conventional synchronous machine, so the integration of such a system to traditional power generating network is more favorable.

Experimental results associated with the normal operation and FPGA-based HIL testing associate with the fault test cases have been provided in order to show the practicality and effectiveness of the introduced internal-model-based control.

REFERENCES

- [1] B. Enayati, "Challenges and solutions of renewable der integration," *T&D World*, March 2020.
- [2] "Standard for interconnection and interoperability of distributed energy resources with associated electric power systems interfaces," *IEEE Standards Coordinating Committee 21*, IEEE P1547 Draft 2, June 2015.
- [3] B. Enayati, "Protection of photovoltaic and wind generators," *PES T&D*, 2012, pp. 1–8, 2012.
- [4] O. Ogunrinde, E. Shittu, and K. K. Dhanda, "Investing in renewable energy: Reconciling regional policy with renewable energy growth," *IEEE Engineering Management Review*, vol. 46, pp. 103–111, Dec 2018.
- [5] J. Matevosyan, S. Sharma, S.-H. Huang, D. Woodfin, K. Ragsdale, S. Moorthy, P. Wattles, and W. Li, "Proposed future ancillary services in electric reliability council of texas," *IEEE Eindhoven PowerTech*, pp. 1–6, 2015.
- [6] S. M. Kaviri, H. Hajebrahimi, M. Pahlevani, P. Jain, and A. Bakhshai, "A new power flow control approach for power converters in singlephase microgrids," *IEEE Applied Power Electronics Conference and Exposition (APEC)*, pp. 1420–1427, 2018.
- [7] R. Rosso, S. Engelken, and M. Liserre, "Robust stability analysis of synchronverters operating in parallel," *IEEE Transactions on Power Electronics*, vol. 34, pp. 11 309–11 319, November 2019.
- [8] O. Mo, S. D'Arco, and J. A. Suul, "Evaluation of virtual synchronous machines with dynamic or quasi-stationary machine models," *IEEE Transactions on Industrial Electronics*, vol. 64, pp. 5952–5962, July 2017.

- [9] B. T. Ooi and X. Wang, "Voltage angle lock loop control of boost type pwm converter for hvdc application," *IEEE Transactions on Power Electronics*, vol. 5, pp. 229–235, April 1990.
- [10] ———, "Voltage angle lock loop control of boost type pwm converter for hvdc application," *IEEE Transactions on Power Electronics*, vol. 5, pp. 229–235, April 1990.
- [11] J. Svensson, "Simulation of power angle controlled voltage source converter using a linear quadratic method in a wind energy application," *IEEE Workshop on Computers in Power Electronics*, pp. 157–163, August 1996.
- [12] Y. Gui, X. Wang, H. Wu, and F. Blaabjerg, "Voltage modulated direct power control for a weak Grid-Connected Voltage Source Inverters," *IEEE Transactions on Power Electronics*, vol. 34, no. 11, pp. 11383–11395, Nov. 2019.
- [13] S. Wang, J. Hu and X. Yuan, "Virtual Synchronous Control for Grid-Connected DFIG-Based Wind Turbines," *IEEE Journal of Emerging and Selected Topics in Power Electronics*, vol. 3, no. 4, pp. 932–944, Dec. 2015.
- [14] M. P. N. van Wesenbeeck, S. W. H. de Haan, P. Varela and K. Visscher, "Grid tied converter with virtual kinetic storage," 2009 *IEEE Bucharest PowerTech*, Bucharest, 2009, pp. 1–7.
- [15] O. Mo, S. D'Arco and J. A. Suul, "Evaluation of Virtual Synchronous Machines With Dynamic or Quasi-Stationary Machine Models," *IEEE Transactions on Industrial Electronics*, vol. 64, no. 7, pp. 5952–5962, July 2017.
- [16] X. Meng, J. Liu, and Z. Liu, "A generalized droop control for grid-supporting inverter based on comparison between traditional droop control and virtual synchronous generator control," *IEEE Transactions on Power Electronics*, vol. 34, pp. 5416–5438, June 2019.
- [17] L. Harnefors, M. Hinkkanen, U. Riaz, F. M. M. Rahman, and L. Zhang, "Robust analytic design of power-synchronization control," *IEEE Transactions on Industrial Electronics*, vol. 66, pp. 5810–5819, August 2019.
- [18] L. Zhang, L. Harnefors, and H.-P. Nee, "Power-synchronization control of grid-connected voltage-source converters," *IEEE Transactions on Power Systems*, vol. 25, pp. 809–820, 2010.
- [19] P. F. de Toledo, "Modelling and control of a line-commutated hvdc transmission system interacting with a vsc statcom," Ph.D. dissertation, *Royal Institute of Technology*, Department of Electrical Engineering, Stockholm, Sweden, 2007.
- [20] L. Harnefors, M. Hinkkanen, U. Riaz, F. M. M. Rahman, and L. Zhang, "Robust analytic design of power-synchronization control," *IEEE Transactions on Industrial Electronics*, vol. 66, August 2019.

- [21] M. Davari, W. Gao, and F. Blaabjerg, "A fault-tolerant, passivity based controller enhanced by the equilibrium-to-equilibrium maneuver capability for the dc-voltage power port vsc in multi-infeed AC/DC modernized grids," *IEEE Journal of Emerging and Selected Topics in Power Electronics*, pp. 1–23, May 2019, Early Access.
- [22] ———, "Analysing dynamics and synthesising a robust vector control for the dc-voltage power port based on the modular multilevel converter in multi-infeed ac/dc smart grids," *IET Smart Grid*, vol. 2, no. 4, pp. 645–658, Dec. 2019.
- [23] M. Davari and Y. A.-R. I. Mohamed, "Robust multi-objective control of vsc-based dc-voltage power port in hybrid AC/DC multi-terminal microgrids," *IEEE Transactions on Smart Grid*, vol. 4, no. 3, pp. 1597–1612, Sep. 2013.
- [24] J. M. Guerrero, J. C. Vasquez, J. Matas, L. G. de Vicuna, and M. Castilla, "Hierarchical control of droop-controlled AC and DC microgrids—a general approach toward standardization," *IEEE Transactions on Industrial Electronics*, vol. 55, pp. 158–172, January 2011.
- [25] R. C. Conant and R. W. Ashby, "Every good regulator of a system must be a model of that system," *International Journal of Systems Science*, vol. 1, pp. 89–97, 1970.
- [26] J. M. Guerrero, J. C. Vasquez, J. Matas, L. G. de Vicuna, and M. Castilla, "Hierarchical control of droop-controlled AC and DC microgrids—a general approach toward standardization," *IEEE Transactions on Industrial Electronics*, vol. 55, pp. 158–172, January 2011.
- [27] L. Zhang, H. P. Nee, and L. Harnefors, "Analysis of stability limitations of a vsc-hvdc link using power-synchronization control," *IEEE Transactions on Power Systems*, vol. 26, pp. 1326–1337, August 2011.
- [28] R. C. Conant and W. R. Ashby, "Every good regulator of a system must be a model of that system," *International Journal of Systems Science*, vol. 1, pp. 89–97, 1970.
- [29] T. Kobaku, S. C. Patwardhan, and V. Agarwal, "Experimental evaluation of internal model control scheme on a dc–dc boost converter exhibiting nonminimum phase behavior," *IEEE Transactions on Power Electronics*, vol. 32, pp. 8880–8891, January 2017.
- [30] M. Yazdani and A. Mehrizi-Sani, "Internal model-based current control of the RL filter-based voltage-sourced converter," *IEEE Transactions on Energy Conversion*, vol. 29, pp. 873–881, December 2014.
- [31] K. Ogata, "Mathematical modeling of control systems in modern control engineering" *Prentice Hall*, New Jersey, U.S., 1997.
- [32] S. H. Mousavi, M. Davari, and H. J. Marquez, "An innovative eventbased filtering scheme using H1 performance for stochastic lti systems considering a practical application in smart modernized microgrids," *IEEE Access*, vol. 7, pp. 48 138–48 138, Apr. 2019.

- [33] M. Davari, “Dynamics of an industrial power amplifier for evaluating phil testing accuracy: An experimental approach via linear system identification methods,” *Proceedings of the IEEE International Conference on Industrial Electronics for Sustainable (IESES)*. IEEE Industrial Electronics Society, Apr. 2018, pp. 540–545.
- [34] M. Davari and F. Katiraei, “Investigation and correction of phase shift delays in power hardware in loop real-time digital simulation testing of power electronic converters,” in *Proceedings of the Grid of the Future Symposium*. CIGRE US National Committee, 2015, pp. 1–12. [Online]. Available: <http://cigre-usnc.tamu.edu/wpcontent/uploads/2015/10/DAVARI.pdf>
- [35] A. Timbus, A. Oudalov, and C. Ho, “Islanding detection in smart grids.” *Energy conversion congress and exposition*, pp. 3631–3637, 2010.

SECTION

2. CONCLUSION

This research proposes to apply new and well-established control methodologies to improve transient response, stability and reliability of three-phase inverters in grid-connected and isolated mode of operation. In the course of studying the effect of these methodologies, internal model-based control (IMC) is extensively applied and the application of this concept has been studied on developing “grid-forming” controls to allow wind and solar inverters to support voltage and frequency levels like traditional generators.

In the first paper, a new approach applied from control theory, an optimal switching control has been utilized to emulate a virtual synchronous machine which regulates power both in grid-connected and standalone modes. Along with it, this approach offers a seamless transition with no need of PLL and is robust during transitions. This optimized switching rule and an inherent islanding detection mechanism and it is able to perform efficiently in the presence of parameter uncertainties and loading conditions.

In the second paper, the interaction of a grid-forming inverter with a grid-following unit has been discussed. In this approach a nonlinear control has been utilized to limit the current and a hierarchical control method which emulates a virtual synchronous machine and regulates voltage magnitude and frequency through the grid-forming inverter has been adopted. This method possesses power-sharing capabilities by controlling the active and reactive power through both grid-forming and grid-following inverters. The autonomous operation in the isolated mode through the grid-forming inverter is attainable by using the proposed control structure and it is capable of withstanding grid unbalanced and faulty conditions.

In the third paper, by considering the non-minimum phase problem in power synchronization transfer functions, an internal model based control was applied to reduce the effects of non-minimum phase phenomena and offer excellent tracking capabilities. This method is capable of offering an excellent performance during weak-grid conditions with no dedicated synchronization unit and it possesses FRT and current-limiting capabilities. Along with it, the operation is possible by switching back and forth between islanded and grid-connected modes.

REFERENCES

- [1] "IEEE Standard for Interconnection and Interoperability of Distributed Energy Resources with Associated Electric Power Systems Interfaces," in IEEE Std 1547-2018 (Revision of IEEE Std 1547-2003) , vol., no., pp.1-138, 6 April 2018
- [2] "IEEE Standard for Inertial Systems Terminology," in IEEE Std 1559-2009 , vol., no., pp.c1-30, 26 Aug. 2009
- [3] "IEEE Recommended Practice for Industrial and Commercial Power Systems Analysis (Brown Book)," *IEEE Std 399-1997* , vol., no., pp.1-488, 31 Aug. 1998,
- [4] "Distributed Energy Resources - Connection, Modeling, and Reliability Considerations", *NREC IEEE 1547 - 404-446-2560*, 2018.
- [5] J. Svensson, "Grid-connected voltage source converter," *Ph.D. dissertation*, Chalmers University of Technology, Gothenburg, Sweden, 1998.
- [6] G. Joos, L. Moran, and P. Ziogas, "Performance analysis of a PWM inverter VAR compensator," *IEEE Transactions on Power Electronics*, vol. 6, no.3, pp. 380–391, Jul. 1999.
- [7] L. Zhang, L. Harnefors, and H.-P. Nee, "Power-synchronization control of grid-connected voltage-source converters," *IEEE Transactions on Power Systems*, vol. 25, no. 2, pp. 809 - 820, May 2010.
- [8] M. Durrant, H. Werner, and K. Abbott, "Model of a VSC HVDC terminal attached to a weak ac system," *IEEE Conference on Control Applications*, Istanbul, Turkey, 2003.
- [9] Q.C.Zhong, G. Weiss: "Synchronverters: inverters that mimic synchronous generators", *IEEE Transactions on Industrial Electronics*, 2011, 58, (4), pp. 1259–1267
- [10] K. Sakimoto, Y. Miura, and T. Ise, "Stabilization of a power system with a distributed generator by a virtual synchronous generator function," *IEEE 8th International Conference on Power Electronics, ECCE*, pp. 1498-1505, 2011.
- [11] N. Pogaku, M. Prodanovic, and T. C. Green, "Modeling, Analysis and Testing of Autonomous Operation of an Inverter-Based Microgrid," *IEEE Transactions on Power Electronics*, vol. 22, no. 2, pp. 613–625, Mar. 2007.
- [12] K. J. Åström and T. Hägglund, "Advanced PID Control." *Research Triangle Park, NC, USA: ISA*, 2006.

VITA

Sara Yazdani received the B.Sc. degree from the K. N. Toosi University of Technology, Tehran, Iran, and the M.Sc. degree from the Amirkabir University of Technology, Tehran, both in condensed matter physics. She worked as Graduate Research Assistant with the subject of "*Advanced Control Methods on Three-Phase Inverters in Distributed Energy Resources*". Her research interests include the application of control in power electronics and distributed energy resources. In August 2020, she received her Ph.D. degree in Electrical Engineering from Missouri University of Science and Technology, Rolla, MO, USA.